ANNALS OF GEOPHYSICS, 69, 5, S553, 2026; doi:10.4401/ag-9625
OPEN ACCESS

Baseline characterization of seismicity for risk-informed planning of geological CO_2 storage: insights from Campo Colorado area, Valle Medio del Magdalena Basin, Colombia

Sergio García-Arias[*,1], Geraldine Ariza[2], Jose David Sanabria-Gómez[2], Diego Armando Vargas-Silva[3]

(1) Universidad Industrial de Santander, Escuela de Geología, Bucaramanga, Colombia
(2) Universidad Industrial de Santander, Escuela de Física, Bucaramanga, Colombia
(3) Universidad Industrial de Santander, Escuela de Ingeniería de Petróleos, Bucaramanga, Colombia

Article history: received June 4, 2026; accepted July 27, 2026

Abstract

Geological CO_2 storage in sedimentary basins associated with depleted hydrocarbon reservoirs represents a relevant strategy for climate change mitigation. In Colombia, the Valle Medio del Magdalena Basin, with a long history of hydrocarbon exploration and production, has been identified as a potential target region, particularly the Campo Colorado field. An additional factor supporting the selection of Campo Colorado is its proximity to the Barrancabermeja refinery, a major CO_2 emission source. However, baseline seismic studies are required to assess its feasibility from a seismic risk management perspective. Given that the Valle Medio del Magdalena is tectonically active, a regional seismic characterization was conducted using the Colombian National Seismological Network catalog. The analysis focused on Campo Colorado within a 100 × 100 km polygon and included the Bucaramanga Seismic Nest as a comparative reference. Results indicate that progressive improvements in the seismic network enhanced catalog completeness, while the estimated b-value for cortical seismicity in Campo Colorado, slightly higher than that estimated for the Bucaramanga Seismic Nest. Higher probabilities of occurrence for cortical events with magnitudes below 5.0 are observed in the study area. The estimated fractal dimension (Dc = 1.45) indicates a moderately clustered spatial distribution of seismicity, consistent with the regional structural framework and providing complementary information for the characterization of seismicity patterns. No significant temporal anomalies were identified, indicating that current seismicity is predominantly related to natural tectonic processes. Strengthening the local seismic network is recommended to improve baseline characterization, support real-time monitoring, and facilitate future geological CO_2 storage initiatives in the region.

Keywords: Seismic baseline; b-value; Fractal dimension; Seal integrity; Depleted hydrocarbon reservoirs

1. Introduction

Carbon capture, utilization, and storage (CCUS) technologies aim to mitigate climate change by reducing atmospheric CO_2 concentrations (Metz et al., 2005). Among the available storage pathways, geological storage in sedimentary basins has emerged as the most viable and widely studied option. The suitability of a storage site depends on multiple criteria, including tectonic and structural conditions, stratigraphic and lithological characteristics, hydrodynamic and hydrogeochemical factors, geothermal conditions, and socio-economic aspects (Rivas, 2007). Basins located in plate interiors or along stable continental margins are considered favorable targets, whereas those situated in tectonically active regions require careful evaluation due to the potential risk of CO_2 leakage (Cook and Benson, 2005). Deep CO_2 injection at pressures exceeding the in situ hydrostatic pressure may induce fracturing or reactivation of pre-existing faults, potentially compromising seal integrity and creating migration pathways (Sminchak et al., 2001; Streit et al., 2005; Wo et al., 2005).

The international literature consistently identifies pore pressure increase as the primary triggering mechanism of induced seismicity in CO_2 storage projects, as it may promote the reactivation of pre-existing faults through relatively small stress perturbations, particularly in geological settings close to critical failure conditions (Cheng et al., 2023; Rutqvist, 2012; Vilarrasa et al., 2019). Geomechanical studies emphasize the importance of defining operational pressure limits, typically established as conservative thresholds below the minimum principal stress (σ_3) and the capillary entry pressure of the caprock (Rutqvist et al., 2016). The seismic response associated with CO_2 injection has been largely restricted to microseismic events ($M < 3$), with no documented cases of damaging seismicity linked to injection in deep saline aquifers or depleted reservoirs. Exceptions include certain CO_2-enhanced oil recovery projects where events of up to M 4.4 have been reported (Cheng et al., 2023; Hosseini et al., 2022; Mitchell and Green, 2017). No robust or universal relationship has been established between injected volume and the maximum magnitude of induced events (Evans et al., 2012; Foulger et al., 2018). Comprehensive site characterization, systematic operational control, and continuous multiparametric monitoring throughout the entire project lifecycle are therefore essential (Aminu et al., 2017; Kiyingi et al., 2025).

Colombia has committed to reducing the equivalent of 51% of its projected greenhouse gas emissions by 2030 (Ministerio de Ambiente y Desarrollo Sostenible, 2020). Campo Colorado, located within the Valle Medio del Magdalena (VMM) Basin in the western foothills of the Eastern Cordillera, has been identified as a potential candidate site for CO_2 storage. Its proximity to the Barrancabermeja refinery, a major CO_2 emission source, further supports its suitability.

Recognizing that the VMM is tectonically complex and that each sedimentary basin requires site-specific evaluation prior to CO_2 injection, this study conducts a seismicity analysis for the Campo Colorado area. The analysis integrates bibliographic review with quantitative characterization of regional seismicity, providing locally grounded considerations and recommendations for future work. These results contribute to the development of a methodological framework for seismic risk assessment in potential CO_2 storage projects within depleted hydrocarbon reservoirs and deep saline aquifers.

In addition, they provide key insights for evaluating caprock integrity, considering seismicity as an indicator of its geomechanical state. In this context, microseismic monitoring is proposed as a tool to detect stress changes, fracture activation, and potential pathways that may compromise the sealing capacity of the system.

This document presents a general framework of the geological context of the study area, corresponding to Campo Colorado, along with a review of the methodologies used in the literature for its analysis. Subsequently, the methodology implemented for seismicity analysis and stress field estimation is described. Finally, the results are presented together with their respective discussion, and future considerations and research directions are proposed to further enhance the understanding of the system.

2. Geological Context

2.1 Valle Medio del Magdalena Basin

The Valle Medio del Magdalena (VMM), located in northeastern Colombia (Fig. 1), is a sedimentary basin situated along the central Magdalena River valley, between the Central and Eastern Cordilleras of the Colombian Andes. Three main deformational phases are recognized: rifting, thrusting, and strike-slip shearing, reflecting multiple

tectonic events during the Late Triassic, Middle Cretaceous, Early Paleogene, and Middle Neogene (Acosta, 2002; Barrero et al., 2007).

The basin corresponds to a SW-NE-oriented intermontane depression, bound to the north by the Espíritu Santo fault system, to the south by the Girardot fold belt, to the northeast by the Bucaramanga-Santa Marta fault system, and to the southeast by the Bituima and La Salina fault systems (Barrero et al., 2007; Londoño et al., 2020; Roncancio and Martínez, 2011). Structurally, the VMM is characterized as an asymmetric tectonic depression, with a passive margin toward the Central Cordillera and a compressional margin toward the Eastern Cordillera (Londoño et al., 2020; Mojica and Franco, 1990). This asymmetry favored the development of asymmetric folds and major strike-slip structures, including the sinistral Bucaramanga Fault (Londoño et al., 2019).

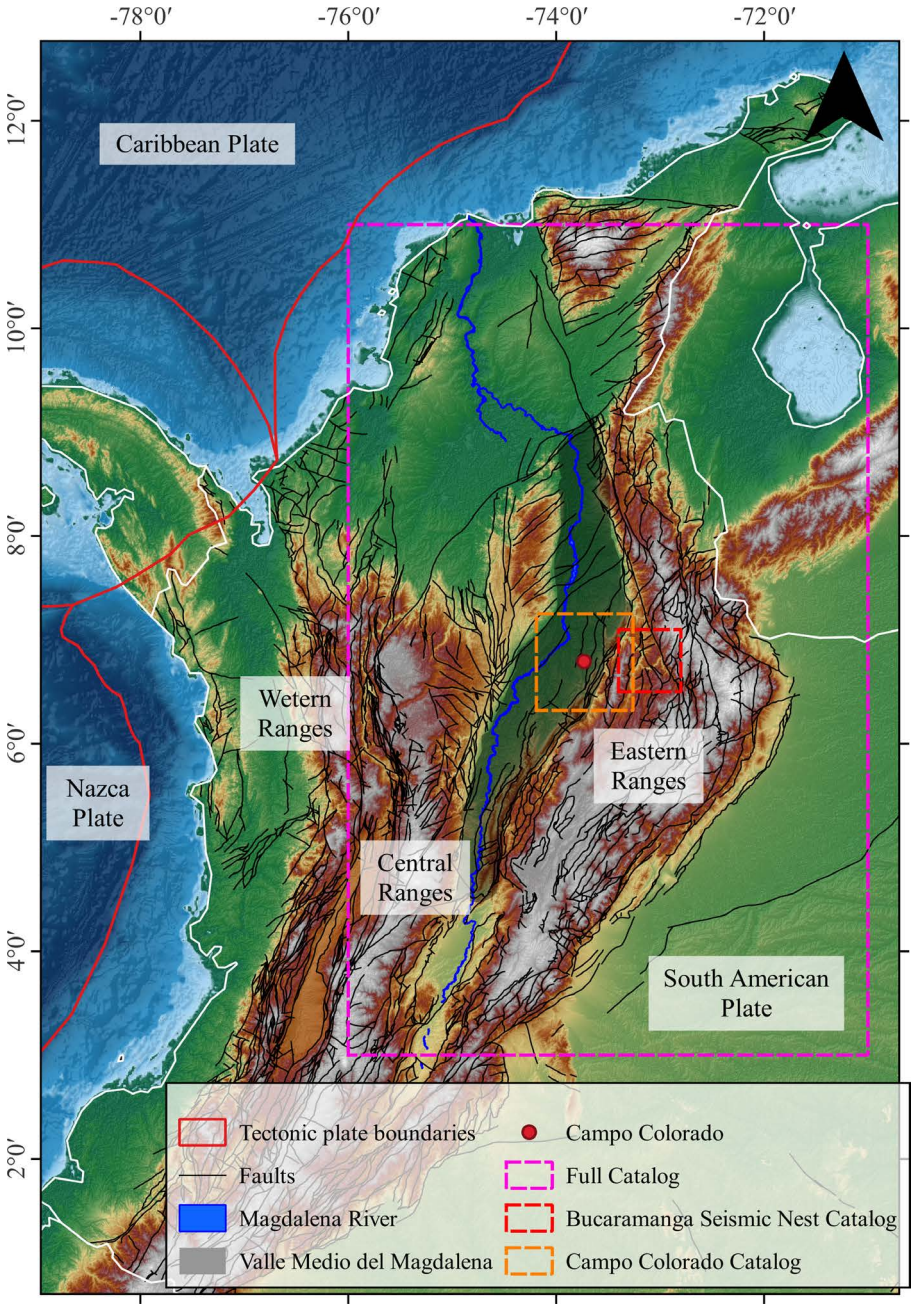


Figure 1. Location map of the study area and the spatial extent of the three seismic subcatalogs analyzed in Colombia: the Full Catalog (FC), the Bucaramanga Seismic Nest Catalog (BSN), and the Campo Colorado Catalog (CC). The FC represents the complete dataset used for regional-scale analysis. The BSN is restricted to events associated with the Bucaramanga Seismic Nest, recognized as the most seismically active zone in Colombia. The CC corresponds to the local study area, focusing on seismicity in the vicinity of the Campo Colorado field.

2.2 Campo Colorado

The Campo Colorado field is located along the crest of an asymmetric anticline plunging northward, within the hanging wall block of the Colorado Fault (Fig. 2). Wells drilled in the field penetrate Quaternary to Cenozoic units overlying the Middle Eocene unconformity. The stratigraphic sequence comprises, from base to top: the La Paz Formation (coarse- to conglomeratic sandstones, up to 610 m; Jaramillo and Dilcher, 2001), the Esmeraldas Formation (fine- to medium-grained sandstones with thick claystone intervals, up to 460 m; Royero and Clavijo, 2001), the Mugrosa Formation (mudstones intercalated with coarse- to conglomeratic sandstones, 600-1330 m; Caballero et al., 2010; Sarmiento et al., 2015), the Colorado Formation (fossiliferous and conglomeratic intervals, up to 1250 m; Caballero et al., 2010; Morales, 1958), the Real Group (heterogeneous deposits up to 3500 m; Sarmiento et al., 2015), and the Mesa Group (volcano-sedimentary deposits; Morales, 1958; Sarmiento et al., 2015). The principal hydrocarbon-bearing units are the Colorado, Mugrosa, and Esmeralda formations (Mier et al., 2013).

The Colorado Fault constitutes the principal structure, from which a system of satellite faults branches within its hanging wall, trending SW-NE. Alternative structural interpretations include reverse faults with backthrusts (Chajin et al., 2013), normal faults with sinistral strike-slip components (Zafra, 2013), and a thin-skinned triangular zone controlled by a backthrust system (Anaya et al., 2018). Ochoa (2010) identified up to ten fault segments, expanding the previously defined seven structural blocks.

At the scale of Campo Colorado, faults may act as potential migration pathways for saline waters from deeper formations, affecting freshwater aquifers detected at approximately 2 km depth (Sarmiento, 2021). Sandy intervals

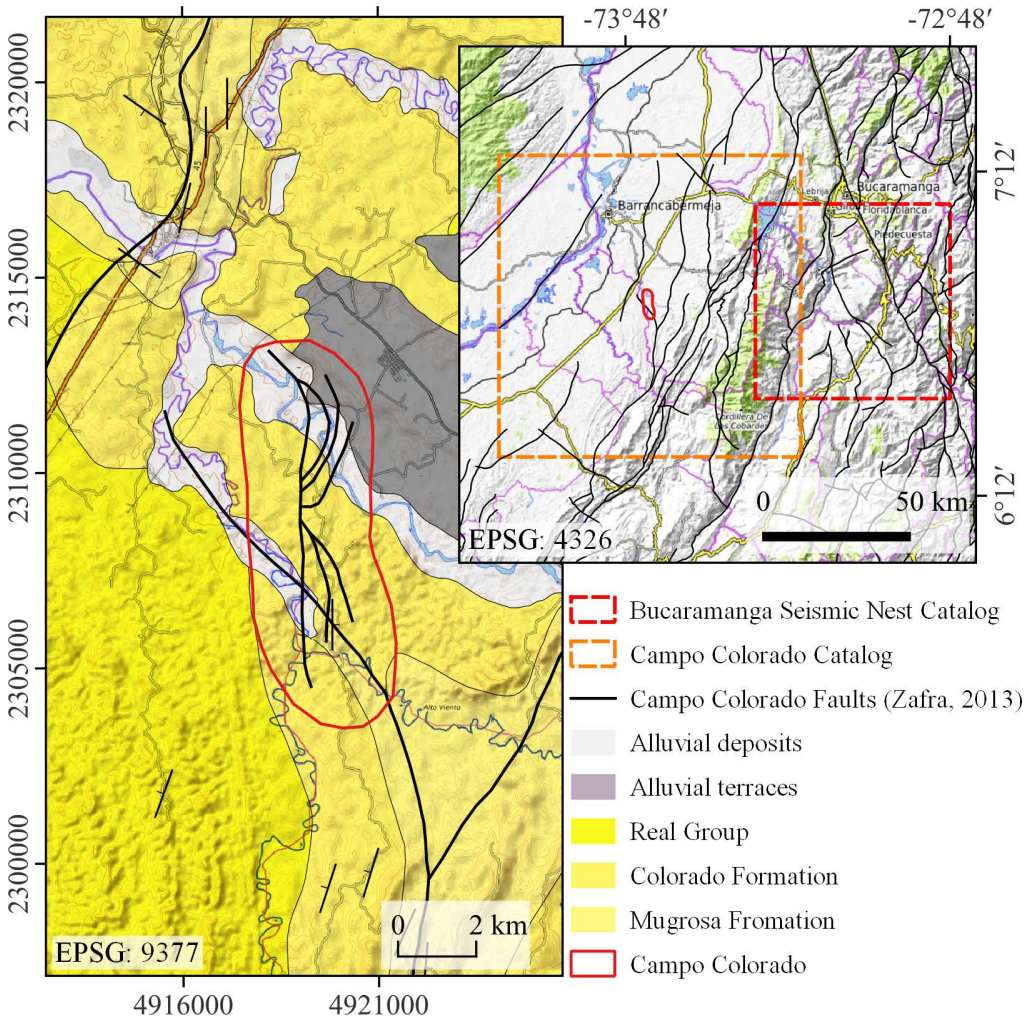


Figure 2. Location of Campo Colorado within the Campo Colorado Catalog (CC) area and geological characterization of the sector considered for potential CO_2 injection. The area exhibits a well-developed fault system and is mainly composed of clastic sedimentary rocks.

within the Mugrosa Formation contain interbedded aquifers with freshwater, brackish water, saline water, and brines, suggesting heterogeneous hydraulic connectivity influenced by fault systems. Regional groundwater flow is directed toward the northwest within the Campo Colorado area, with no hydraulic interconnection between different aquifers, as evidenced by varying salinity across stratigraphic levels (Sarmiento, 2021).

2.3 Induced Seismicity and CO_2 Storage: Context for Campo Colorado

Geomechanical modeling of CO_2 storage consistently shows that even moderate overpressures may bring the stress state closer to the failure envelope if pressure is not properly managed (Cappa and Rutqvist, 2011a, 2011b; Rutqvist, 2011, 2012). In well-designed storage sites, recorded microseismicity has been of very low magnitude (Rutqvist et al., 2016). Proximity of injection wells to fault systems significantly increases the likelihood of seismic activation, and injection in sedimentary formations should not be assumed to be inherently less seismogenic than in crystalline units (Evans et al., 2012; Vilarrasa et al., 2019). Caprock architecture, including multilayered configurations and lateral facies variations, controls trapping mechanisms and the timing of potential fault reactivation (Rinaldi et al., 2015).

Traffic light systems constitute the main operational tool for linking seismic observations to injection management actions. A four-level protocol proposed by Kohli et al. (2023) defines thresholds based on the combined evaluation of event location relative to the reservoir and mapped faults, seismic characteristics (magnitude, spatiotemporal density), and surface ground motion levels. Monitoring should begin during early injection stages and continue throughout the operational lifecycle, integrating seismic techniques (4D surveys, VSP, DAS), electromagnetic and electrical methods, gravimetry, InSAR, and downhole sensors (Furre et al., 2017; Goertz-Allmann et al., 2024; Kiyingi et al., 2025). An adaptive management framework with periodic protocol reviews is recommended (Kiyingi et al., 2025; Kohli et al., 2023).

At the national scale, the Colombian CO_2 Storage Atlas (Díaz et al., 2024) identifies depleted oil fields and associated aquifers in the VMM as potential storage candidates. One-dimensional geomechanical models for the Sinú-San Jacinto Basin indicate that injection pressures on the order of 1,500 psi may bring fractures to a critical state (Garcia Ariza, 2024). Laboratory experiments on VMM rocks show that CO_2 exposure may increase porosity without a corresponding gain in permeability, and mineralogical alterations have been observed under higher temperature and salinity conditions (Rojas Orduz and Pabón Uribe, 2024; Sierra Reyes, 2025). The La Luna Formation exhibits significant storage potential through adsorption mechanisms (Acevedo Acosta, 2023; Vesga Esparza and Mendoza Vecino, 2020), while non-miscible WAG schemes enhance CO_2 retention through combined structural (70-75%), capillary (22-25%), and solubility (3-5%) trapping (Gutiérrez Barrera, 2025).

For the VMM, mixed seismicity has been documented, with the crustal regime predominantly controlled by strike-slip mechanisms (Londoño et al., 2019). Intrinsic attenuation predominates over scattering attenuation, with anomalies spatially aligned with strike-slip fault systems and exhibiting sensitivity to rainfall cycles (Londoño et al., 2022). Local magnitude (Ml) has been calibrated specifically for the VMM region (Londoño and Romero, 2017). Automated monitoring approaches based on deep learning enable continuous catalog updating and real-time estimation of seismic parameters (Castillo et al., 2024; Prada Velásquez, 2024). To date, no studies have specifically characterized the historical seismicity of the Campo Colorado area.

3. Methodology

A bibliometric analysis of induced seismicity associated with CO_2 injection was performed using the SCOPUS database and VOSviewer software (van Eck and Waltman, 2010) (see Appendix A).

3.1 Seismic Data and Seismicity Characterization

Seismic events were retrieved from the Servicio Geológico Colombiano (SGC) online catalog, where four catalogs were available (Table 1). Data extraction used a geographic bounding box with latitudes between 3° and 11° N and longitudes between −76° and −71° W, retaining all events with magnitudes greater than zero recorded prior to 2025.

Table 1. List of the four seismic catalogs obtained from the SGC platform, including the direct link to each catalog. A total of 303240 events were downloaded.

Reference Name	Time Coverage	Direct Link to SGC Catalog	Total Events
SGC Catalog 1	June 1, 1993 – February 28, 2018	https://bdrsnc.sgc.gov.co/paginas1/catalogo/Consulta_Experta/consultaexperta_2.php	145061
SGC Catalog 2	March 1, 2018 – Present	https://bdrsnc.sgc.gov.co/paginas1/catalogo/Consulta_Experta_Seiscomp/consultaexperta.php	134030
TECTO Catalog	February 14, 2014 – Present	https://bdrsnc.sgc.gov.co/paginas1/catalogo/Consulta_Valle_Medio/index.php	16481
LBG Catalog (General Baseline Seismicity of the Middle Magdalena Valley and La Loma, Cesar)	June 3, 1993 – December 31, 2021	https://bdrsnc.sgc.gov.co/paginas1/catalogo/Catalogo_LBG/index.php	7668

The four catalogs were merged into a single unified dataset reprojected into MAGNA-SIRGAS 2018/Origen-Nacional (EPSG: 9377). As a preliminary quality-control step for the catalog integration, the workflow described by Londoño et al. (2019) was replicated to verify the consistency of the compiled datasets. During this process, duplicate records corresponding to the same seismic event were identified. Among these duplicated records, only the SGC 1 catalog contained events with more than one reported magnitude scale (Ml and Mw). In the remaining catalogs, although different magnitude labels (e.g., MLr_2, MLr_3, MLr_vmm and related suffixes) are reported, these correspond to local magnitude (Ml) determinations rather than different magnitude scales. Consequently, no magnitude conversion was applied during the integration process. After removing duplicate records, the unified catalog contained 281,086 seismic events. Three subcatalogs were subsequently defined according to the distance from the Campo Colorado reference point (Table 2): the Full Catalog (FC), the Bucaramanga Seismic Nest Catalog (BSN), defined following García-Arias et al. (2026a), and the Campo Colorado Catalog (CC), corresponding to a 100 × 100 km area centered on Campo Colorado.

Table 2. Spatial boundaries of the three study quadrants and corresponding number of events considered, relative to the total of 281086 available events.

Subcatalog	Longitude (min, max)	Latitude (min, max)	Total Events
Full Catalog (FC)	−76.00, −71.00	3.00, 11.00	281086 (100%)
Bucaramanga Seismic Nest Catalog (BSN)	−73.40, −72.80	6.50, 7.10	161158 (57.33%)
Campo Colorado Catalog (CC)	−74.19, −73.26	6.32, 7.25	22052 (7.85%)

Although the TECTO and LBG catalogs only report earthquakes with depths up to 50 km, and Londoño et al. (2019) adopted the same threshold for the analysis of shallow regional seismicity, the preliminary exploratory analysis of the merged catalog suggested that a slightly higher limit was more appropriate. The depth distribution (see Appendix B, Fig. B1) shows a clear transition around 60 km, separating the shallow crustal seismicity from the deeper events associated with the Bucaramanga Seismic Nest. In addition, the first quartile of the depth distribution is approximately 62 km, indicating that at least 25% of the earthquakes occur at shallower depths. Therefore, a depth threshold of

60 km was adopted to distinguish crustal from deeper seismicity throughout this study. The Gutenberg-Richter parameters were estimated from the frequency-magnitude distribution

$$\log_{10} N(m) = a - bm \tag{1}$$

Where $N(m)$ represents the cumulative number of events with magnitude M or greater, the a-value reflects seismic productivity, and the b-value corresponds to the slope of the exponential decay. The Mc was estimated using the maximum curvature method. Parameters were estimated using a resampling approach without replacement, randomly selecting 80% of the data across 1,000 iterations. The annual rate of occurrence was estimated as

$$\log_{10} N_1(m) = \log_{10} N(m) - \log_{10} T \tag{2}$$

The probability of occurrence of at least one event with magnitude $\geq m$ within a future time window of t years is given by

$$P(m,t) = 1 - e^{-N_1(m)\times t} \tag{3}$$

and the return period θ in years is

$$\theta = \frac{1}{N_1(m)} \tag{4}$$

The fractal dimension (*Dc*) was estimated from the correlation integral $C(r)$ for cortical events in the CC area:

$$C(r) = \frac{2N(R < r)}{N(N-1)}, \tag{5}$$

$$Dc = lim\left[\frac{\log C(r)}{\log r}\right] \tag{6}$$

Where r is the separation distance between epicenters and N is the number of event pairs separated by distance $R < r$.

3.2 Stress Field Estimation

The data used to estimate the stress field from focal mechanisms were compiled from both international and national repositories. Focal mechanism information was obtained from the Servicio Geológico Colombiano (SGC; https://bdrsnc.sgc.gov.co/sismologia1/sismologia/focal_seiscomp_3/index.html#advanced), the International Seismological Centre (ISC; https://www.isc.ac.uk/iscbulletin/search/fmechanisms/), and the Global Centroid-Moment-Tensor Project (Global CMT; https://www.globalcmt.org/).

The stress field was estimated through the approximation of the principal stress axes (σ_1, σ_2, and σ_3) following the methodology proposed by Pérez et al. (2026). The stress field was calculated using the Right Dihedral Method for stress inversion (Angelier and Mechler, 1977; Delvaux et al., 1995). Focal mechanisms were imported into WinTensor (Delvaux, 2001) using the Focal mechanism: Movement plane, slip line and slip sense definition, where each mechanism is represented by a fault plane defined by strike (φ), dip (δ), and rake (λ), were used as input in the WinTensor software (Delvaux, 2001).

The inversion provides the orientations of the three principal stress axes σ_1 (maximum compressive stress), σ_2 (intermediate compressive stress), σ_3 (minimum compressive stress), and the stress shape factor

$$R = \frac{(\sigma_2 - \sigma_3)}{(\sigma_1 - \sigma_3)} \tag{7}$$

To facilitate tectonic interpretation, the stress regime was characterized using the stress regime index (R′), which allows classification into the following regimes: radial extension (0.00-0.25), pure extension (0.25-0.75), transtension (0.75-1.25), pure strike-slip (1.25-1.75), transpression (1.75-2.25), pure compression (2.25-2.75), and radial compression (2.75-3.00) (Ali et al., 2021; Delvaux et al., 1997).

4. Results

4.1 Exploratory Data Analysis

Because the original catalogs and previous regional studies adopted different maximum depths for shallow seismicity (50 km), the exploratory analysis initially reports statistics considering both the historical reference and the depth threshold adopted in this study. Unless otherwise indicated, all subsequent analyses are based on the 60 km threshold defined for the unified catalog. In the unified catalog (see Appendix B), the spatial distribution of events shows concentration near the central portion of both coordinate axes (Fig. 3). In terms of depth, 25% of events occur at depths shallower than 62 km and 90% at depths less than 150 km. Location uncertainties at the 75^{th} and 90^{th} percentiles are smaller than 9 km and 13 km, respectively (Table 3).

A total of 67,986 events were classified as cortical earthquakes (≤50 km). For these events, the magnitude distribution is characterized by P10 = 0.9, Q1 = 1.2, Q2 = 1.5, Q3 = 2.0, and P90 = 2.5. No events with magnitudes lower than 1.5 were recorded prior to 2009, and a marked increase in cortical events with magnitudes as low as 0.5 is observed beginning in 2014.

To investigate the spatial relationship between the seismicity and the proposed CO_2 storage site, earthquake epicenters were referenced to the Campo Colorado location (X = 4,919,222.973 m; Y = 2,308,553.476 m; EPSG:9377). The planar epicentral distance was calculated from the projected X and Y coordinates, allowing comparison between crustal (≤50 km) and deeper (>50 km) seismicity. The resulting heat maps (Fig. 4) show that deep earthquakes are strongly concentrated approximately 50-60 km east of Campo Colorado, coinciding with the Bucaramanga Seismic Nest, whereas crustal seismicity is more dispersed and no significant clustering is observed in the immediate vicinity of the study area.

The planar distance histogram (Fig. 5) further highlights these differences. Deep earthquakes exhibit a pronounced peak at approximately 60 km from Campo Colorado, reflecting the dominant contribution of the Bucaramanga Seismic Nest, while crustal earthquakes show a broader spatial distribution without a comparable concentration near the study site. This analysis indicates that the concentration of deep seismicity is spatially consistent with the location of the Bucaramanga Seismic Nest, whereas crustal events show a broader distribution around Campo Colorado. Based on these observations, a 100 × 100 km study area centered on Campo Colorado was adopted to define the CC subcatalog used in the subsequent analyses.

Based on the exploratory analyses, a depth threshold of 60 km was adopted to distinguish crustal from deeper seismicity (see Appendix C). For cortical events (≤60 km), 90% of the events have magnitudes lower than 2.5 Ml,

Table 3. Percentiles 10 (P10), 25 (Q1), 50 (Q2), 75 (Q3), and 90 (P90) of the event location coordinates and their corresponding location uncertainties for the unified catalog.

	Y [km]	Y Error [km]	X [km]	X Error [km]	Depth [km]	Depth Error [km]
P10	2110.57	1.20	4834.54	1.20	5.96	1.90
Q1	2280.70	2.09	4923.09	2.18	62.00	3.40
Q2	2308.06	3.50	4980.67	4.20	138.00	6.10
Q3	2313.04	5.40	4987.08	7.21	146.00	8.70
P90	2380.01	7.90	4998.23	12.60	150.1	12.30

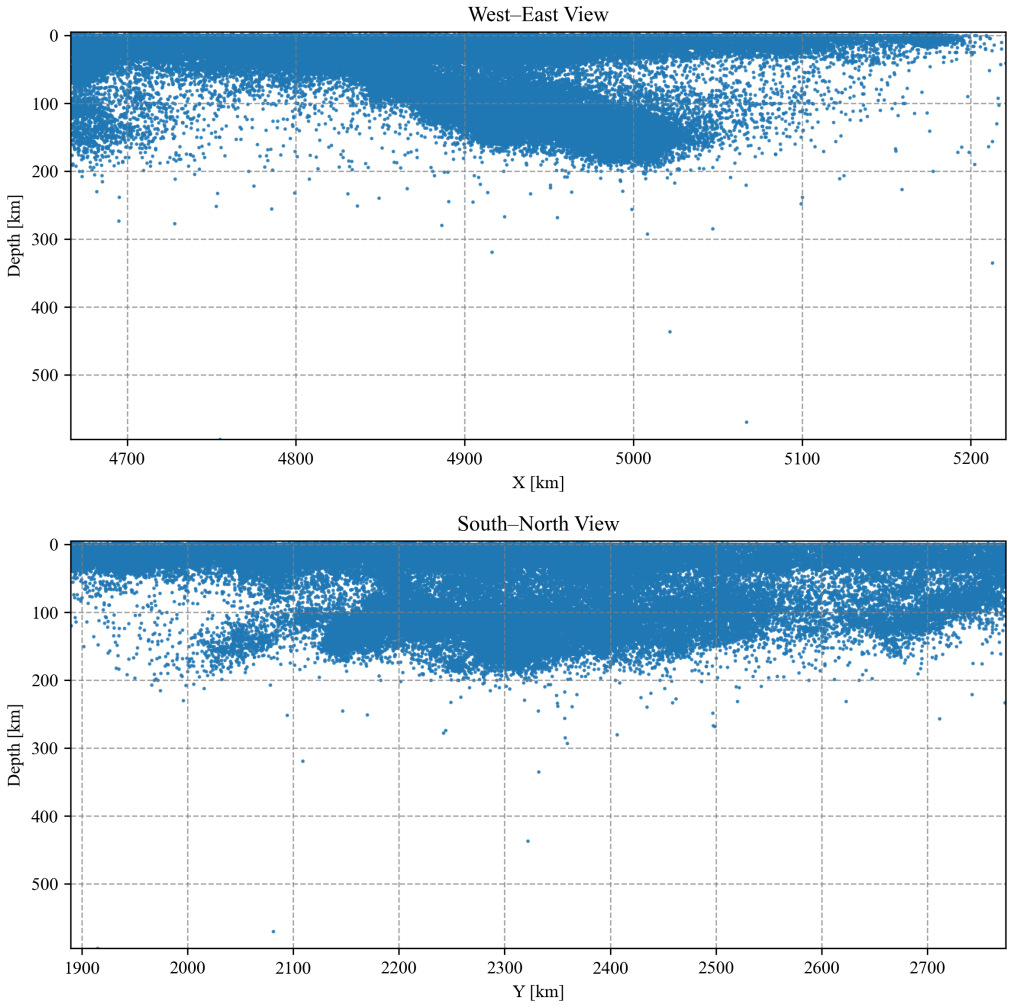


Figure 3. Cross-sections generated from the X and Y projections of the events in the unified catalog.

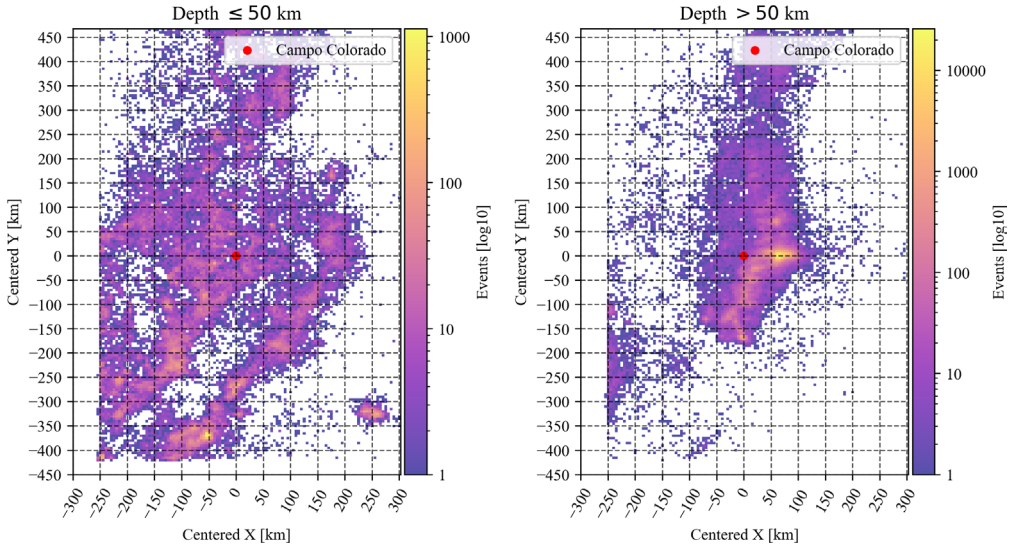


Figure 4. Heat maps of the spatial distribution of seismic events from the unified catalog, centered relative to Campo Colorado (red point). Separate heat maps are shown for crustal events (≤50 km) and deep events (>50 km), highlighting a greater concentration of deep seismicity compared to crustal events. This pattern reflects the dominance of seismic activity associated with the Bucaramanga Seismic Nest, located approximately 50 km east (X direction) of Campo Colorado.

whereas for deeper earthquakes the P90 reaches approximately 2.9 Ml (Fig. 6). The magnitude histograms further show that the highest event frequencies are concentrated around Ml ≈ 1.0-1.5 for the FC and BSN subcatalogs and around Ml ≈ 1.1 for the CC subcatalog. These distributions provide the preliminary basis for the formal estimation

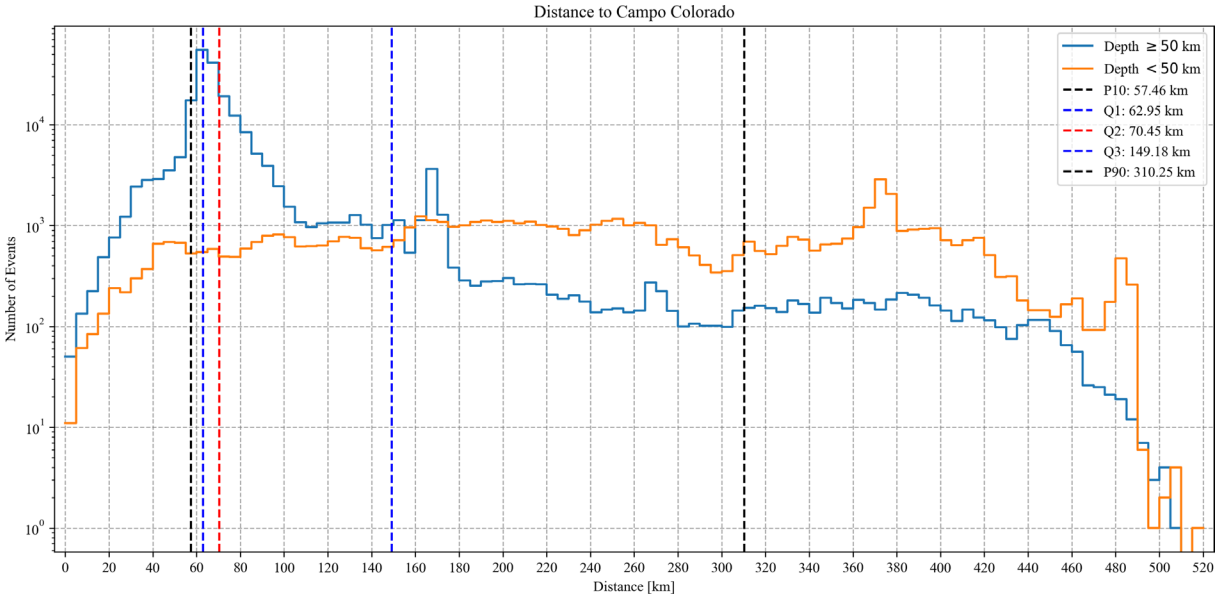


Figure 5. Histogram of the planar (XY) distance of seismic events relative to Campo Colorado. Crustal events (≤50 km depth, orange) and deep events ((>50 km depth, blue) are shown separately. A marked increase in the number of deep events is observed at a distance of approximately 60 km, corresponding to the location of the Bucaramanga Seismic Nest. In contrast, crustal events are sparse near Campo Colorado and increase progressively with distance.

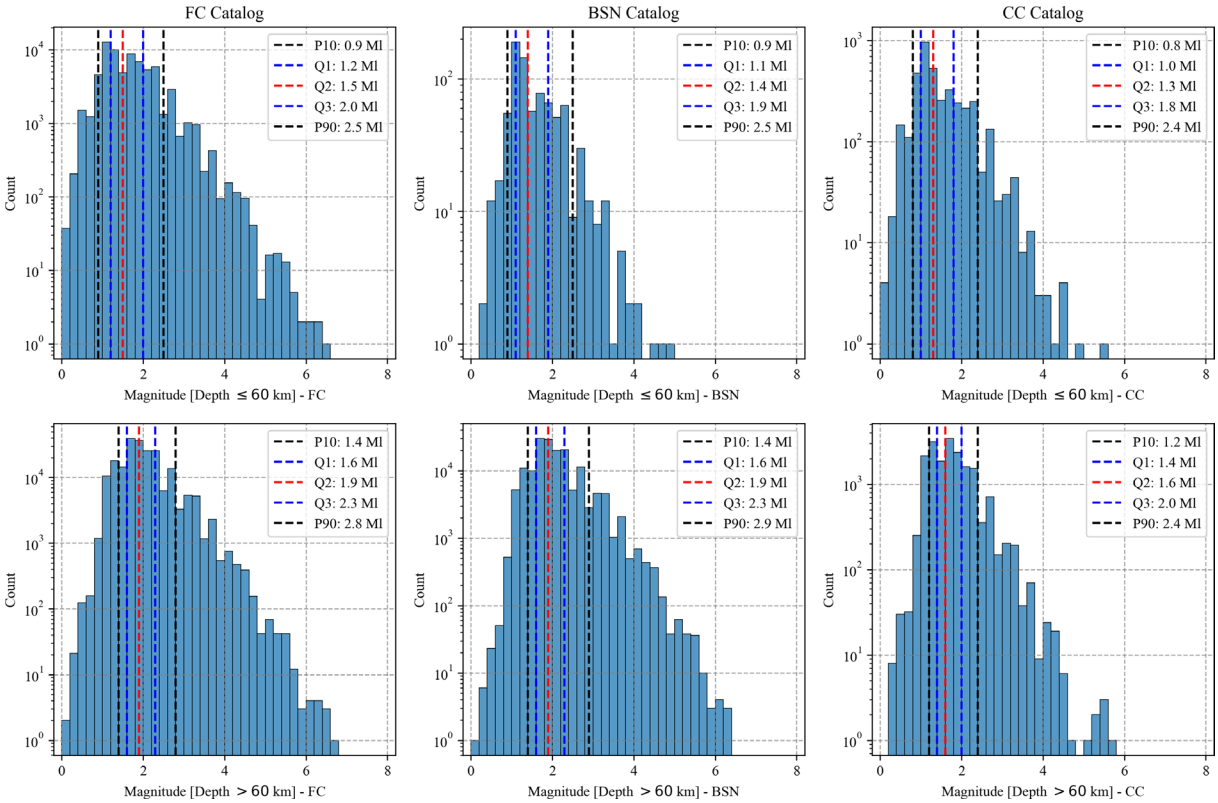


Figure 6. Magnitude histograms for the three subcatalogs, separated into crustal events (≤60 km depth) and deep events (>60 km depth).

of the magnitude of completeness (Mc) presented in the following section using the maximum curvature method. In addition, the progressive increase in the annual number of recorded earthquakes (Fig. 7) indicates that the catalog characteristics may vary through time. Therefore, the estimation and interpretation of the Gutenberg-Richter parameters in the following section consider the possible influence of temporal changes in catalog completeness.

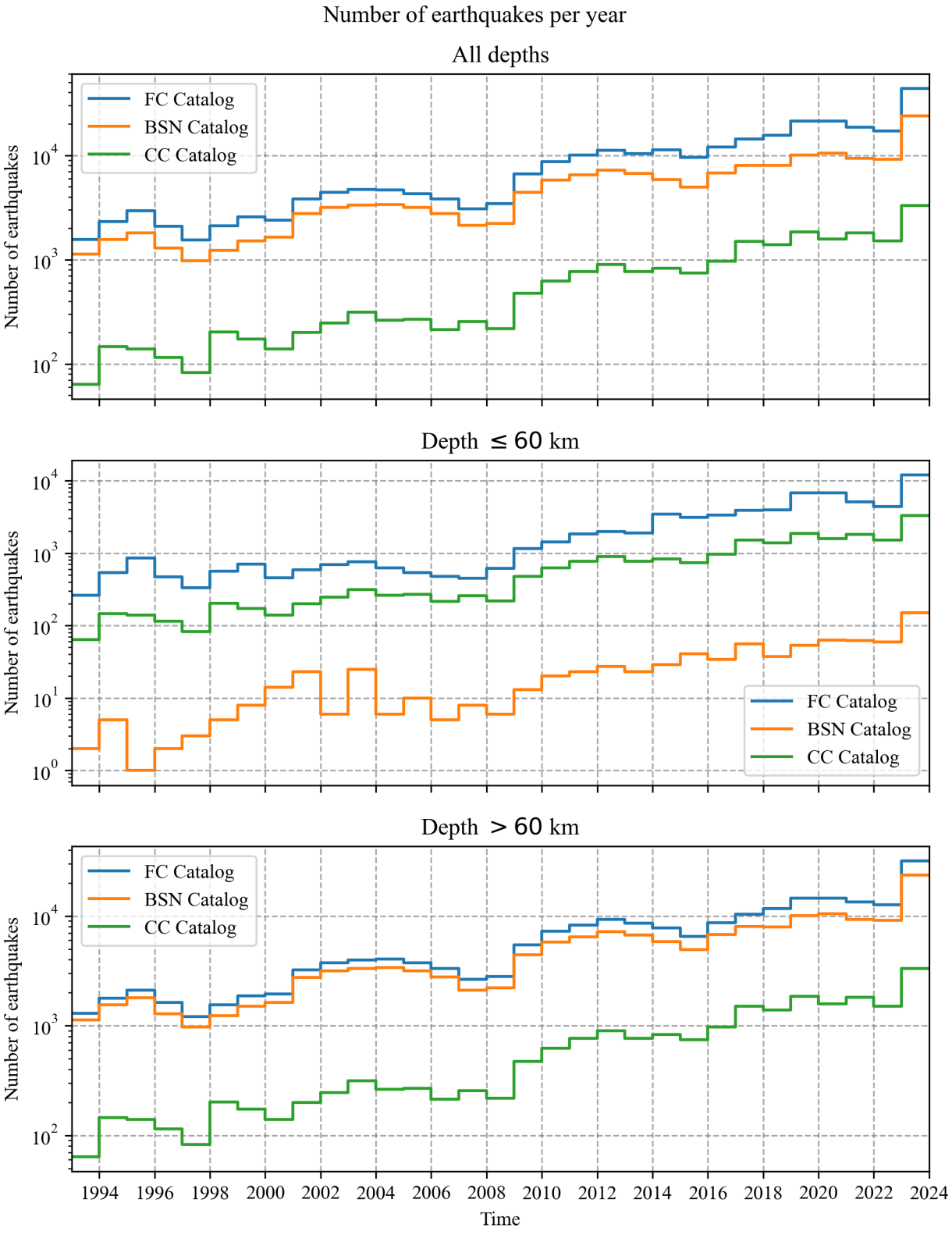


Figure 7. Yearly seismicity rates for the three subcatalogs, shown for the complete dataset, crustal events (≤60 km), and deep events (>60 km).

4.2 Gutenberg-Richter Parameters

The estimated a-values vary among the three subcatalogs, primarily reflecting differences in their spatial extent and the corresponding number of recorded earthquakes. In contrast, the estimated Mc and b-values are generally comparable across the datasets (see Appendix D). Considering all earthquakes, Mc values of 1.6, 1.6, and 1.4 were obtained for the FC, BSN, and CC subcatalogs, respectively, with corresponding b-values of 0.985 ± 0.011, 0.991 ± 0.014, and 0.960 ± 0.019. For crustal events (>60 km), Mc values decrease to 1.2, 1.2, and 1.0, whereas the corresponding b-values are 0.878 ± 0.012, 0.756 ± 0.039, and 0.871 ± 0.029. Deep earthquakes (>60 km) show Mc values of 1.6, 1.6, and 1.4, with corresponding b-values of 0.996 ± 0.012, 0.990 ± 0.013, and 0.964 ± 0.024 for the FC, BSN, and CC subcatalogs, respectively (Fig. 8).

Given the progressive increase in the number of recorded earthquakes through time, the Gutenberg-Richter parameters (a, b, and Mc) were subsequently recalculated using a cumulative approach. The analysis started with the 1993-1994 period and progressively incorporated earthquakes on an annual basis until the complete 1993-2024 catalog (see Appendix D). Because the a-value is strongly dependent on the total number of earthquakes, it is not directly comparable among the three subcatalogs, whose spatial extents and event counts differ substantially.

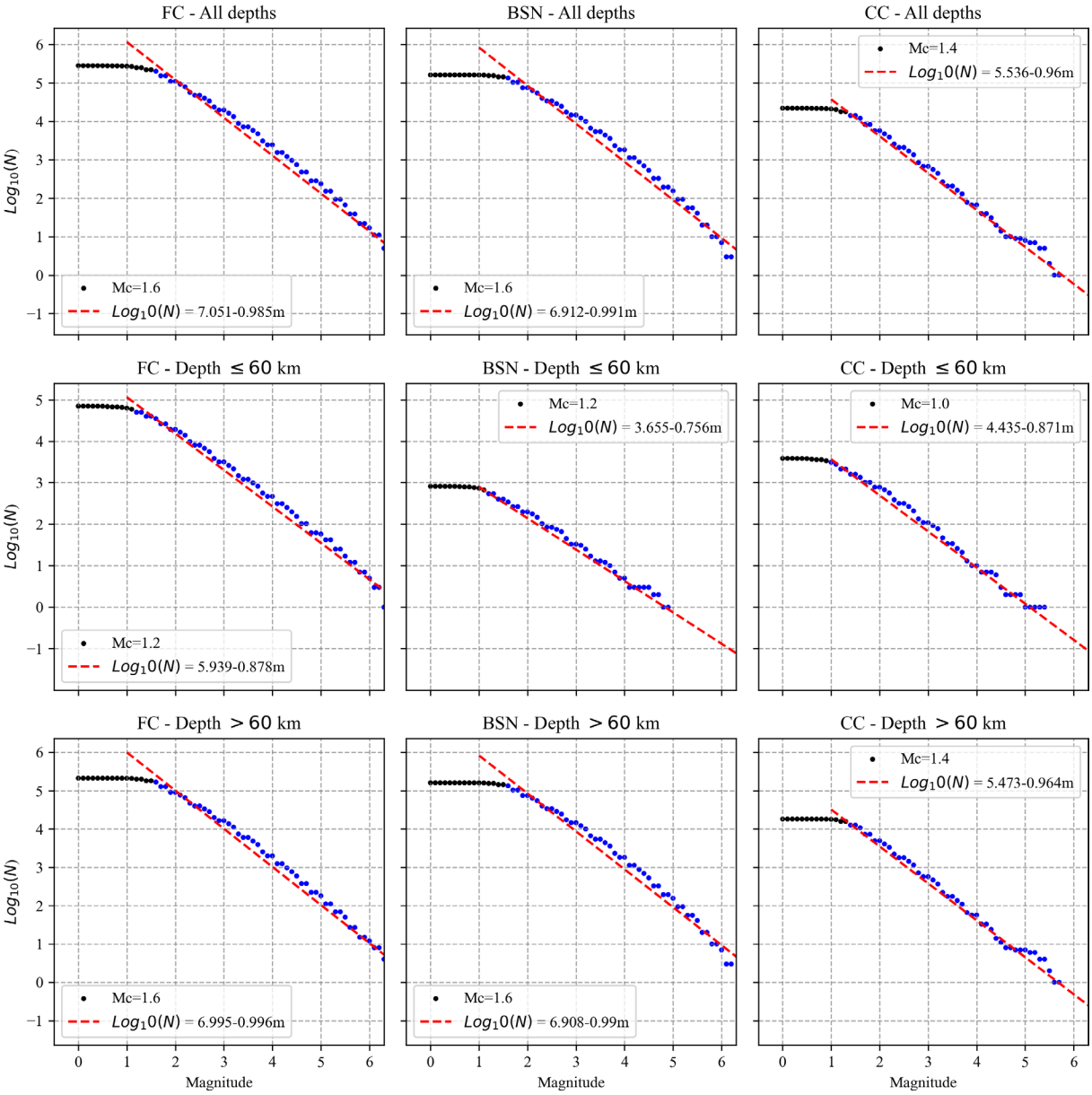


Figure 8. Estimated Gutenberg-Richter parameters (a-value, b-value, and Mc) for the three subcatalogs, computed for the complete dataset, crustal events (≤60 km), and deep events (>60 km).

The cumulative temporal analysis (Figs. 9-11) indicates that the b-value for crustal events remains relatively stable after approximately 2002, reaching values close to 0.87 for the FC and CC subcatalogs and about 0.76 for the BSN. For deeper events, the FC and BSN exhibit similar temporal behavior, whereas the CC subcatalog shows a gradual increase in b-value over time. In contrast, Mc exhibits a systematic decrease from values greater than 2.75 to approximately 1.0-1.5. This reduction is consistent with the progressive improvement of the regional seismic monitoring network rather than reflecting changes in the seismic source process itself. Vergara (2024) documented a significant increase in the number of seismic stations operating in the Valle Medio del Magdalena and the Bucaramanga Seismic Nest region since approximately 2005, accompanied by a reduction in earthquake location uncertainties and a corresponding increase in the number of detected events. These improvements in network coverage and catalog completeness likely

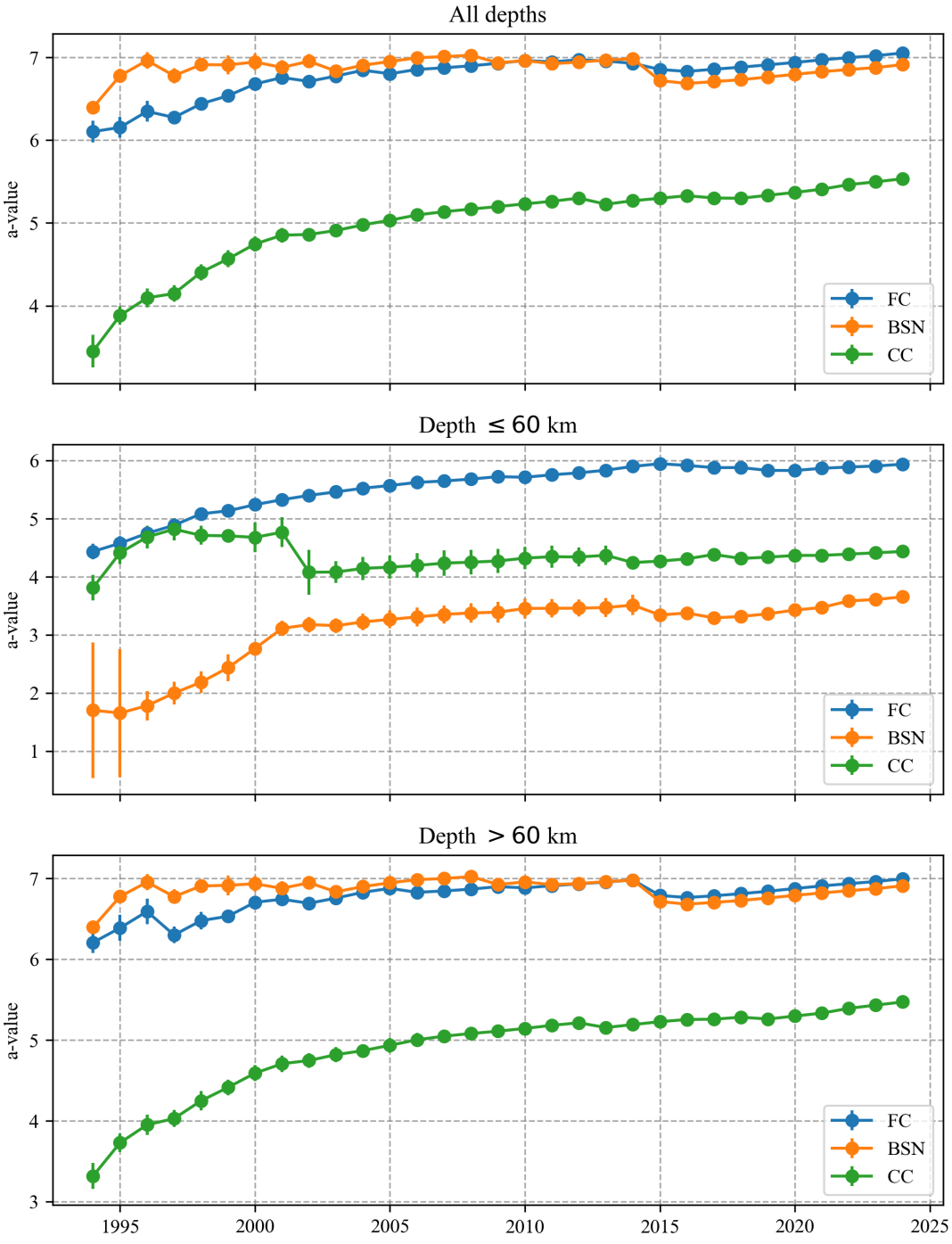


Figure 9. Temporal evolution of the cumulative a-value for the three subcatalogs, calculated by progressively extending the catalog year by year, for all events, crustal events (≤60 km), and deep events (>60 km). Vertical bars indicate the standard deviation obtained through resampling.

explain part of the temporal variations observed during the early years of the catalog, particularly the decrease in Mc and the initial variability of the Gutenberg-Richter parameters. Conversely, the stabilization of both Mc and the b-value during the most recent years suggests that the catalog has reached a more consistent level of completeness, providing a more reliable basis for the seismic characterization presented in this study.

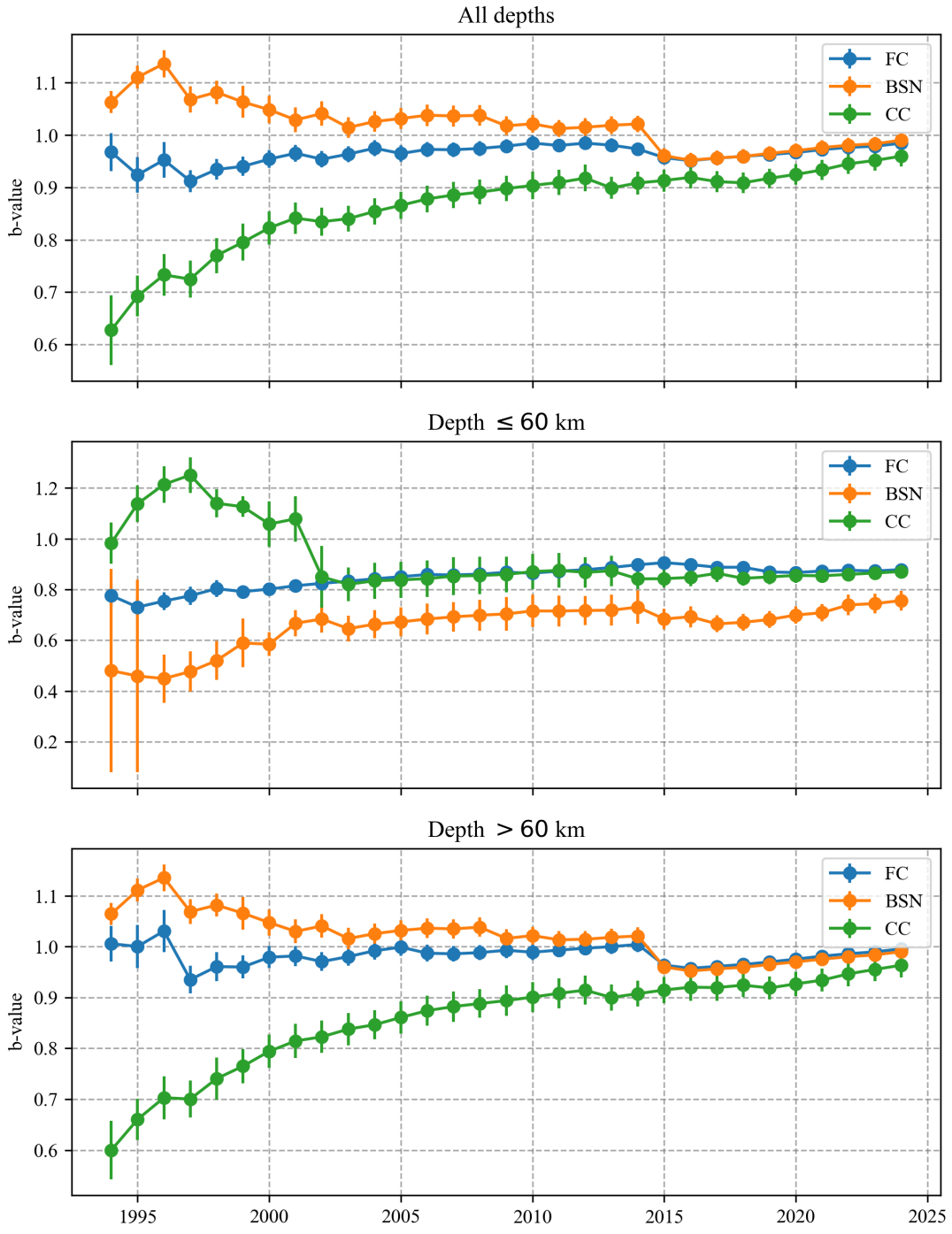


Figure 10. Temporal evolution of the cumulative b-value for the three subcatalogs, calculated by progressively extending the catalog year by year, for the complete dataset, crustal events (≤60 km), and deep events (>60 km). Vertical bars indicate the standard deviation obtained through resampling.

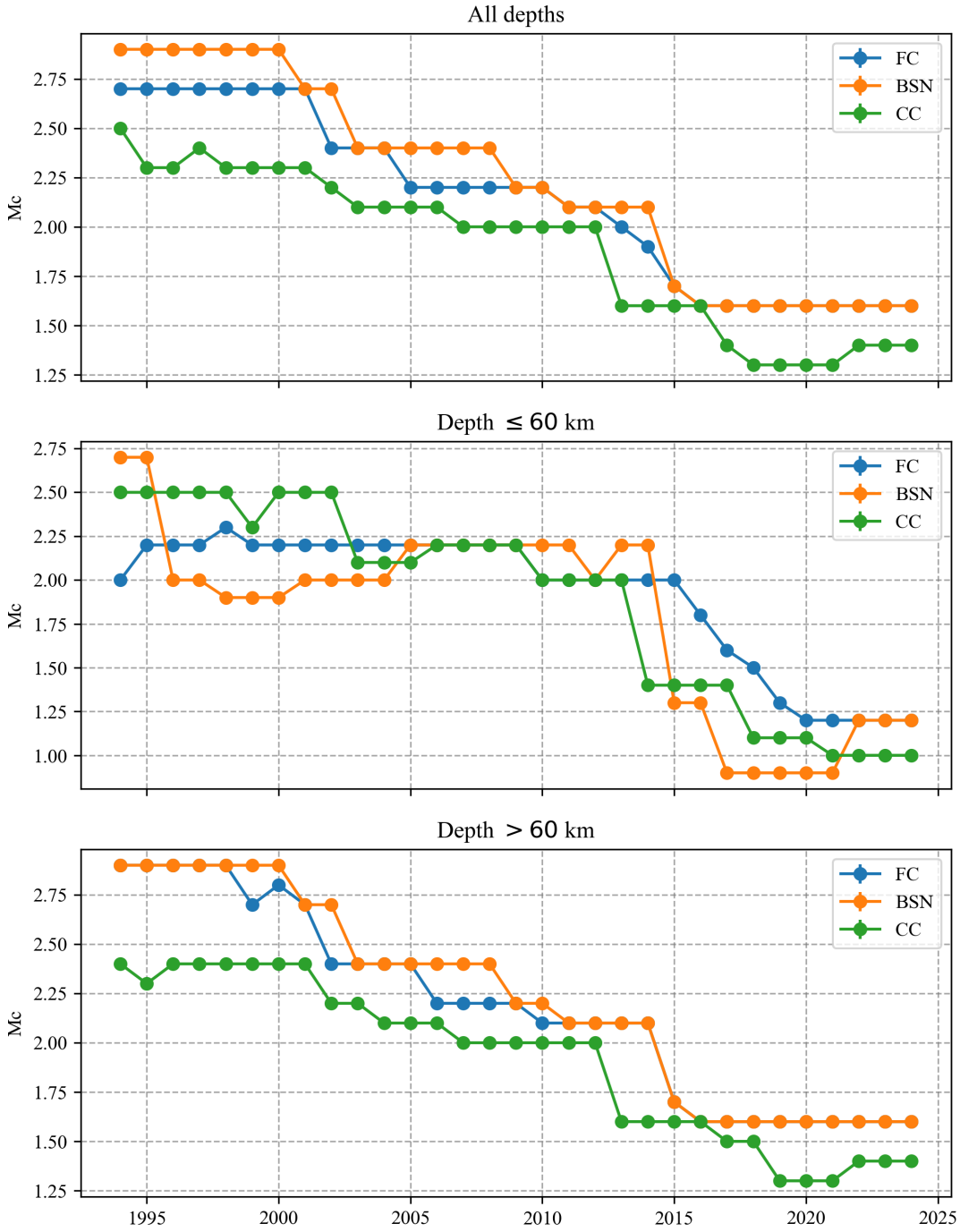


Figure 11. Temporal evolution of the cumulative magnitude of completeness (Mc) for the three subcatalogs, calculated by progressively extending the catalog year by year, for the complete dataset, crustal events (≤60 km), and deep events (>60 km). Vertical bars indicate the standard deviation obtained through resampling.

4.3 Recurrence Intervals and Occurrence Probabilities

For cortical events (≤60 km), magnitudes with a high probability of occurring within one year are those below 5.3, 3.1, and 3.5 for the FC, BSN, and CC subcatalogs, respectively (see Appendix E). Considering a probability threshold lower than 50% within one year, the corresponding magnitudes for cortical events are 5.1 (46%) for the BSN and 5.3 (48%) for the CC. For deep events in the BSN, no magnitude falls below the 50% threshold; even at magnitude 7.1, the annual probability remains 53%.

4.4 Fractal Dimension – Campo Colorado

The estimated fractal dimension (Dc) for cortical events in the CC subcatalog is 1.45 (Fig. 12). To provide context for the interpretation of this parameter, the depth distribution and depth location errors of the analyzed earthquakes are shown in Fig. 13. The depth histogram indicates that 25% of events occur at depths shallower than 4 km, 50% at depths less than 14 km, and 75% at depths below 26 km, with 90% located shallower than 35 km. A higher concentration of earthquakes is observed within the 0-6 km depth interval, whereas between approximately 6 and 30 km the event frequency remains relatively stable. Beyond 30 km depth, the number of earthquakes progressively decreases. The estimated depth uncertainties are generally smaller than 15 km for most of the analyzed events.

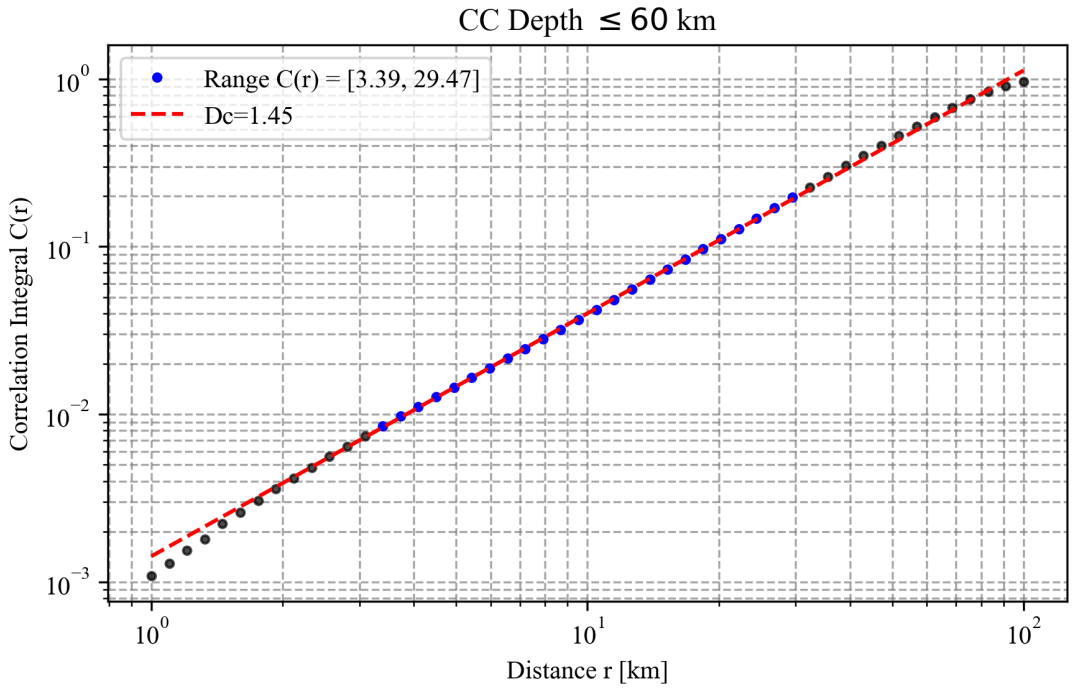


Figure 12. Estimation of the fractal dimension (Dc) for the complete set of seismic events in the Campo Colorado area.

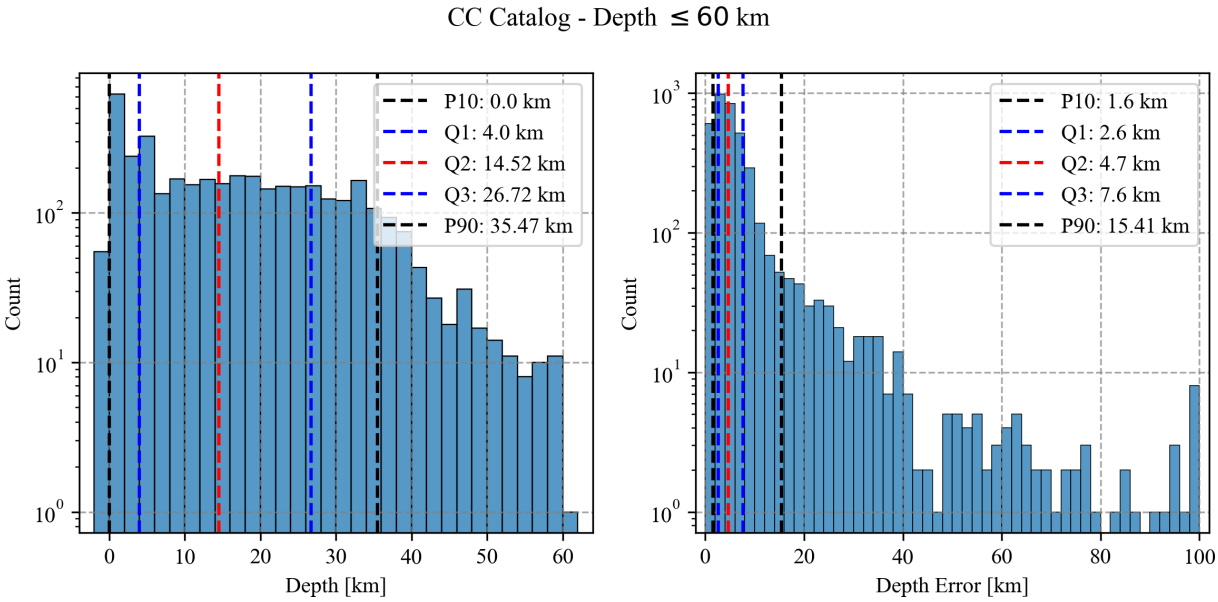


Figure 13. Frequency distribution of seismic event depths and their corresponding depth location errors in the Campo Colorado area.

Incremental depth analysis (Fig. 14) shows Dc values ranging between 1.20 and 1.45 (see Appendix F). Within the first 10 km, Dc remains near 1.20-1.25, increasing progressively beyond 10 km to approximately 1.43 at 30 km depth, and reaching 1.45 when the full crustal depth range is considered. A minor decrease to 1.41 is observed near 38 km, after which Dc increases again, attaining a value of 1.45 when considering the full depth range of the CC dataset. In contrast, analysis using a sliding 5 km depth window (Fig. 15), considering that 50% of the earthquakes have depth uncertainties smaller than 5 km, reveals considerable variability. Dc decreases from approximately 1.25 to 0.93 within the 5-10 km interval, increases to values approaching 1.6 between 10 and 18 km, and subsequently decreases to approximately 0.8 between 25 and 39 km before increasing again at greater depths. These results indicate that the estimated fractal dimension is sensitive to the selected depth interval and the spatial distribution of the analyzed earthquakes.

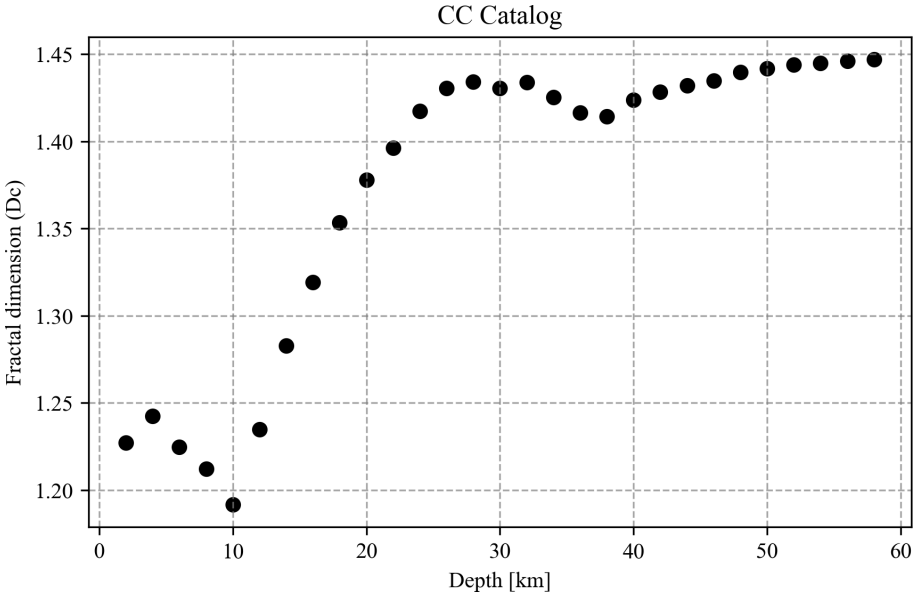


Figure 14. Fractal dimension (Dc) values calculated for cortical seismic events in the CC area, estimated incrementally as a function of depth.

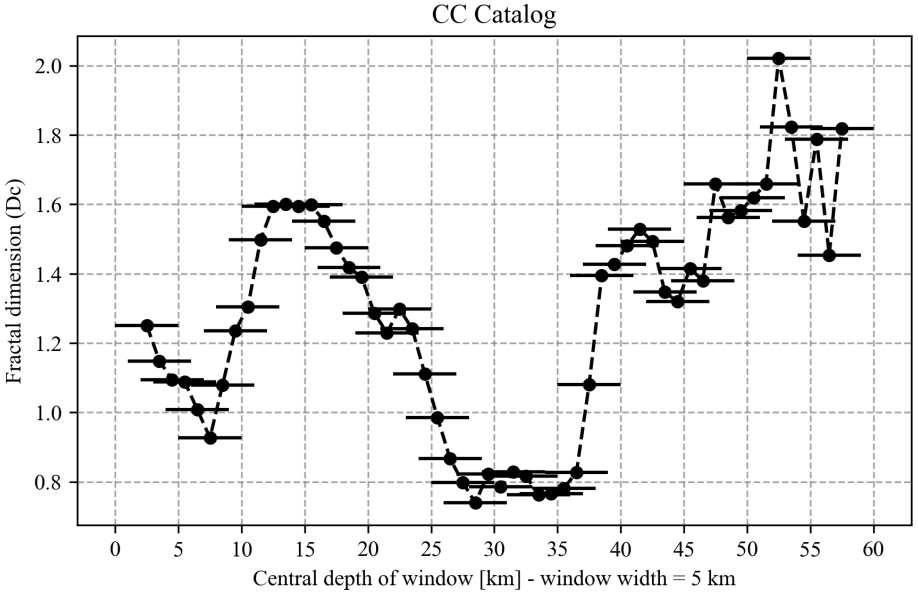


Figure 15. Fractal dimension (Dc) calculated for cortical seismic events in the CC area using a moving depth window. Points along the X-axis represent the center of each depth window, while the associated horizontal bars indicate the window width (5 km).

4.5 Estimated Stress Field

Focal mechanisms show a general pattern with most events associated with compressional and strike-slip regimes (Fig. 16). Events within the VMM are predominantly shallow (<20 km), whereas events to the west (Central Cordillera) are deeper (20-60 km). The stress field for Campo Colorado, based on 16 nodal planes and 2 P- and T-axis solutions, yields SHmax = 078°, R′ = 2.13 (R = 0.13), indicating a transpressive regime, with σ_1 = 16/259, σ_2 = 29/359, and σ_3 = 56/144. For the broader VMM (22 nodal planes and 5 P- and T-axis solutions), SHmax = 084°, R′ = 2.15 (R = 0.15), likewise corresponding to transpression stress regime.

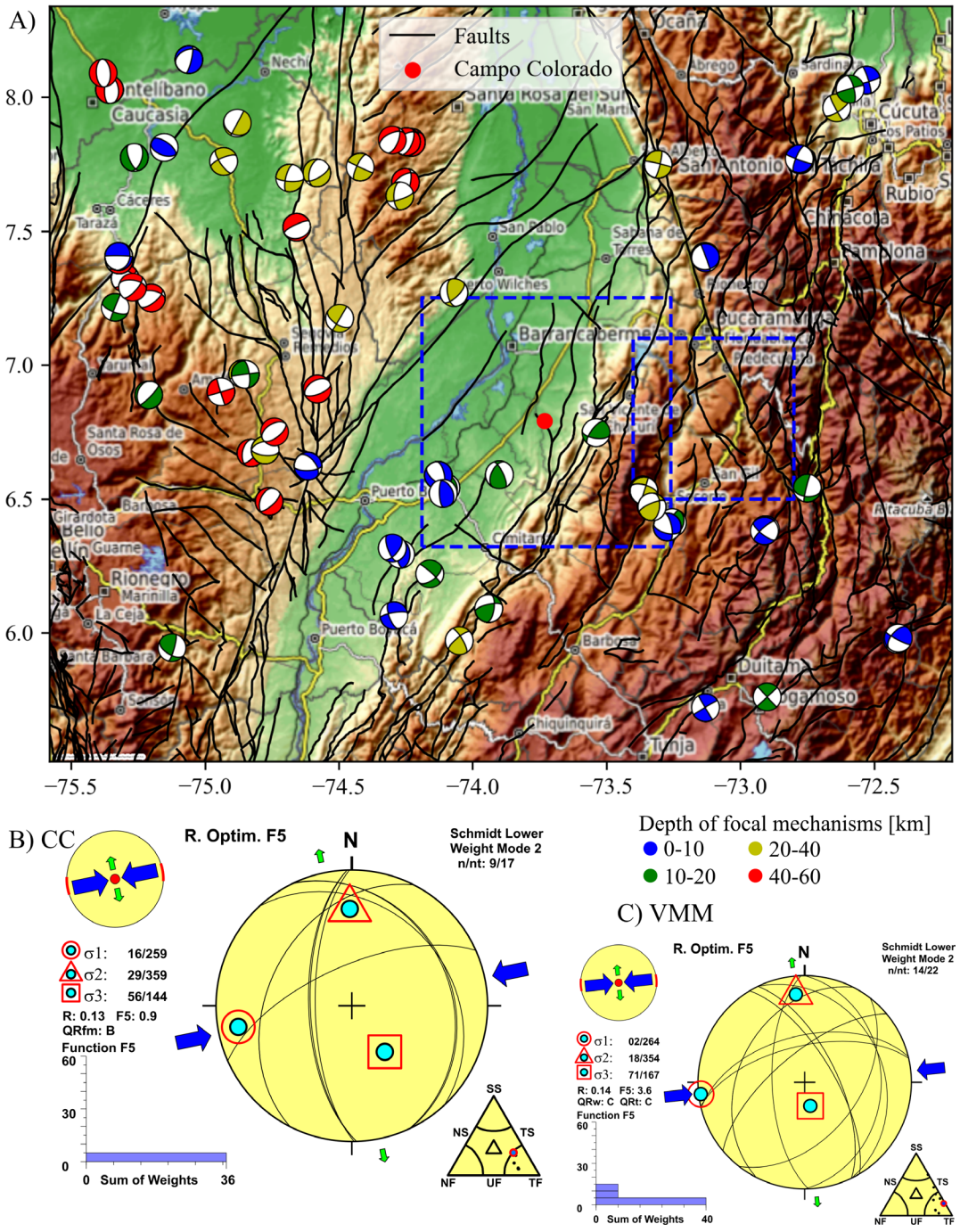


Figure 16. A) Focal mechanisms compiled from the SGC, ISC, and CMT catalogs for the regional study area. Based on this information, a stress inversion analysis was performed using the WinTensor software to estimate the stress field distribution. B) Stress inversion results for the Campo Colorado (CC) area. C) Stress inversion results for the Middle Magdalena Valley (VMM).

5. Discussion

5.1 Seismicity Characterization and Implications for CO_2 Storage

The EDA confirms a clear differentiation between shallow (crustal) and deep seismic events, with the latter primarily associated with the subducting slab. This depth-dependent distribution has been extensively documented in regional studies (Chiarabba et al., 2016; Cortés and Angelier, 2005; Londoño et al., 2010, 2019, 2020; Prieto et al., 2012; Taboada et al., 2000; Zarifi et al., 2007). The improvement in event location accuracy and detection capability is primarily related to progressive upgrades of the regional seismic network rather than changes in the underlying tectonic regime(García-Arias et al., 2026; Vergara, 2024). Consequently, temporal increases in the number of detected earthquakes and decreases in Mc should be interpreted mainly as reflecting improved catalog completeness. This also reinforces the need to strengthen local monitoring near Campo Colorado.

Crustal seismicity is more pronounced in the CC area compared to the BSN, consistent with the tectonically active character of the VMM. The estimated b-value for crustal events in the CC area (0.871) is slightly lower than the reference value of 1.0 commonly reported for tectonically active regions (Frohlich and Davis, 1993). The BSN exhibits a lower crustal b-value (0.756), although its overall shallow seismic activity is lower than that observed in the CC area, as reflected by the corresponding a-value.

Overall, the estimated b-values and their associated uncertainties, obtained through the resampling procedure, allow for a robust statistical comparison. For instance, the crustal b-value in the CC subcatalog (0.871 ± 0.029) is statistically higher than that of the BSN subcatalog (0.756 ± 0.039), as the difference exceeds their combined standard errors. This indicates a genuinely higher frequency of smaller-magnitude events in the VMM crust compared to the Bucaramanga Nest. Nevertheless, when evaluating absolute values, it is important to contextualize them within the temporal evolution of the regional seismic network and catalog completeness.

The temporal evolution of the Gutenberg-Richter parameters show that, despite the progressive decrease in Mc, associated with improvements in the detection capability of the seismic network, the b-value remains relatively stable throughout the study period, particularly for the CC subcatalog. After accounting for the temporal improvement in catalog completeness, the relative stability of the b-value suggests that a crustal b-value close to 0.87 is representative of the current tectonic conditions in the Campo Colorado area.

The divergent temporal trends in deep b-values among subcatalogs, stable for FC and BSN but increasing for CC, suggest that deep seismicity beneath CC evolves independently from shallow crustal activity. This supports the interpretation that no direct coupling exists between deep slab-related seismicity and crustal seismicity in the CC area and justifies restricting recurrence analysis to crustal events as the domain most relevant for evaluating interactions with future CO_2 injection.

In the context of induced seismicity monitoring, the IEAGHG (2013) report highlights that b-value variations are commonly linked to changes in stress conditions and permeability: higher values are associated with fluid-rock interactions promoting small tensile fractures (Shapiro and Dinske, 2009), whereas lower values relate to reactivation of pre-existing fractures (Bachmann et al., 2012; Maxwell et al., 2009). A stable baseline b-value, as observed for CC, provides a reference against which injection-induced perturbations can be assessed.

Although the Gutenberg-Richter parameters provide valuable information for the baseline characterization of regional seismicity, they represent only one component of a comprehensive seismic hazard assessment. Additional parameters describing earthquake occurrence, ground-motion severity (e.g., Peak Ground Acceleration PGA, Peak Ground Velocity PGV, and spectral response), together with local geological conditions and seismic-wave propagation effects, should also be considered when evaluating seismic hazard and risk. Consequently, these parameters should be interpreted within the tectonic framework of the study area and should not be directly extrapolated between different regions (Cabañas and Benito, 1999; Villalobos-Escobar et al., 2024).

For crustal events, the FC shows at least 90% probability that an event with magnitude ≤ 6.5 will occur annually, whereas corresponding magnitudes for BSN and CC are 4.5 and 4.7, respectively. Probabilities are nearly identical between BSN and CC for magnitudes below 3.9; however, for magnitudes ≥ 3.9, events become progressively more probable in CC, reaching a maximum contrast of approximately 18% at M 4.9 (Table 4 and Table 5). This suggests that the BSN could serve as a regional benchmark for baseline probability behavior, though a more robust comparison would require identifying a VMM zone not associated with prospective injection or hydrocarbon activities.

The estimated Dc of 1.45 for crustal events suggests a moderately clustered distribution consistent with fault-controlled seismicity. The intermediate value between 1.0 (linear distribution) and 2.0 (two-dimensional fault

Table 4. Gutenberg-Richter relationship parameters estimated for cortical seismic events in the three analyzed subcatalogs.

	FC crustal	BSN crustal	CC crustal
Mc mean	1,2	1,2	1
Mc std	6,66E-16	6,66E-16	0,00E+00
b mean	0,87829	0,75602	0,87054
b std	0,01178	0,03912	0,02908
a mean	5,93899	3,65526	4,43531
a std	0,03079	0,07907	0,05965

Table 5. Annual probability of occurrence of seismic events by magnitude range in the Bucaramanga Seismic Nest (BSN) and Campo Colorado (CC). The CC-BSN column represents the difference between these probabilitie.

Magnitude	BSN crustal probability	CC crustal probability	CC-BSN
0,1-3,7	100%	100%	0%
3,9	99%	100%	1%
4,1	97%	100%	3%
4,3	92%	99%	7%
4,5	83%	96%	13%
4,7	72%	89%	17%
4,9	59%	77%	18%
5,1	47%	63%	16%
5,3	36%	48%	13%
5,5	27%	36%	9%
5,7	20%	26%	6%
5,9	14%	18%	4%
6,1	10%	12%	2%
6,3	8%	9%	1%
6,5	5%	6%	0%
6,7	4%	4%	0%
6,9	3%	3%	0%
7,1	2%	2%	0%

plane) is coherent with the structural configuration: regional faults exhibit NE orientation, shallow events (<10 km) display more linear distributions (Dc ~ 1.20), while deeper events align with broader fault-plane geometries. Although the estimated fractal dimension is influenced by the selected depth interval and the spatial distribution of earthquakes, it provides complementary information on the geometric characteristics of seismicity. Therefore, the fractal dimension should not be interpreted as a uniquely robust, standalone structural parameter. Instead, it should be viewed as a general structural trend and an additional monitoring indicator to evaluate possible changes in the spatial organization and clustering of seismicity during future CO_2 injection operations.

The SHmax orientations for Campo Colorado (078°) and the VMM (084°) differ by only 6°, indicating consistent stress orientation near east-west. Considering an average SHmax of approximately 81°, fractures oriented between 51° and 111° are expected to be favorably oriented for dilation, potentially enhancing fluid flow (Barton et al., 1995; Ferrill et al., 1999; Mortimer et al., 2011). Sarmiento (2021) indicates that faulting in the Campo Colorado area may either facilitate or hinder groundwater flow and hydraulic interactions, and that the occurrence of interstratified saline waters within the Mugrosa, Colorado, and Esmeraldas formations is attributed to hydrocarbon migration from Cretaceous units, driven by pore pressure exceeding hydrostatic conditions.

The plan-view distribution of cortical events (Fig. 17) reveals concentration near faults to the east of the study area, with additional clusters along the periphery. A potential concentration of events is identified near the western block of the Mugrosa Fault, whereas the eastern block, where approximately 65 wells are located, does not exhibit representative seismicity. No seismic events were identified within the polygon directly associated with the

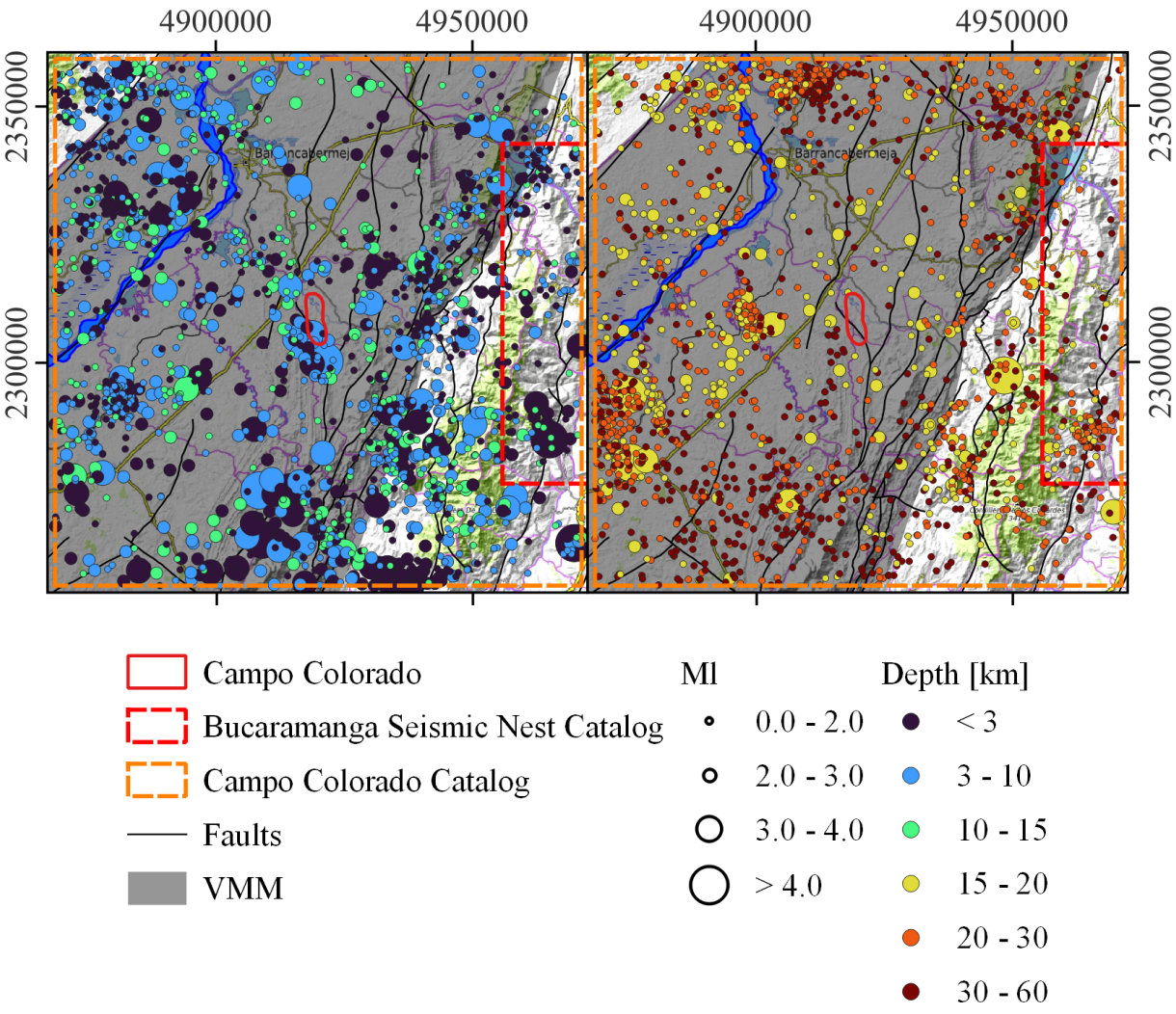


Figure 17. Spatial distribution of cortical seismic events associated with the CC within a 100 × 100 km polygon centered on the study area. Shallower events are displayed in cool colors, whereas deeper events are represented in warm colors.

immediate Campo Colorado field during the analyzed period, though seismicity is concentrated along peripheral fault systems (e.g., the eastern block of the Mugrosa Fault), which must be considered in future geomechanical modeling.

5.2 Recommendations and Future Work

To date, no CO_2 injection has been initiated at Campo Colorado. The field is a mature depleted conventional oil field that has been identified as a promising candidate for geological CO_2 storage. The principal storage targets correspond to the intraformational Mugrosa B and Mugrosa C sandstone units, which exhibit effective porosities of approximately 18-25% and permeabilities on the order of 100-200 mD. These reservoir units are overlain by the basal Colorado Formation, which constitutes the regional caprock, together with intraformational sealing intervals that compartmentalize the reservoir. Mugrosa B represents the shallowest proposed injection interval, whereas Mugrosa C reaches depths of approximately 5400 ft (~1646 m), where pressure and temperature conditions are suitable for supercritical CO_2 storage.

Current efforts focus on detailed geological characterization, caprock integrity assessment, and geomechanical modeling to evaluate reservoir behavior under future injection scenarios. The geomechanical modeling domain (Fig. 18) encompasses the candidate storage area together with the surrounding fault network, legacy wells, and four available 2D seismic lines, providing the structural framework required for upscaling petrophysical properties from well logs to the seismic scale and for subsequent coupled reservoir-geomechanical simulations. The baseline seismic characterization presented in this study provides a key input for these ongoing activities. Accordingly, the following recommendations are proposed to support the safe implementation of potential CO_2 storage operations and long-term seal integrity monitoring at Campo Colorado:

(I) Definition of a local area of interest, minimizing contamination from BSN seismicity and prioritizing crustal events (<60 km) as the primary domain of analysis. The 100 × 100 km polygon should be refined, differentiating subareas according to clustering patterns and structural domains.

(II) Deployment of a dedicated local seismic network for at least one year prior to injection onset, enabling refined baseline characterization and improved discrimination between natural and injection-induced seismicity. Local monitoring should capture low-magnitude seismicity associated with reservoir-scale processes.

(III) Sectorized pressure limits integrating in situ stress measurements with overpressure mapping, considering structural blocks and fault configurations individually. Parameters should include σ_3, fracture gradient, and caprock entry pressure, continuously updated using downhole data and surface deformation measurements.

(IV) Implementation of a multiparametric traffic light system based on seismic occurrence rate, b-value variations, migration patterns, structural alignments, and locally calibrated Ml thresholds, following frameworks such as (Kohli et al., 2023). Operational responses should include injection rate modulation, temporary pauses, or pressure relief measures. Post-injection monitoring must be explicitly incorporated, as significant events may occur after injection ceases.

(V) Monitoring network design integrating surface and downhole microseismic monitoring, pressure and temperature sensors, geochemical tracers, seismic imaging (3D/4D surveys, VSP), and geodetic observations (InSAR). Continuous estimation of seismicity parameters (e.g., a-value, b-value, Mc, and Dc), ground-motion parameters (e.g., PGA, PGV, and spectral response), and the spatial and temporal evolution of seismicity, including potential migration patterns, should support real-time operational decision-making.

(VI) Assessment and, if necessary, retrofitting of legacy wells with multiple barrier systems to ensure long-term CO_2 containment. Further investigation of the local aquifer system is required, as evidence suggests possible interactions between fresh and saline waters with implications for regional groundwater protection.

(VII) Variations in a-value, b-value, and Dc may constitute early indicators in the context of CO_2 injection, but this requires strengthening the local seismic network to enhance microseismic detection and establish a robust baseline prior to injection operations.

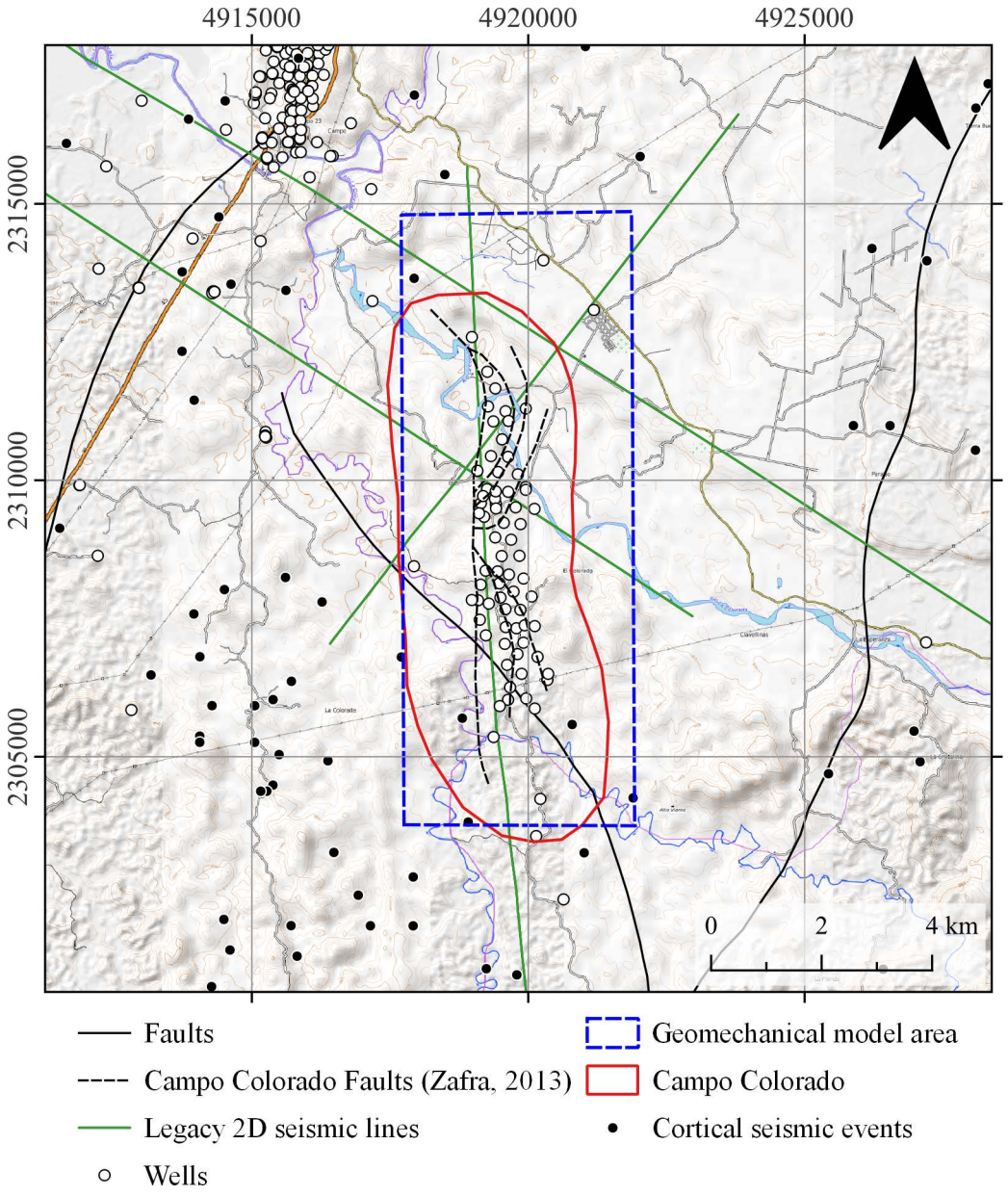


Figure 18. Location of the proposed CO_2 storage site at Campo Colorado showing the geomechanical modeling domain, existing wells, interpreted faults, legacy 2D seismic lines, and the distribution of crustal seismicity.

6. Conclusions

Site selection for CO_2 injection must consider reservoir porosity and permeability, pressure-temperature conditions, caprock entry pressure, the presence and orientation of faults and wells, and the regional hydrodynamic regime. Depleted hydrocarbon reservoirs offer advantages due to existing infrastructure, whereas saline aquifers provide the greatest volumetric potential; in both cases, storage security depends on rigorous site selection, careful operational management, and continuous monitoring.

For the Campo Colorado area, a clear differentiation is confirmed between shallow (crustal) seismicity and intermediate deep seismicity. Although the region is tectonically active, crustal seismic activity within the study area exhibits a higher frequency of events compared to the Bucaramanga Seismic Nest.

The completeness of the seismic catalog has improved, with Mc estimated at 1.0 for the Campo Colorado area. Crustal events exhibit a stable b-value with an average of aprox. 0.87 (std = 0.03), slightly higher than that estimated for the Bucaramanga Seismic Nest (aprox. 0.76 with std = 0.04).

A probability close to 100% was obtained for events with Ml 3.5, decreasing to approximately 48% for Ml 5.3. Within the magnitude range Ml 3.9-6.3, probabilities are higher in the Campo Colorado area than in the BSN, reinforcing the interpretation of relatively greater crustal tectonic activity.

The estimated fractal dimension (Dc = 1.45) suggests an intermediate spatial distribution between linear and two-dimensional geometries. For events shallower than 11 km, Dc values are below 1.25, increasing progressively with depth. No seismic events were identified within the polygon directly associated with the Campo Colorado field.

The orientation of SHmax is approximately 81°. Under this stress regime, fractures oriented between 51° and 111° are expected to be favorably oriented for dilation. The monitoring network design should integrate multiparametric seismic monitoring, downhole sensors, geochemical tracers, seismic imaging, and geodetic observations, coupled with a traffic light system linked to predefined operational actions and post-injection monitoring.

Acknowledgements. The authors acknowledge the financial support provided by the Colombian Ministry of Science, Technology and Innovation (MINCIENCIAS) through project No. 111979, Contract CT 044-2025: Evaluación y monitoreo del riesgo en el almacenamiento de CO_2 en Valle Medio del Magdalena, estudiando integridad de sello, geomecánica y sísmica, mediante simulación, laboratorio y aprendizaje de máquina.

Author contributions. Sergio García-Arias: Conceptualization, Investigation, Data curation, Formal analysis, Methodology, Visualization, Writing – original draft. Geraldine Ariza: Conceptualization, Investigation, Writing – original draft. Jose David Sanabria-Gómez: Conceptualization, Methodology, Supervision, Writing – original draft Validation. Diego Armando Vargas-Silva: Conceptualization, Methodology, Supervision, Validation.

Declaration of competing interest. The authors declare that they have no known competing financial interests or personal relationships that could have appeared to influence the work reported in this paper.

Declaration of generative AI use. During the preparation of this work, the authors used ChatGPT to assist with grammar revision. After using this tool, the authors carefully reviewed and edited the content as needed and take full responsibility for the content of the published article.

Data availability statement. The seismic event data downloaded from the Colombian Geological Survey (SGC) platform and the Notebooks used in this study are publicly available at the following repository: https://github.com/sergioGarcia91/SeismicUP.

Appendix A.

Two advanced searches were conducted in the SCOPUS database to perform the bibliographic review. The second query was refined by expanding and adjusting selected keywords to broaden the thematic coverage. After completing both searches, the resulting records were exported in CSV format and analyzed using VOSviewer in order to identify priority publications and thematic clusters relevant to this study.

- First Search Query:
  TITLE-ABS-KEY ((“seismicity” OR “earthquake*” OR “seismotectonic*” OR “earthquake catalog*” OR “microseismic catalog” OR “induced seismicity” OR “triggered seismicity” OR “injection-induced” OR “anthropogenic seismicity” OR “microseismic*” OR “fault reactivation” OR “fault stability” OR “probabilistic seismic hazard” OR “risk analysis” OR “risk management”) AND (“CO2” OR “CO2 injection” OR “geologic carbon storage” OR “geological carbon storage” OR “carbon capture and storage” OR “carbon dioxide” OR “CCS” OR “carbon storage” OR “carbon sequestration” OR “CO2-EOR” OR “enhanced oil recovery”)) AND PUBYEAR > 2009 AND PUBYEAR < 2027 AND (LIMIT-TO (SUBJAREA ; “EART”) OR LIMIT-TO (SUBJAREA ; “ENER”) OR LIMIT-TO (SUBJAREA ; “ENGI”) OR LIMIT-TO (SUBJAREA ; “ENVI”) OR LIMIT-TO (SUBJAREA ; “COMP”) OR LIMIT-TO (SUBJAREA ; “PHYS”) OR LIMIT-TO (SUBJAREA ; “DECI”)) AND (LIMIT-TO (EXACTKEYWORD ; “Carbon Dioxide”) OR LIMIT-TO (EXACTKEYWORD ; “Risk Assessment”) OR LIMIT-TO (EXACTKEYWORD ; “Risk Management”) OR LIMIT-TO (EXACTKEYWORD ; “Earthquakes”) OR LIMIT-TO (EXACTKEYWORD ; “Risk Analysis”) OR LIMIT-TO (EXACTKEYWORD ; “Seismology”) OR LIMIT-TO (EXACTKEYWORD ; “Induced Seismicity”) OR LIMIT-TO (EXACTKEYWORD ; “Seismicity”) OR LIMIT-TO (EXACTKEYWORD ; “Carbon Capture”) OR LIMIT-TO (EXACTKEYWORD ; “Faulting”) OR LIMIT-TO (EXACTKEYWORD ; “Risk Perception”) OR LIMIT-TO (EXACTKEYWORD ; “Fracture”) OR LIMIT-TO (EXACTKEYWORD ; “Monitoring”) OR LIMIT-TO (EXACTKEYWORD ; “Carbon Storage”) OR LIMIT-TO (EXACTKEYWORD ; “Injection (oil Wells)”) OR LIMIT-TO (EXACTKEYWORD ; “Earthquake”) OR LIMIT-TO (EXACTKEYWORD ; “Co2 Storage”) OR LIMIT-TO (EXACTKEYWORD ; “Decision Making”) OR LIMIT-TO (EXACTKEYWORD ; “Fault Zone”) OR LIMIT-TO (EXACTKEYWORD ; “Carbon Capture And Storage”) OR LIMIT-TO (EXACTKEYWORD ; “Seismic Response”) OR LIMIT-TO (EXACTKEYWORD ; “Fault”) OR LIMIT-TO (EXACTKEYWORD ; “Co 2 Injections”) OR LIMIT-TO (EXACTKEYWORD ; “Earthquake Swarm”) OR LIMIT-TO (EXACTKEYWORD ; “Tectonics”) OR LIMIT-TO (EXACTKEYWORD ; “Ccs”) OR LIMIT-TO (EXACTKEYWORD ; “Microseismic Events”) OR LIMIT-TO (EXACTKEYWORD ; “Risks Assessments”))

- Second Search Query. The second search expanded the keyword combinations to include additional monitoring, modeling, and reservoir-related terms:
  TITLE-ABS-KEY((“seismicity” OR “earthquake” OR “seismotectonic*” OR “earthquake catalog*” OR “microseismic catalog” OR “induced seismicity” OR “triggered seismicity” OR “injection-induced seismicity” OR “anthropogenic seismicity” OR “microseismic*” OR “fault reactivation” OR “fault stability” OR “probabilistic seismic hazard” OR “risk analysis” OR “risk management” OR “Seismic monitoring” OR “Passive seismics” OR “Injection induced seismicity” OR “Seismic magnitude prediction” OR “Fault reactivation” OR “Fault failure” OR “Seismic events” Or “Microseismicity” OR “Induced seismicity”) AND (“CO2” OR “CO2 injection” OR “geologic carbon storage” OR “geological carbon storage” OR “carbon capture and storage” OR “carbon dioxide” OR “CCS” OR “carbon storage” OR “carbon sequestration” OR “CO2-EOR” OR “enhanced oil recovery” OR “CO2--rock interactions” OR “Injection of CO2” OR “depleted reservoirs” OR “CO2 plume migration” OR “Carbon dioxide” OR “CO2 utilization” OR “CO2 capture” OR “CO2 storage” OR “CO2 sequestration” OR “CCUS” OR “Depleted natural gas reservoir” OR “Geological storage” OR “Geological carbon sequestration” OR “Geological carbon storage”)) AND (LIMIT-TO (SUBJAREA,”EART”) OR LIMIT-TO (SUBJAREA,”ENER”) OR LIMIT-TO (SUBJAREA,”ENGI”) OR LIMIT-TO (SUBJAREA,”ENVI”)) AND PUBYEAR > 2010 AND PUBYEAR < 2026

Appendix B.

This appendix presents selected results obtained during the exploratory data analysis of the complete seismic dataset. All analyses can be replicated using the Notebooks available in the public repository referenced in the Data Availability section. After merging the downloaded catalogs into a unified dataset, duplicate events were identified and removed. Subsequently, the exploratory data analysis was conducted to examine spatial distribution, depth patterns, magnitude characteristics, and location uncertainties.

Table B1. Berum ant optassi sapit, ape pligend issinissum quia sa il mil enditiust, es ad ut autassi omnistrum facescipsunt.

	SGC 1	SGC 2	TECTO	LBG
Minimum date	1993-06-01	2018-03-01	2014-02-15	1993-06-03
Maximum date	2018-02-28	2024-12-31	2024-02-12	2021-12-31
Total duration (days)	9038	2497	3649	10438
Total number of events	145061	134030	7668	16481
Total number of duplicate events	7059	0	0	0
Percentage of duplicate events	4.87%	0.0%	0.0%	0.0%
Minimum depth (km)	0.0	−4.97	−2.0	0.0
Maximum depth (km)	594.8	319.0	50.0	50.0
Reported magnitude types	‘Ml’ ‘Mw’	‘MLr_3’ ‘MLr_4’ ‘MLr_vmm’ ‘MLr_2’ ‘M_MLr’ ‘M’ ‘MLr_1’ ‘MLr_PtoGtn’ ‘MLr’ ‘Mw’ ‘Mw(mB)’ ‘mb’ ‘mB’ ‘MLr_5’ ‘MLv’ ‘Mwp’ ‘M_Pac’	‘MLr_vmm’ ‘MLr_4’	‘MLr_vmm’ ‘MLr_4’ ‘MLr_2’ ‘MLr_3’ ‘MLr’ ‘ML’ ‘Mw’ ‘M’ ‘M_MLr’
Minimum magnitude	0.1	0.0	0.0	0.0
Maximum magnitude	6.8	6.1	4.3	5.4

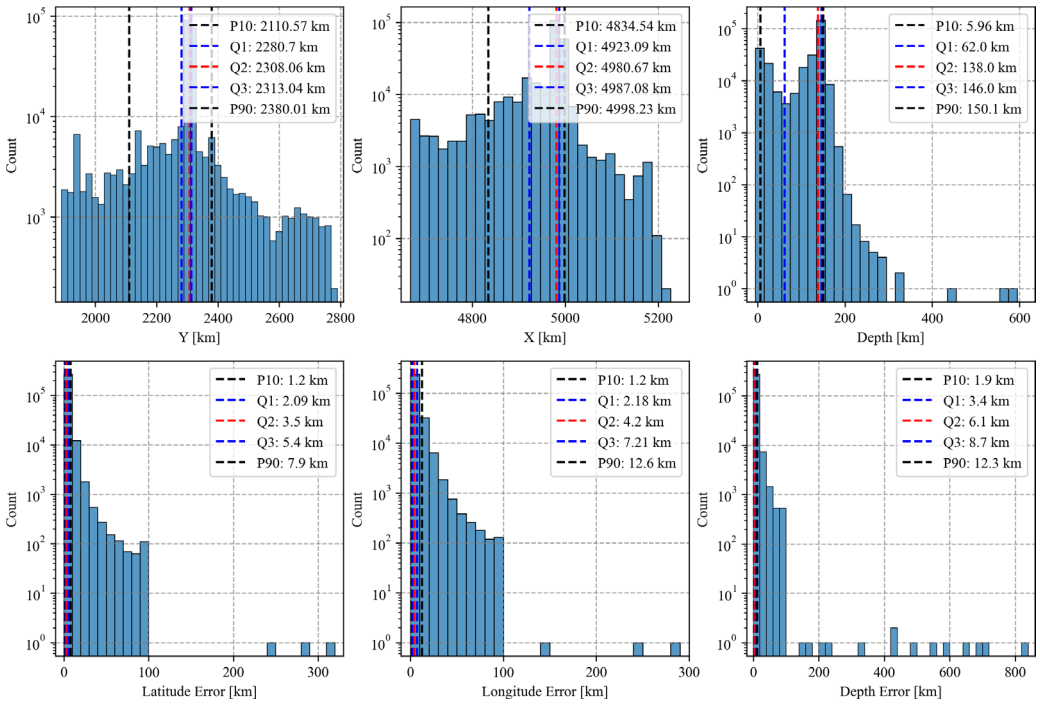


Figure B1. Histograms showing the distribution of event location coordinates and their corresponding location uncertainties.

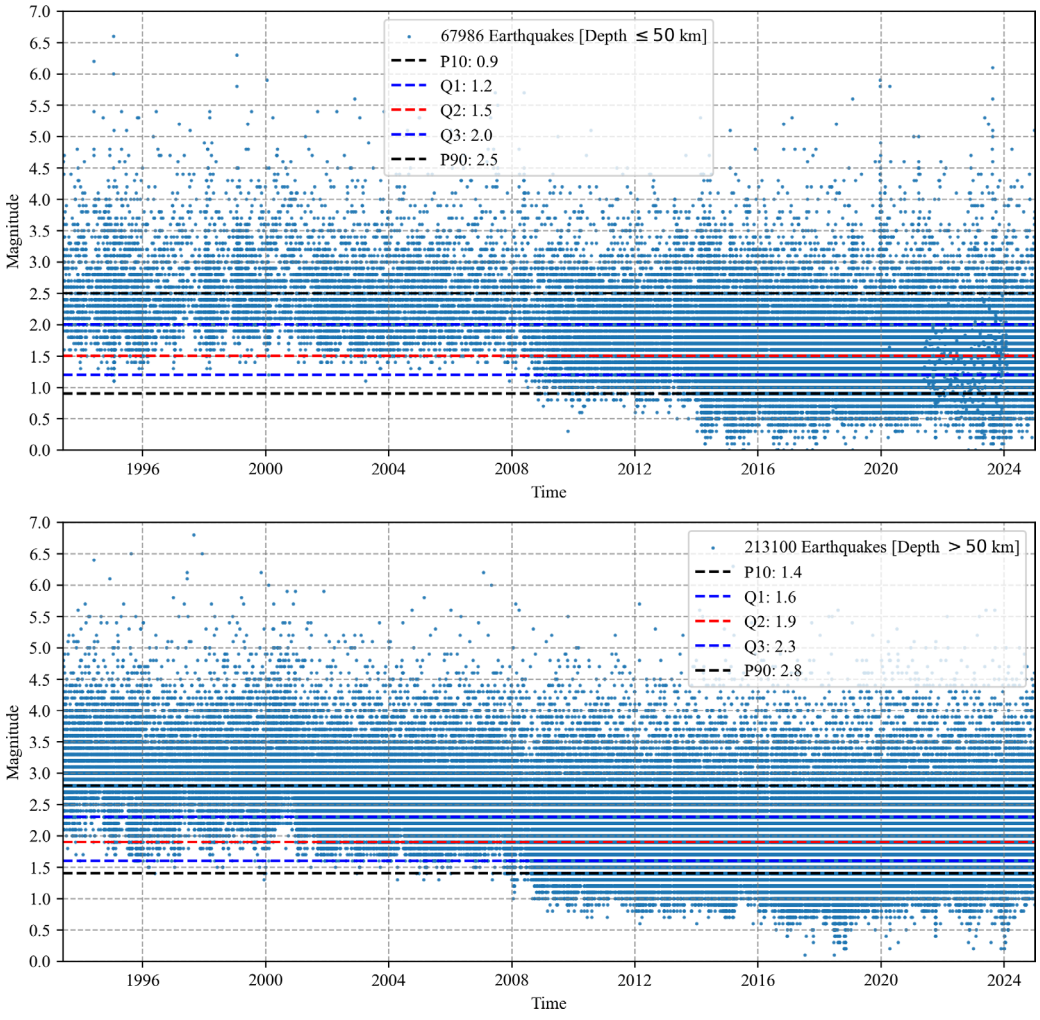


Figure B2. Time-magnitude plot of the unified catalog, differentiating events up to a depth of 50 km, considering that the TECTO and LBG catalogs only include events within this depth range.

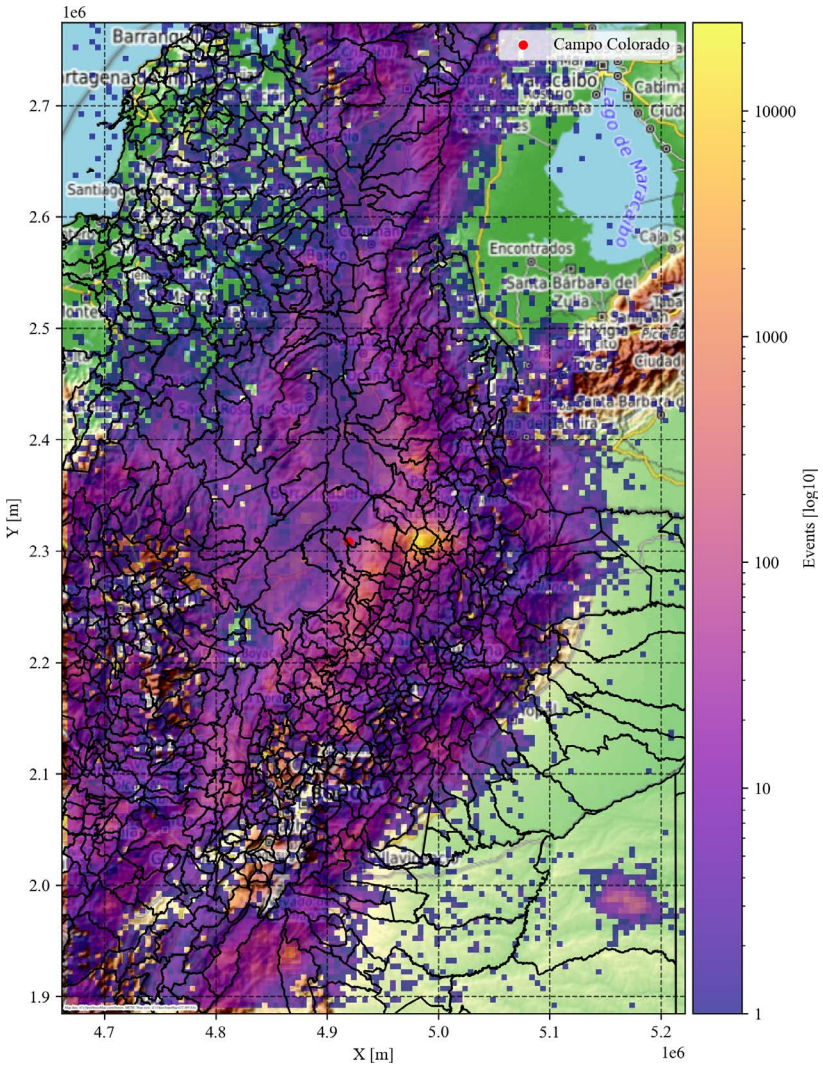


Figure B3. Heatmap showing the spatial distribution of events from the unified catalog. The red point marks the location of Campo Colorado. The highest event concentration coincides with the Bucaramanga Seismic Nest.

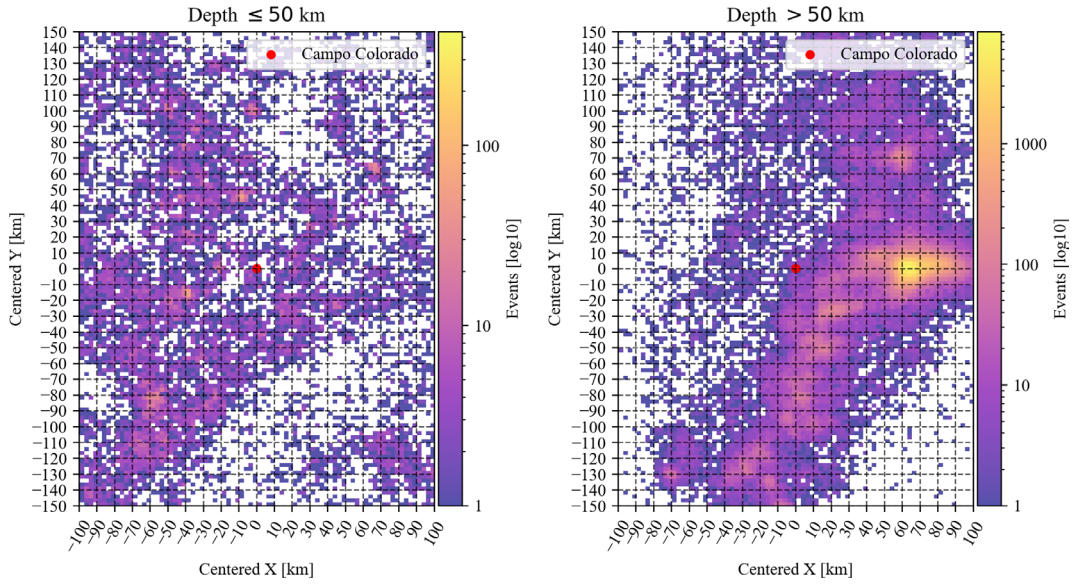


Figure B4. Zoomed view of the area of interest centered on the coordinates of Campo Colorado. Separate density maps are shown for cortical events (≤50 km) and deep events (>50 km).

Appendix C.

This appendix presents selected results from the exploratory data analysis performed on the three subcatalogs developed in this study: the Full Catalog (FC), the Bucaramanga Seismic Nest Catalog (BSN), and the Campo Colorado Catalog (CC). All results can be replicated using the Jupyter Notebooks available in the public repository referenced in the Data Availability section.

Table C1. Summary statistics of the Full Catalog (FC) subcatalog.

FC	X [m]	Y [m]	Depth [km]	Magnitude	Latitude Error [km]	Longitude Error [km]	Depth Error [km]	Distance [m]
count	281086.00	281086.00	281086.00	281086.00	280952.00	280952.00	280952.00	281086.00
mean	4947836.35	2284614.83	106.61	1.91	4.46	6.05	7.35	122479.14
min	4666612.52	1889660.69	−4.97	0.00	0.00	0.00	0.00	1091.10
25%	4923091.88	2280697.52	62.00	1.50	2.09	2.18	3.40	62947.77
50%	4980671.67	2308063.05	138.00	1.80	3.50	4.20	6.10	70454.22
75%	4987076.76	2313039.48	146.00	2.20	5.40	7.21	8.70	149181.45
max	5220800.48	2774223.43	594.80	6.80	313.47	283.69	832.90	516596.81
std	79483.07	133966.62	55.74	0.64	4.88	7.01	8.22	103224.07

Table C2. Summary statistics of the Bucaramanga Seismic Nest Catalog (BSN).

BSN	X [m]	Y [m]	Depth [km]	Magnitude	Latitude Error [km]	Longitude Error [km]	Depth Error [km]	Distance [m]
count	161158.00	161158.00	161158.00	161158.00	161082.00	161082.00	161082.00	161158.00
mean	4985506.79	2309107.12	143.15	2.05	4.63	6.78	7.01	66566.99
min	4955795.61	2276239.85	−4.88	0.10	0.00	0.00	0.00	36596.20
25%	4980781.29	2306190.25	139.96	1.60	2.60	3.04	4.10	61790.25
50%	4984205.77	2309277.97	144.50	1.90	4.00	5.10	6.41	65167.23
75%	4989396.25	2311940.30	148.47	2.30	5.80	8.50	8.80	70397.07
max	5022102.37	2342553.36	436.50	6.30	99.90	99.90	99.90	106621.98
std	8881.56	5928.84	12.31	0.61	3.28	6.05	4.96	8759.00

Table C3. Summary statistics of the Campo Colorado Catalog (CC).

CC	X [m]	Y [m]	Depth [km]	Magnitude	Latitude Error [km]	Longitude Error [km]	Depth Error [km]	Distance [m]
count	22052.00	22052.00	22052.00	22052.00	22050.00	22050.00	22050.00	22052.00
mean	4940085.94	2299776.78	99.88	1.69	3.73	4.97	6.68	40659.54
min	4868446.70	2256362.49	−2.00	0.00	0.00	0.00	0.00	1091.10
25%	4929473.56	2280390.12	98.80	1.30	1.41	1.41	2.40	33698.66
50%	4943755.71	2300571.52	113.30	1.60	2.76	2.83	4.90	42132.48
75%	4960591.90	2316475.44	123.70	2.00	4.70	5.40	8.20	49136.62
max	4971307.59	2359270.80	244.90	5.70	99.90	99.90	99.90	72000.42
std	25037.58	25351.30	41.47	0.56	4.24	7.02	7.34	11340.77

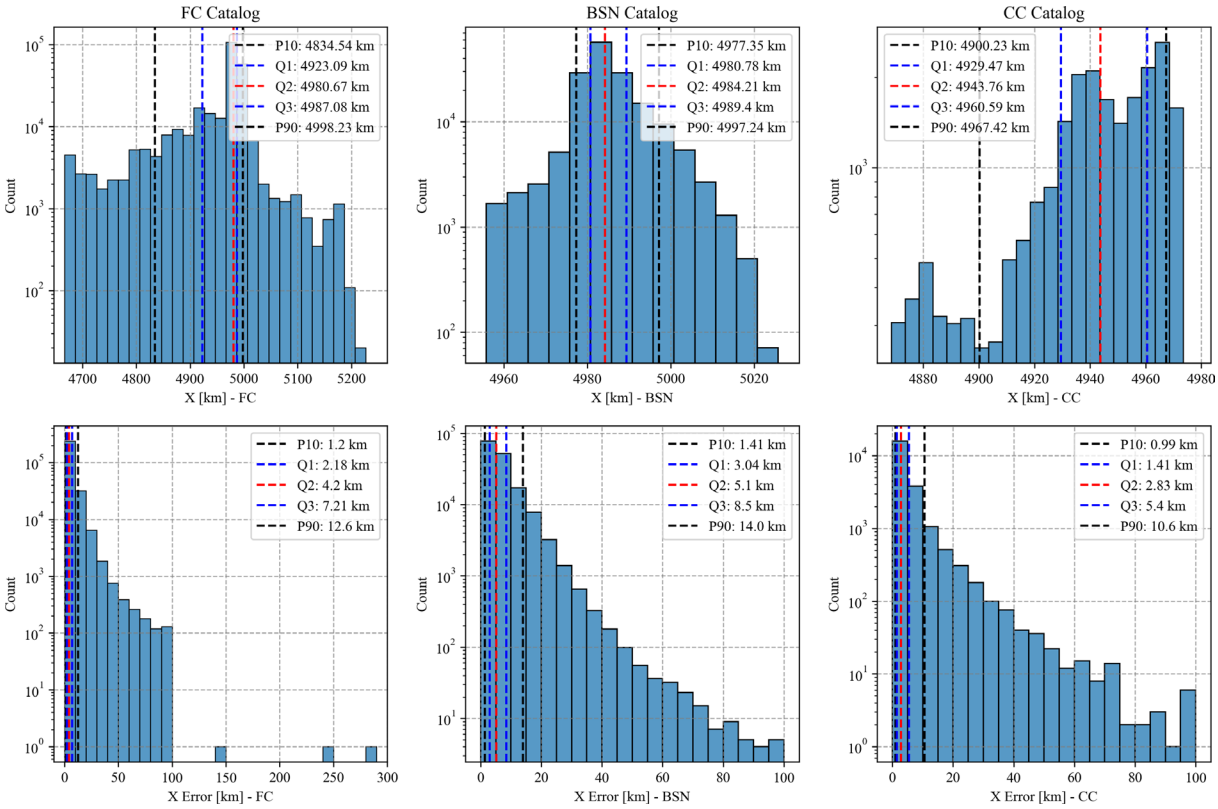


Figure C1. Histograms of the X-coordinate location and corresponding location uncertainties for seismic events in the three analyzed subcatalogs.

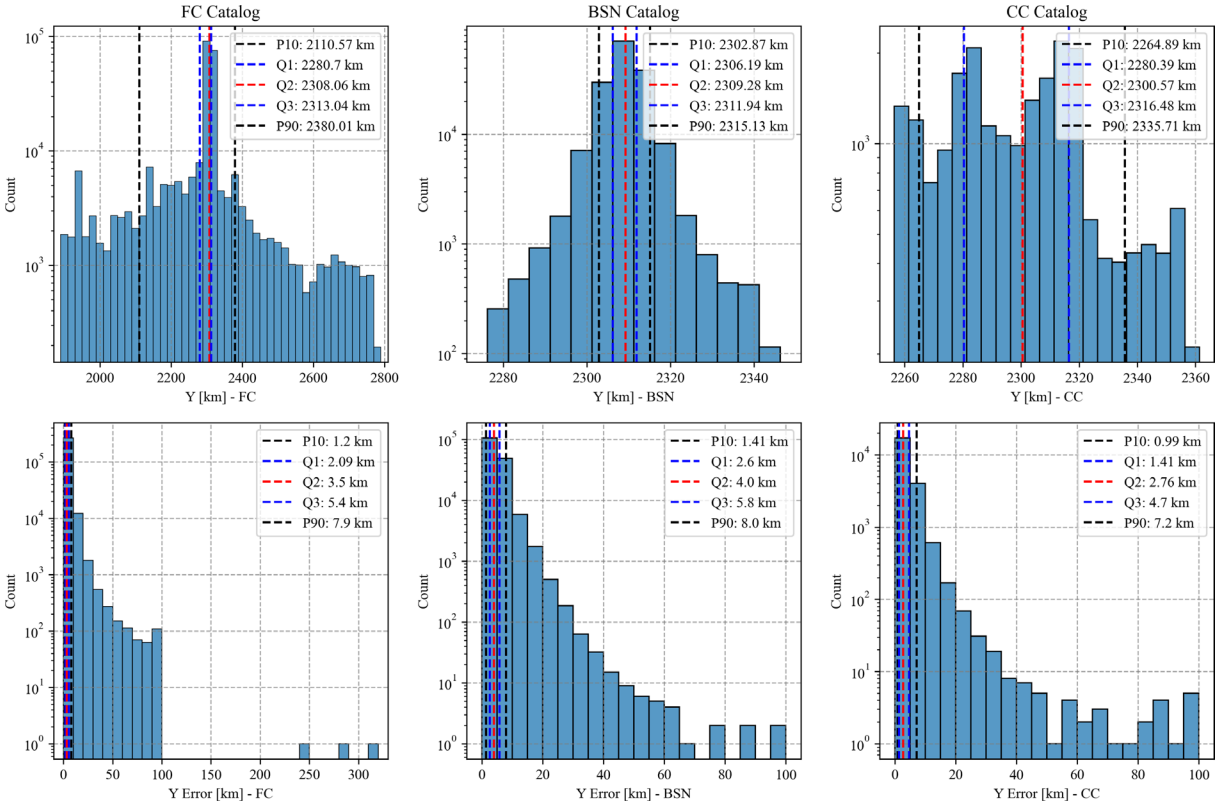


Figure C2. Histograms of the Y-coordinate location and corresponding location uncertainties for seismic events in the three analyzed subcatalogs.

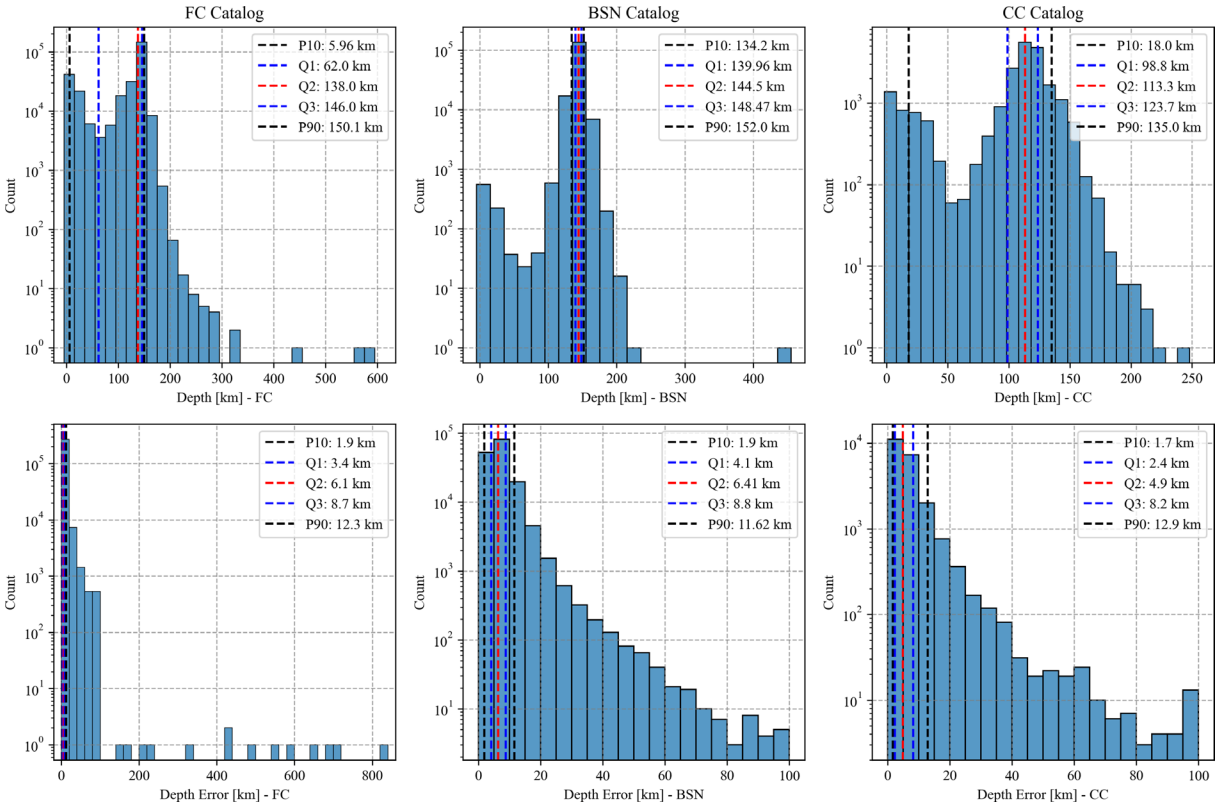


Figure C3. Histograms of the Depth location and corresponding location uncertainties for seismic events in the three analyzed subcatalogs.

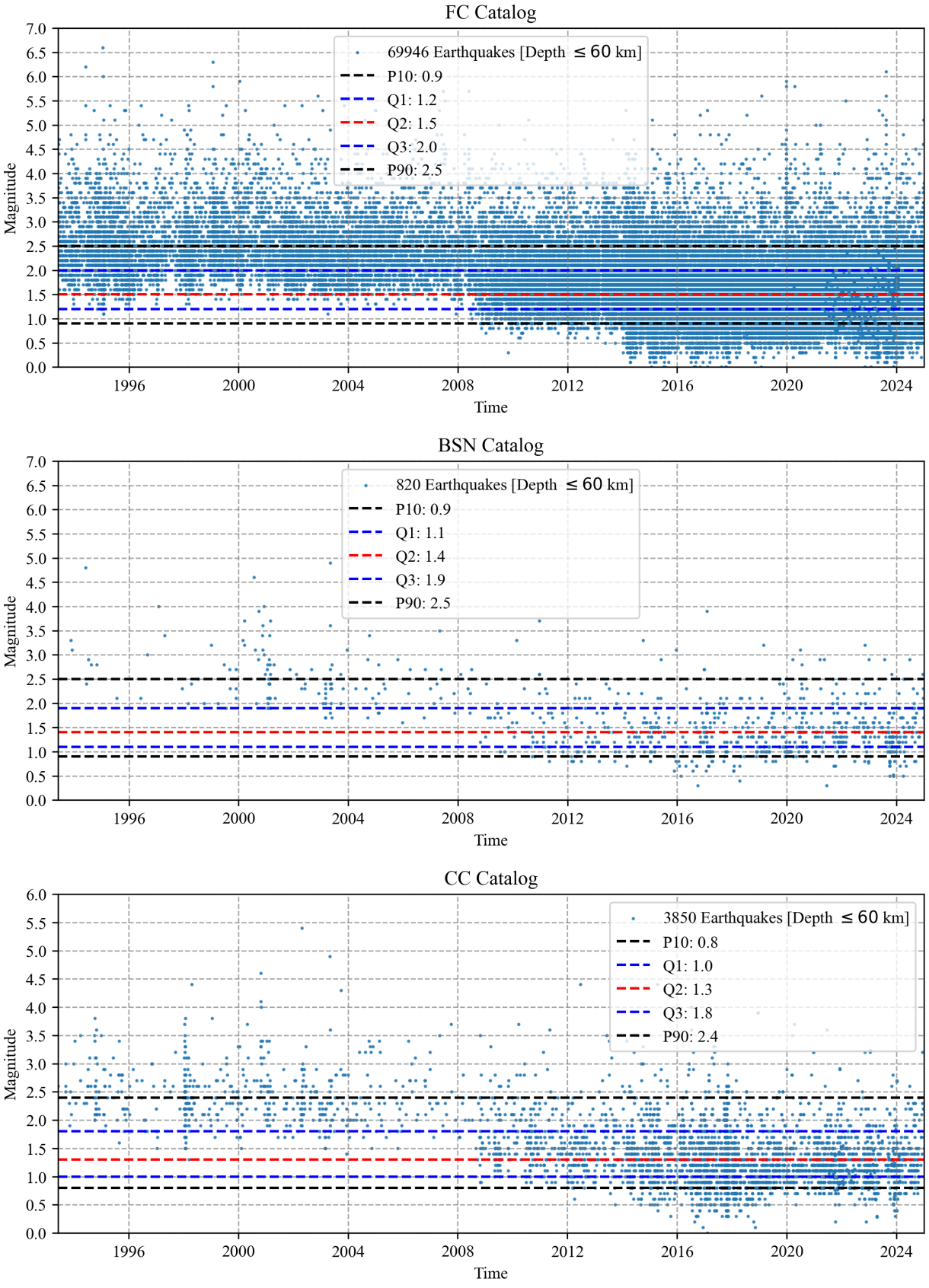


Figure C4. Time-magnitude plots of seismic events from the three subcatalogs, considering only cortical events (≤60 km).

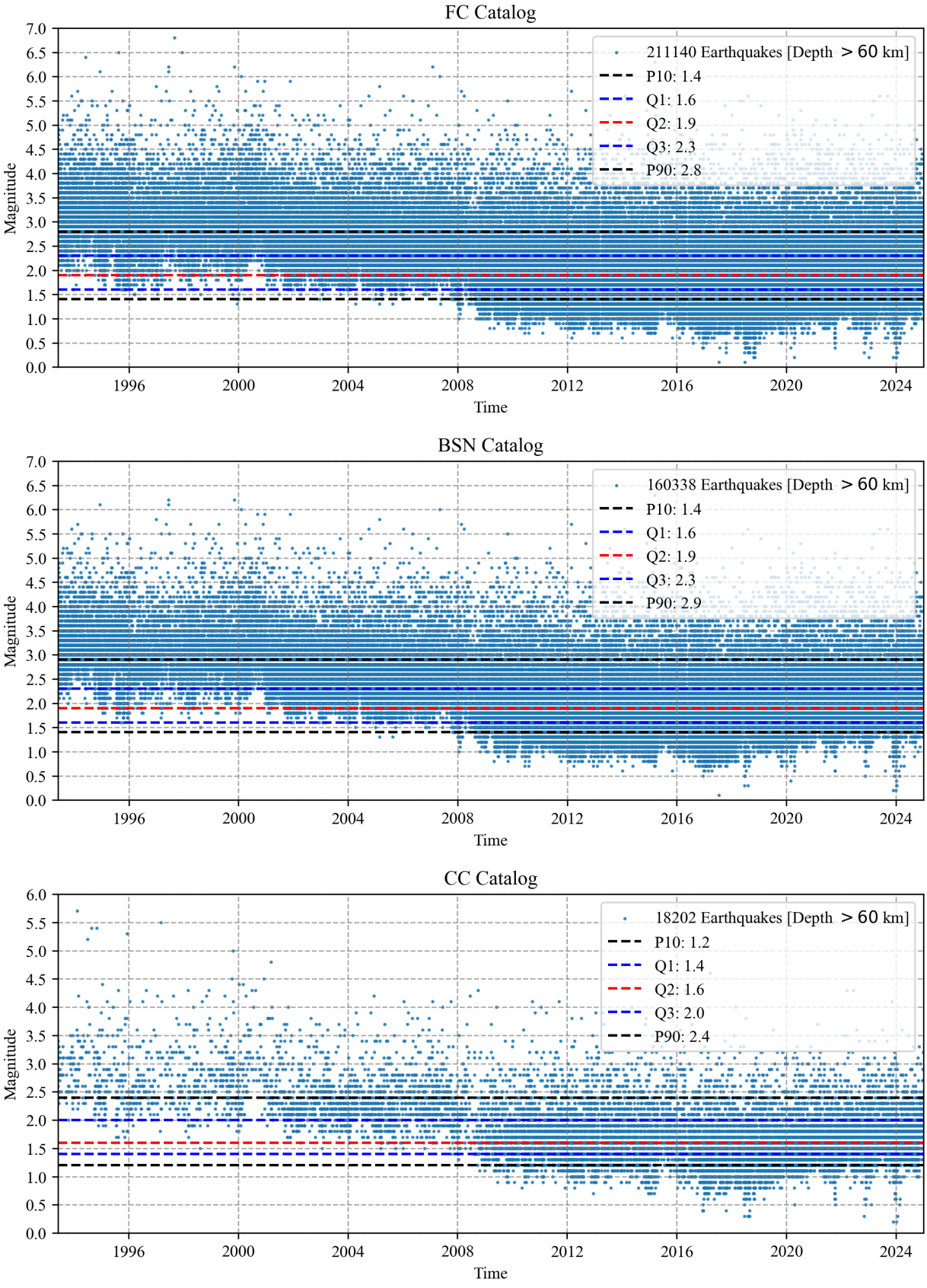


Figure C5. Time-magnitude distribution of deep seismic events (>60 km) for the three analyzed subcatalogs.

Appendix D.

This appendix presents the Gutenberg-Richter parameters estimated for the three subcatalogs analyzed in this study. The results can be replicated using the Notebooks available in the public repository referenced in the Data Availability section.

Table D1. Estimated Gutenberg-Richter parameters derived from the complete dataset of the three subcatalogs.

	FC	BSN	CC	FC crustal	BSN crustal	CC crustal	FC deep	BSN deep	CC deep
Mc mean	1,6	1,6	1,4	1,2	1,2	1	1,6	1,6	1,4
Mc std	2,22E-16	2,22E-16	4,44E-16	6,66E-16	6,66E-16	0,00E+00	2,22E-16	2,22E-16	4,44E-16
b mean	0,98466	0,99091	0,96042	0,87829	0,75602	0,87054	0,99551	0,98972	0,96402
b std	0,01156	0,01476	0,01955	0,01178	0,03912	0,02908	0,01202	0,01336	0,02396
a mean	7,05053	6,91241	5,53575	5,93899	3,65526	4,43531	6,99504	6,90775	5,47311
a std	0,03558	0,04366	0,0469	0,03079	0,07907	0,05965	0,03572	0,03965	0,05797

Table D2. Estimated Gutenberg-Richter parameters derived from the complete dataset of the three subcatalogs.

Years FC	Mc mean	Mc std	b mean	b std	a mean	a std
1993-1994	2,7	4,44E-16	0,96749	0,03624	6,10193	0,13025
1993-1995	2,7	4,44E-16	0,92400	0,03428	6,15287	0,12578
1993-1996	2,7	4,44E-16	0,95256	0,03390	6,34595	0,12490
1993-1997	2,7	4,44E-16	0,91228	0,02108	6,27274	0,07634
1993-1998	2,7	4,44E-16	0,93435	0,01972	6,43667	0,07201
1993-1999	2,7	4,44E-16	0,94023	0,01838	6,53471	0,06680
1993-2000	2,7	4,44E-16	0,95416	0,01706	6,67607	0,06305
1993-2001	2,7	4,44E-16	0,96529	0,01624	6,75407	0,05975
1993-2002	2,4	1,33E-15	0,95394	0,01597	6,70770	0,05594
1993-2003	2,4	1,33E-15	0,96364	0,01517	6,77171	0,05318
1993-2004	2,4	1,33E-15	0,97494	0,01539	6,84200	0,05403
1993-2005	2,2	4,44E-16	0,96483	0,01561	6,79962	0,05313
1993-2006	2,2	4,44E-16	0,97270	0,01422	6,85141	0,04827
1993-2007	2,2	4,44E-16	0,97200	0,01399	6,87160	0,04750
1993-2008	2,2	4,44E-16	0,97452	0,01430	6,89547	0,04895
1993-2009	2,2	4,44E-16	0,97881	0,01349	6,92573	0,04588
1993-2010	2,2	4,44E-16	0,98473	0,01432	6,95947	0,04880
1993-2011	2,1	8,88E-16	0,98024	0,01307	6,94240	0,04385
1993-2012	2,1	8,88E-16	0,98461	0,01337	6,96871	0,04476
1993-2013	2	0	0,98075	0,01284	6,95283	0,04218
1993-2014	1,9	6,66E-16	0,97344	0,01237	6,92563	0,03981
1993-2015	1,7	6,66E-16	0,95692	0,01165	6,85102	0,03633
1993-2016	1,6	2,22E-16	0,95115	0,01130	6,82771	0,03468

Years FC	Mc mean	Mc std	b mean	b std	a mean	a std
1993-2017	1,6	2,22E-16	0,95589	0,01215	6,85398	0,03721
1993-2018	1,6	2,22E-16	0,95937	0,01177	6,87890	0,03593
1993-2019	1,6	2,22E-16	0,96278	0,01116	6,90705	0,03408
1993-2020	1,6	2,22E-16	0,96674	0,01162	6,93560	0,03550
1993-2021	1,6	2,22E-16	0,97226	0,01163	6,96770	0,03544
1993-2022	1,6	2,22E-16	0,97652	0,01159	6,99389	0,03549
1993-2023	1,6	2,22E-16	0,97878	0,01103	7,01735	0,03405
1993-2024	1,6	2,22E-16	0,98448	0,01140	7,05013	0,03473

Table D3. Gutenberg-Richter relationship parameters estimated cumulatively over time for all events in the Bucaramanga Seismic Nest (BSN) subcatalog.

Years BSN	Mc mean	Mc std	b mean	b std	a mean	a std
1993-1994	2,9	1,33E-15	1,06317	0,02109	6,39476	0,07363
1993-1995	2,9	1,33E-15	1,11058	0,02213	6,77576	0,08218
1993-1996	2,9	1,33E-15	1,13654	0,02594	6,96000	0,09738
1993-1997	2,9	1,33E-15	1,06835	0,02504	6,77567	0,09205
1993-1998	2,9	1,33E-15	1,08183	0,02246	6,90941	0,08333
1993-1999	2,9	1,33E-15	1,06324	0,03044	6,90677	0,11535
1993-2000	2,9	1,33E-15	1,04854	0,02640	6,94092	0,10003
1993-2001	2,7	4,44E-16	1,02902	0,02389	6,87585	0,08741
1993-2002	2,7	4,44E-16	1,04113	0,02334	6,94984	0,08514
1993-2003	2,4	1,33E-15	1,01441	0,02002	6,83166	0,06939
1993-2004	2,4	1,33E-15	1,02595	0,02001	6,90321	0,06937
1993-2005	2,4	1,33E-15	1,03165	0,01995	6,94725	0,06934
1993-2006	2,4	1,33E-15	1,03794	0,02079	6,99278	0,07234
1993-2007	2,4	1,33E-15	1,03656	0,02000	7,00609	0,06966
1993-2008	2,4	1,33E-15	1,03767	0,01944	7,02317	0,06774
1993-2009	2,2	4,44E-16	1,01775	0,01789	6,93185	0,06023
1993-2010	2,2	4,44E-16	1,02156	0,01721	6,95818	0,05788
1993-2011	2,1	8,88E-16	1,01238	0,01624	6,92082	0,05342
1993-2012	2,1	8,88E-16	1,01499	0,01710	6,93999	0,05653
1993-2013	2,1	8,88E-16	1,01880	0,01682	6,96401	0,05546
1993-2014	2,1	8,88E-16	1,02124	0,01603	6,98181	0,05288
1993-2015	1,7	6,66E-16	0,96058	0,01451	6,71722	0,04377
1993-2016	1,6	2,22E-16	0,95204	0,01421	6,68274	0,04190
1993-2017	1,6	2,22E-16	0,95625	0,01414	6,70486	0,04178
1993-2018	1,6	2,22E-16	0,95929	0,01403	6,72787	0,04129
1993-2019	1,6	2,22E-16	0,96501	0,01393	6,75996	0,04115
1993-2020	1,6	2,22E-16	0,97026	0,01365	6,79232	0,04038

Years BSN	Mc mean	Mc std	b mean	b std	a mean	a std
1993-2021	1,6	2,22E-16	0,97616	0,01397	6,82454	0,04139
1993-2022	1,6	2,22E-16	0,98059	0,01374	6,85091	0,04061
1993-2023	1,6	2,22E-16	0,98336	0,01349	6,87401	0,03996
1993-2024	1,6	2,22E-16	0,99008	0,01350	6,91003	0,03989

Table D4. Gutenberg-Richter relationship parameters estimated cumulatively over time for all events in the Campo Colorado (CC) subcatalog.

Years CC	Mc mean	Mc std	b mean	b std	a mean	a std
1993-1994	2,5	0	0,62728	0,06664	3,45471	0,19603
1993-1995	2,3	4,44E-16	0,69224	0,03898	3,88434	0,10879
1993-1996	2,3	4,44E-16	0,73295	0,04000	4,09748	0,11403
1993-1997	2,4	1,33E-15	0,72471	0,03514	4,14895	0,10073
1993-1998	2,3	4,44E-16	0,76986	0,03341	4,40500	0,09661
1993-1999	2,3	4,44E-16	0,79536	0,03551	4,56690	0,10271
1993-2000	2,3	4,44E-16	0,82276	0,03172	4,74613	0,09250
1993-2001	2,3	4,44E-16	0,84137	0,02984	4,85293	0,08740
1993-2002	2,2	4,44E-16	0,83458	0,02722	4,86123	0,07767
1993-2003	2,1	8,88E-16	0,84027	0,02427	4,90970	0,06764
1993-2004	2,1	8,88E-16	0,85414	0,02520	4,97712	0,07076
1993-2005	2,1	8,88E-16	0,86581	0,02555	5,03301	0,07160
1993-2006	2,1	8,88E-16	0,87808	0,02580	5,09679	0,07230
1993-2007	2	0	0,88554	0,02502	5,13603	0,06834
1993-2008	2	0	0,89109	0,02367	5,16752	0,06495
1993-2009	2	0	0,89779	0,02432	5,19801	0,06628
1993-2010	2	0	0,90384	0,02610	5,23012	0,07184
1993-2011	2	0	0,90944	0,02404	5,26172	0,06624
1993-2012	2	0	0,91785	0,02544	5,30002	0,07025
1993-2013	1,6	2,22E-16	0,89911	0,02095	5,22622	0,05221
1993-2014	1,6	2,22E-16	0,90859	0,02187	5,26834	0,05472
1993-2015	1,6	2,22E-16	0,91327	0,02104	5,29798	0,05252
1993-2016	1,6	2,22E-16	0,91920	0,02076	5,32849	0,05220
1993-2017	1,4	4,44E-16	0,91113	0,02012	5,30160	0,04776
1993-2018	1,3	4,44E-16	0,90884	0,01946	5,29773	0,04495
1993-2019	1,3	4,44E-16	0,91750	0,01828	5,33370	0,04248
1993-2020	1,3	4,44E-16	0,92482	0,01986	5,36866	0,04611
1993-2021	1,3	4,44E-16	0,93350	0,01894	5,40733	0,04392
1993-2022	1,4	4,44E-16	0,94515	0,01944	5,46284	0,04607
1993-2023	1,4	4,44E-16	0,95155	0,01952	5,49590	0,04691
1993-2024	1,4	4,44E-16	0,95973	0,01979	5,53365	0,04723

Table D5. Gutenberg-Richter relationship parameters estimated cumulatively over time for cortical events (≤60 km) in the Full Catalog (FC) subcatalo.

Years FC crustal	Mc mean	Mc std	b mean	b std	a mean	a std
1993-1994	2	0	0,77608	0,04399	4,43494	0,13093
1993-1995	2,2	4,44E-16	0,73059	0,03793	4,57846	0,12000
1993-1996	2,2	4,44E-16	0,75425	0,03545	4,74819	0,11266
1993-1997	2,2	4,44E-16	0,77529	0,03572	4,88721	0,11366
1993-1998	2,3	4,44E-16	0,80326	0,03322	5,08475	0,10883
1993-1999	2,2	4,44E-16	0,79144	0,02512	5,13560	0,07967
1993-2000	2,2	4,44E-16	0,80146	0,02131	5,24215	0,06705
1993-2001	2,2	4,44E-16	0,81462	0,02081	5,32772	0,06549
1993-2002	2,2	4,44E-16	0,82420	0,02212	5,40162	0,06974
1993-2003	2,2	4,44E-16	0,83263	0,02184	5,46236	0,06907
1993-2004	2,2	4,44E-16	0,84205	0,02142	5,52519	0,06814
1993-2005	2,2	4,44E-16	0,85030	0,02128	5,57197	0,06753
1993-2006	2,2	4,44E-16	0,85896	0,02242	5,62543	0,07121
1993-2007	2,2	4,44E-16	0,85737	0,01952	5,64949	0,06226
1993-2008	2,2	4,44E-16	0,86019	0,01907	5,68200	0,06075
1993-2009	2,2	4,44E-16	0,86791	0,01870	5,72479	0,05991
1993-2010	2	0	0,86443	0,01757	5,71359	0,05378
1993-2011	2	0	0,87226	0,01801	5,75659	0,05512
1993-2012	2	0	0,87775	0,01721	5,78958	0,05285
1993-2013	2	0	0,88665	0,01917	5,83517	0,05879
1993-2014	2	0	0,89749	0,01771	5,90084	0,05443
1993-2015	2	0	0,90552	0,01848	5,94710	0,05713
1993-2016	1,8	4,44E-16	0,89801	0,01609	5,91788	0,04730
1993-2017	1,6	2,22E-16	0,88761	0,01430	5,87980	0,03982
1993-2018	1,5	0	0,88757	0,01480	5,88093	0,04056
1993-2019	1,3	4,44E-16	0,86914	0,01242	5,83151	0,03243
1993-2020	1,2	6,66E-16	0,86663	0,01192	5,83060	0,03049
1993-2021	1,2	6,66E-16	0,87267	0,01158	5,86818	0,02983
1993-2022	1,2	6,66E-16	0,87551	0,01180	5,89056	0,03034
1993-2023	1,2	6,66E-16	0,87296	0,01124	5,90707	0,02923
1993-2024	1,2	6,66E-16	0,87815	0,01174	5,93874	0,03066

Table D6. Gutenberg-Richter relationship parameters estimated cumulatively over time for cortical seismic events (≤60 km) in the Bucaramanga Seismic Nest (BSN) subcatalog.

Years BSN crustal	Mc mean	Mc std	b mean	b std	a mean	a std
1993-1994	2,7	4,44E-16	0,48025	0,40015	1,70249	1,17016
1993-1995	2,7	4,44E-16	0,45903	0,37905	1,65370	1,10453
1993-1996	2	0	0,44901	0,09527	1,78029	0,25057
1993-1997	2	0	0,47666	0,07924	1,99672	0,19574
1993-1998	1,9	6,66E-16	0,52010	0,07603	2,18499	0,18359
1993-1999	1,9	6,66E-16	0,58901	0,09608	2,43423	0,23515
1993-2000	1,9	6,66E-16	0,58453	0,04750	2,76654	0,11359
1993-2001	2	0	0,66704	0,05192	3,11110	0,13020
1993-2002	2	0	0,68368	0,05304	3,17688	0,13367
1993-2003	2	0	0,64578	0,05017	3,15913	0,12731
1993-2004	2	0	0,66307	0,05546	3,22271	0,14109
1993-2005	2,2	4,44E-16	0,67230	0,05688	3,26731	0,15330
1993-2006	2,2	4,44E-16	0,68363	0,06107	3,30784	0,16263
1993-2007	2,2	4,44E-16	0,69215	0,05818	3,35199	0,15466
1993-2008	2,2	4,44E-16	0,69853	0,06054	3,37733	0,16308
1993-2009	2,2	4,44E-16	0,70372	0,06711	3,39031	0,17908
1993-2010	2,2	4,44E-16	0,71558	0,06318	3,45491	0,16922
1993-2011	2,2	4,44E-16	0,71513	0,06072	3,45764	0,16078
1993-2012	2	0	0,71728	0,05713	3,45924	0,14673
1993-2013	2,2	4,44E-16	0,71826	0,06076	3,47044	0,16365
1993-2014	2,2	4,44E-16	0,73057	0,06503	3,51254	0,17477
1993-2015	1,3	4,44E-16	0,68351	0,04015	3,34210	0,08242
1993-2016	1,3	4,44E-16	0,69285	0,04156	3,37634	0,08635
1993-2017	0,9	2,22E-16	0,66447	0,03315	3,29305	0,05964
1993-2018	0,9	2,22E-16	0,67065	0,03332	3,31594	0,05948
1993-2019	0,9	2,22E-16	0,68165	0,03387	3,36298	0,06051
1993-2020	0,9	2,22E-16	0,69921	0,03356	3,42661	0,05995
1993-2021	0,9	2,22E-16	0,70864	0,03348	3,47139	0,06100
1993-2022	1,2	6,66E-16	0,73927	0,04003	3,58445	0,08099
1993-2023	1,2	6,66E-16	0,74447	0,03904	3,60970	0,07872
1993-2024	1,2	6,66E-16	0,75620	0,03865	3,65465	0,07876

Table D7. Gutenberg-Richter relationship parameters estimated cumulatively over time for cortical seismic events (≤60 km) in the Campo Colorado (CC) subcatalog.

Years CC crustal	Mc mean	Mc std	b mean	b std	a mean	a std
1993-1994	2,5	0	0,98246	0,08155	3,81315	0,21861
1993-1995	2,5	0	1,13766	0,07160	4,41338	0,19577
1993-1996	2,5	0	1,21385	0,07201	4,68391	0,19227
1993-1997	2,5	0	1,25077	0,07010	4,82038	0,19022
1993-1998	2,5	0	1,13947	0,05476	4,71318	0,16207
1993-1999	2,3	4,44E-16	1,12599	0,04078	4,70442	0,11365
1993-2000	2,5	0	1,05769	0,08952	4,67888	0,25793
1993-2001	2,5	0	1,07842	0,08937	4,76822	0,25770
1993-2002	2,5	0	0,84955	0,12177	4,07828	0,38540
1993-2003	2,1	8,88E-16	0,82029	0,06674	4,08191	0,18694
1993-2004	2,1	8,88E-16	0,83442	0,07140	4,14441	0,20077
1993-2005	2,1	8,88E-16	0,83776	0,07125	4,16580	0,19901
1993-2006	2,2	4,44E-16	0,84278	0,07194	4,19496	0,20910
1993-2007	2,2	4,44E-16	0,85253	0,07521	4,23576	0,21779
1993-2008	2,2	4,44E-16	0,85519	0,07358	4,25107	0,21277
1993-2009	2,2	4,44E-16	0,85930	0,07025	4,27215	0,20478
1993-2010	2	0	0,87039	0,06895	4,32138	0,18992
1993-2011	2	0	0,87522	0,06869	4,34622	0,18951
1993-2012	2	0	0,86757	0,05958	4,34083	0,16521
1993-2013	2	0	0,87353	0,05985	4,37037	0,16521
1993-2014	1,4	4,44E-16	0,84170	0,04078	4,24519	0,09423
1993-2015	1,4	4,44E-16	0,84254	0,03609	4,26984	0,08413
1993-2016	1,4	4,44E-16	0,84770	0,03399	4,30843	0,07861
1993-2017	1,4	4,44E-16	0,86372	0,03475	4,38487	0,08075
1993-2018	1,1	2,22E-16	0,84391	0,02903	4,31527	0,06078
1993-2019	1,1	2,22E-16	0,84943	0,02848	4,33811	0,05971
1993-2020	1,1	2,22E-16	0,85525	0,02905	4,36729	0,06105
1993-2021	1	0	0,85395	0,02666	4,36916	0,05451
1993-2022	1	0	0,85937	0,02715	4,39016	0,05464
1993-2023	1	0	0,86486	0,02832	4,41303	0,05820
1993-2024	1	0	0,87088	0,02920	4,43610	0,06023

Table D8. Gutenberg-Richter relationship parameters estimated cumulatively over time for deep seismic events (>60 km) in the Full Catalog (FC) subcatalog.

Years FC deep	Mc mean	Mc std	b mean	b std	a mean	a std
1993-1994	2,9	1,33E-15	1,00561	0,03486	6,20684	0,12921
1993-1995	2,9	1,33E-15	1,00013	0,04216	6,38770	0,16029
1993-1996	2,9	1,33E-15	1,03056	0,04120	6,59132	0,15639
1993-1997	2,9	1,33E-15	0,93508	0,02721	6,29982	0,10239
1993-1998	2,9	1,33E-15	0,96062	0,02868	6,47751	0,10814
1993-1999	2,7	4,44E-16	0,95983	0,02267	6,53182	0,08254
1993-2000	2,8	8,88E-16	0,97912	0,02151	6,70528	0,08025
1993-2001	2,7	4,44E-16	0,98155	0,01966	6,74248	0,07218
1993-2002	2,4	1,33E-15	0,97051	0,01818	6,69244	0,06327
1993-2003	2,4	1,33E-15	0,98020	0,01755	6,75691	0,06081
1993-2004	2,4	1,33E-15	0,99180	0,01772	6,82820	0,06167
1993-2005	2,4	1,33E-15	0,99886	0,01731	6,87688	0,06009
1993-2006	2,2	4,44E-16	0,98699	0,01644	6,82826	0,05503
1993-2007	2,2	4,44E-16	0,98575	0,01545	6,84472	0,05204
1993-2008	2,2	4,44E-16	0,98816	0,01484	6,86715	0,04992
1993-2009	2,2	4,44E-16	0,99278	0,01561	6,89832	0,05256
1993-2010	2,1	8,88E-16	0,98891	0,01517	6,88342	0,04987
1993-2011	2,1	8,88E-16	0,99307	0,01421	6,90939	0,04702
1993-2012	2,1	8,88E-16	0,99671	0,01448	6,93328	0,04751
1993-2013	2,1	8,88E-16	0,99993	0,01407	6,95544	0,04645
1993-2014	2,1	8,88E-16	1,00421	0,01476	6,98036	0,04880
1993-2015	1,7	6,66E-16	0,96344	0,01259	6,78939	0,03827
1993-2016	1,6	2,22E-16	0,95732	0,01157	6,76349	0,03450
1993-2017	1,6	2,22E-16	0,96099	0,01175	6,78541	0,03507
1993-2018	1,6	2,22E-16	0,96480	0,01232	6,81118	0,03688
1993-2019	1,6	2,22E-16	0,96973	0,01193	6,84112	0,03570
1993-2020	1,6	2,22E-16	0,97530	0,01177	6,87490	0,03516
1993-2021	1,6	2,22E-16	0,98118	0,01221	6,90744	0,03640
1993-2022	1,6	2,22E-16	0,98592	0,01157	6,93540	0,03447
1993-2023	1,6	2,22E-16	0,98963	0,01177	6,96168	0,03529
1993-2024	1,6	2,22E-16	0,99549	0,01130	6,99503	0,03378

Table D9. Gutenberg-Richter relationship parameters estimated cumulatively over time for deep seismic events (>60 km) in the Bucaramanga Seismic Nest (BSN) subcatalog.

Years BSN deep	Mc mean	Mc std	b mean	b std	a mean	a std
1993-1994	2,9	1,33E-15	1,06424	0,02164	6,39642	0,07516
1993-1995	2,9	1,33E-15	1,11102	0,02263	6,77595	0,08386
1993-1996	2,9	1,33E-15	1,13528	0,02612	6,95437	0,09832
1993-1997	2,9	1,33E-15	1,06860	0,02464	6,77490	0,09049
1993-1998	2,9	1,33E-15	1,08153	0,02282	6,90676	0,08428
1993-1999	2,9	1,33E-15	1,06563	0,03217	6,91497	0,12173
1993-2000	2,9	1,33E-15	1,04718	0,02603	6,93419	0,09866
1993-2001	2,7	4,44E-16	1,02983	0,02346	6,87733	0,08597
1993-2002	2,7	4,44E-16	1,04058	0,02311	6,94659	0,08447
1993-2003	2,4	1,33E-15	1,01570	0,02107	6,83448	0,07295
1993-2004	2,4	1,33E-15	1,02536	0,01971	6,89939	0,06853
1993-2005	2,4	1,33E-15	1,03175	0,01974	6,94599	0,06858
1993-2006	2,4	1,33E-15	1,03614	0,01926	6,98496	0,06696
1993-2007	2,4	1,33E-15	1,03477	0,01895	6,99860	0,06597
1993-2008	2,4	1,33E-15	1,03815	0,01906	7,02318	0,06634
1993-2009	2,2	4,44E-16	1,01603	0,01776	6,92459	0,05932
1993-2010	2,2	4,44E-16	1,02159	0,01768	6,95700	0,05921
1993-2011	2,1	8,88E-16	1,01340	0,01706	6,92282	0,05605
1993-2012	2,1	8,88E-16	1,01430	0,01667	6,93644	0,05491
1993-2013	2,1	8,88E-16	1,01820	0,01691	6,96066	0,05573
1993-2014	2,1	8,88E-16	1,02083	0,01666	6,97931	0,05486
1993-2015	1,7	6,66E-16	0,96005	0,01446	6,71426	0,04362
1993-2016	1,6	2,22E-16	0,95199	0,01385	6,68140	0,04076
1993-2017	1,6	2,22E-16	0,95619	0,01412	6,70338	0,04151
1993-2018	1,6	2,22E-16	0,95931	0,01365	6,72669	0,04025
1993-2019	1,6	2,22E-16	0,96475	0,01340	6,75782	0,03943
1993-2020	1,6	2,22E-16	0,96991	0,01391	6,78998	0,04110
1993-2021	1,6	2,22E-16	0,97529	0,01381	6,82083	0,04086
1993-2022	1,6	2,22E-16	0,98011	0,01373	6,84816	0,04067
1993-2023	1,6	2,22E-16	0,98354	0,01412	6,87338	0,04173
1993-2024	1,6	2,22E-16	0,99010	0,01425	6,90891	0,04207

Table D10. Gutenberg-Richter relationship parameters estimated cumulatively over time for deep seismic events (>60 km) in the Campo Colorado (CC) subcatalog.

Years CC deep	Mc mean	Mc std	b mean	b std	a mean	a std
1993-1994	2,4	1,33E-15	0,59970	0,05743	3,31734	0,16085
1993-1995	2,3	4,44E-16	0,66036	0,04041	3,72863	0,11301
1993-1996	2,4	1,33E-15	0,70302	0,04222	3,95073	0,12350
1993-1997	2,4	1,33E-15	0,70028	0,03636	4,02808	0,10427
1993-1998	2,4	1,33E-15	0,74037	0,04124	4,24770	0,12098
1993-1999	2,4	1,33E-15	0,76489	0,03335	4,41385	0,09798
1993-2000	2,4	1,33E-15	0,79416	0,03290	4,58963	0,09966
1993-2001	2,4	1,33E-15	0,81449	0,03391	4,70675	0,10128
1993-2002	2,2	4,44E-16	0,82267	0,03187	4,74632	0,09061
1993-2003	2,2	4,44E-16	0,83769	0,03204	4,81904	0,09201
1993-2004	2,1	8,88E-16	0,84636	0,02835	4,86857	0,07978
1993-2005	2,1	8,88E-16	0,86071	0,03203	4,93462	0,09037
1993-2006	2,1	8,88E-16	0,87410	0,02957	5,00279	0,08375
1993-2007	2	0	0,88210	0,03008	5,04784	0,08315
1993-2008	2	0	0,88802	0,02802	5,08055	0,07761
1993-2009	2	0	0,89385	0,03000	5,10907	0,08292
1993-2010	2	0	0,90063	0,02949	5,14379	0,08171
1993-2011	2	0	0,90810	0,02926	5,18180	0,08126
1993-2012	2	0	0,91433	0,02869	5,21338	0,07977
1993-2013	1,6	2,22E-16	0,89991	0,02601	5,15446	0,06515
1993-2014	1,6	2,22E-16	0,90752	0,02505	5,19123	0,06302
1993-2015	1,6	2,22E-16	0,91459	0,02578	5,22658	0,06502
1993-2016	1,6	2,22E-16	0,92013	0,02647	5,25434	0,06656
1993-2017	1,5	0	0,91943	0,02566	5,25741	0,06328
1993-2018	1,5	0	0,92419	0,02381	5,28319	0,05875
1993-2019	1,3	4,44E-16	0,91868	0,02285	5,26007	0,05360
1993-2020	1,3	4,44E-16	0,92669	0,02384	5,29670	0,05563
1993-2021	1,3	4,44E-16	0,93396	0,02251	5,33283	0,05262
1993-2022	1,4	4,44E-16	0,94643	0,02487	5,39210	0,05977
1993-2023	1,4	4,44E-16	0,95505	0,02315	5,43186	0,05571
1993-2024	1,4	4,44E-16	0,96329	0,02427	5,47159	0,05846

Appendix E.

This appendix presents the return period and occurrence probability estimates calculated for the three subcatalogs analyzed in this study. All results can be reproduced using the Notebooks available in the public repository referenced in the Data Availability section.

Table E1. Return periods (in years) and probability of occurrence of an event with local magnitude Ml for time horizons of 1, 10, 50, and 100 years, considering all events from the Full Catalog (FC) subcatalog. Note: Probabilities are expressed as values between 0 and 1.

Magnitude	Return period FC	1-year probability	10-year probability	50-year probability	100-year probability
0,1	0,00000353	1,0	1,0	1,0	1,0
0,3	0,00000555	1,0	1,0	1,0	1,0
0,5	0,00000874	1,0	1,0	1,0	1,0
0,7	0,00001375	1,0	1,0	1,0	1,0
0,9	0,00002164	1,0	1,0	1,0	1,0
1,1	0,00003405	1,0	1,0	1,0	1,0
1,3	0,00005358	1,0	1,0	1,0	1,0
1,5	0,00008433	1,0	1,0	1,0	1,0
1,7	0,00013271	1,0	1,0	1,0	1,0
1,9	0,00020884	1,0	1,0	1,0	1,0
2,1	0,00032866	1,0	1,0	1,0	1,0
2,3	0,00051723	1,0	1,0	1,0	1,0
2,5	0,00081398	1,0	1,0	1,0	1,0
2,7	0,00128099	1,0	1,0	1,0	1,0
2,9	0,00201594	1,0	1,0	1,0	1,0
3,1	0,00317256	1,0	1,0	1,0	1,0
3,3	0,00499277	1,0	1,0	1,0	1,0
3,5	0,00785729	1,0	1,0	1,0	1,0
3,7	0,01236530	1,0	1,0	1,0	1,0
3,9	0,01945970	1,0	1,0	1,0	1,0
4,1	0,03062440	1,0	1,0	1,0	1,0
4,3	0,04819468	1,0	1,0	1,0	1,0
4,5	0,07584565	1,0	1,0	1,0	1,0
4,7	0,11936093	1,0	1,0	1,0	1,0
4,9	0,18784244	1,0	1,0	1,0	1,0
5,1	0,29561417	1,0	1,0	1,0	1,0
5,3	0,46521829	1,0	1,0	1,0	1,0
5,5	0,73213018	1,0	1,0	1,0	1,0
5,7	1,15217869	1,0	1,0	1,0	1,0
5,9	1,81322363	0,99999997	1,0	1,0	1,0
6,1	2,85353299	0,99998442	1,0	1,0	1,0
6,3	4,49070397	0,99911836	1,0	1,0	1,0
6,5	7,06717680	0,98854635	1,0	1,0	1,0
6,7	11,12186156	0,94157582	1,0	1,0	1,0
6,9	17,50285980	0,83546640	0,99999999	1,0	1,0
7,1	27,54485832	0,68232445	0,99998953	1,0	1,0

Table E2. Return periods (in years) and probability of occurrence of an event with local magnitude Ml for time horizons of 1, 10, 50, and 100 years, considering all events from the Bucaramanga Seismic Nest (BSN) subcatalog. Note: Probabilities are expressed as values between 0 and 1.

Magnitude	Return period BSN	1-year probability	10-year probability	50-year probability	100-year probability
0,1	0,00000485	1,0	1,0	1,0	1,0
0,3	0,00000766	1,0	1,0	1,0	1,0
0,5	0,00001209	1,0	1,0	1,0	1,0
0,7	0,00001909	1,0	1,0	1,0	1,0
0,9	0,00003012	1,0	1,0	1,0	1,0
1,1	0,00004754	1,0	1,0	1,0	1,0
1,3	0,00007504	1,0	1,0	1,0	1,0
1,5	0,00011843	1,0	1,0	1,0	1,0
1,7	0,00018691	1,0	1,0	1,0	1,0
1,9	0,00029500	1,0	1,0	1,0	1,0
2,1	0,00046559	1,0	1,0	1,0	1,0
2,3	0,00073482	1,0	1,0	1,0	1,0
2,5	0,00115975	1,0	1,0	1,0	1,0
2,7	0,00183040	1,0	1,0	1,0	1,0
2,9	0,00288888	1,0	1,0	1,0	1,0
3,1	0,00455944	1,0	1,0	1,0	1,0
3,3	0,00719604	1,0	1,0	1,0	1,0
3,5	0,01135733	1,0	1,0	1,0	1,0
3,7	0,01792497	1,0	1,0	1,0	1,0
3,9	0,02829050	1,0	1,0	1,0	1,0
4,1	0,04465014	1,0	1,0	1,0	1,0
4,3	0,07047014	1,0	1,0	1,0	1,0
4,5	0,11122115	1,0	1,0	1,0	1,0
4,7	0,17553740	1,0	1,0	1,0	1,0
4,9	0,27704602	1,0	1,0	1,0	1,0
5,1	0,43725440	1,0	1,0	1,0	1,0
5,3	0,69010703	1,0	1,0	1,0	1,0
5,5	1,08917763	1,0	1,0	1,0	1,0
5,7	1,71902019	0,99999999	1,0	1,0	1,0
5,9	2,71308402	0,99999121	1,0	1,0	1,0
6,1	4,28198860	0,99937425	1,0	1,0	1,0
6,3	6,75814914	0,99066342	1,0	1,0	1,0
6,5	10,66620768	0,94825083	1,0	1,0	1,0
6,7	16,83419292	0,84684741	0,99999999	1,0	1,0
6,9	26,56896055	0,69542676	0,99999313	1,0	1,0
7,1	41,93308633	0,52916889	0,99946463	1,0	1,0

Table E3. Return periods (in years) and probability of occurrence of an event with local magnitude Ml for time horizons of 1, 10, 50, and 100 years, considering all events from the Campo Colorado (CC) subcatalog. Note: Probabilities are expressed as values between 0 and 1.

Magnitude	Return period CC	1-year probability	10-year probability	50-year probability	100-year probability
0,1	0,00011469	1,0	1,0	1,0	1,0
0,3	0,00017849	1,0	1,0	1,0	1,0
0,5	0,00027778	1,0	1,0	1,0	1,0
0,7	0,00043230	1,0	1,0	1,0	1,0
0,9	0,00067277	1,0	1,0	1,0	1,0
1,1	0,00104701	1,0	1,0	1,0	1,0
1,3	0,00162943	1,0	1,0	1,0	1,0
1,5	0,00253583	1,0	1,0	1,0	1,0
1,7	0,00394643	1,0	1,0	1,0	1,0
1,9	0,00614170	1,0	1,0	1,0	1,0
2,1	0,00955813	1,0	1,0	1,0	1,0
2,3	0,01487500	1,0	1,0	1,0	1,0
2,5	0,02314948	1,0	1,0	1,0	1,0
2,7	0,03602677	1,0	1,0	1,0	1,0
2,9	0,05606729	1,0	1,0	1,0	1,0
3,1	0,08725568	1,0	1,0	1,0	1,0
3,3	0,13579315	1,0	1,0	1,0	1,0
3,5	0,21133041	1,0	1,0	1,0	1,0
3,7	0,32888658	1,0	1,0	1,0	1,0
3,9	0,51183539	1,0	1,0	1,0	1,0
4,1	0,79655262	1,0	1,0	1,0	1,0
4,3	1,23964868	1,0	1,0	1,0	1,0
4,5	1,92922454	0,99999992	1,0	1,0	1,0
4,7	3,00238882	0,99997285	1,0	1,0	1,0
4,9	4,67251914	0,99883610	1,0	1,0	1,0
5,1	7,27168812	0,98697836	1,0	1,0	1,0
5,3	11,31668947	0,93854552	1,0	1,0	1,0
5,5	17,61179227	0,83344062	0,99999998	1,0	1,0
5,7	27,40865406	0,68391132	0,99999004	1,0	1,0
5,9	42,65518841	0,52291513	0,99938912	1,0	1,0
6,1	66,38286922	0,37844811	0,99139454	1,0	1,0
6,3	103,30947983	0,26329067	0,95290642	0,99999977	1,0
6,5	160,77715151	0,17826950	0,85962362	0,99994549	1,0
6,7	250,21220211	0,11852854	0,71680698	0,99817857	0,99999668
6,9	389,39703495	0,07786854	0,55544202	0,98263631	0,99969850
7,1	606,00582046	0,05075750	0,40602009	0,92606352	0,99453340

Table E4. Return periods (in years) and probability of occurrence of an event with local magnitude Ml for time horizons of 1, 10, 50, and 100 years, considering only cortical events (≤60 km) from the Full Catalog (FC) subcatalog. Note: Probabilities are expressed as values between 0 and 1.

Magnitude	Return period FC crustal	1-year probability	10-year probability	50-year probability	100-year probability
0,1	0,00004450	1,0	1,0	1,0	1,0
0,3	0,00006668	1,0	1,0	1,0	1,0
0,5	0,00009992	1,0	1,0	1,0	1,0
0,7	0,00014973	1,0	1,0	1,0	1,0
0,9	0,00022437	1,0	1,0	1,0	1,0
1,1	0,00033622	1,0	1,0	1,0	1,0
1,3	0,00050383	1,0	1,0	1,0	1,0
1,5	0,00075498	1,0	1,0	1,0	1,0
1,7	0,00113135	1,0	1,0	1,0	1,0
1,9	0,00169532	1,0	1,0	1,0	1,0
2,1	0,00254044	1,0	1,0	1,0	1,0
2,3	0,00380686	1,0	1,0	1,0	1,0
2,5	0,00570458	1,0	1,0	1,0	1,0
2,7	0,00854832	1,0	1,0	1,0	1,0
2,9	0,01280966	1,0	1,0	1,0	1,0
3,1	0,01919529	1,0	1,0	1,0	1,0
3,3	0,02876417	1,0	1,0	1,0	1,0
3,5	0,04310314	1,0	1,0	1,0	1,0
3,7	0,06459011	1,0	1,0	1,0	1,0
3,9	0,09678835	1,0	1,0	1,0	1,0
4,1	0,14503745	1,0	1,0	1,0	1,0
4,3	0,21733879	1,0	1,0	1,0	1,0
4,5	0,32568243	1,0	1,0	1,0	1,0
4,7	0,48803550	1,0	1,0	1,0	1,0
4,9	0,73132176	1,0	1,0	1,0	1,0
5,1	1,09588650	1,0	1,0	1,0	1,0
5,3	1,64218718	1,0	1,0	1,0	1,0
5,5	2,46081939	0,99999734	1,0	1,0	1,0
5,7	3,68754070	0,99980947	1,0	1,0	1,0
5,9	5,52578400	0,99670773	1,0	1,0	1,0
6,1	8,28039370	0,97795342	1,0	1,0	1,0
6,3	12,40817952	0,92157470	1,0	1,0	1,0
6,5	18,59367134	0,81709162	0,99999996	1,0	1,0
6,7	27,86263797	0,67814240	0,99998807	1,0	1,0
6,9	41,75219517	0,53070325	0,99948183	1,0	1,0
7,1	62,56571267	0,39640456	0,99358112	1,0	1,0

Table E5. Return periods (in years) and probability of occurrence of an event with local magnitude Ml for time horizons of 1, 10, 50, and 100 years, considering only cortical events (≤60 km) from the Bucaramanga Seismic Nest (BSN) subcatalog. Note: Probabilities are expressed as values between 0 and 1.

Magnitude	Return period BSN crustal	1-year probability	10-year probability	50-year probability	100-year probability
0,1	0,00831453	1,0	1,0	1,0	1,0
0,3	0,01177719	1,0	1,0	1,0	1,0
0,5	0,01668190	1,0	1,0	1,0	1,0
0,7	0,02362922	1,0	1,0	1,0	1,0
0,9	0,03346981	1,0	1,0	1,0	1,0
1,1	0,04740860	1,0	1,0	1,0	1,0
1,3	0,06715232	1,0	1,0	1,0	1,0
1,5	0,09511849	1,0	1,0	1,0	1,0
1,7	0,13473141	1,0	1,0	1,0	1,0
1,9	0,19084147	1,0	1,0	1,0	1,0
2,1	0,27031905	1,0	1,0	1,0	1,0
2,3	0,38289575	1,0	1,0	1,0	1,0
2,5	0,54235601	1,0	1,0	1,0	1,0
2,7	0,76822486	1,0	1,0	1,0	1,0
2,9	1,08815875	1,0	1,0	1,0	1,0
3,1	1,54133188	1,0	1,0	1,0	1,0
3,3	2,18323288	0,99999948	1,0	1,0	1,0
3,5	3,09245910	0,99996335	1,0	1,0	1,0
3,7	4,38034046	0,99926153	1,0	1,0	1,0
3,9	6,20457116	0,99384701	1,0	1,0	1,0
4,1	8,78851852	0,97251311	1,0	1,0	1,0
4,3	12,44857312	0,92092404	1,0	1,0	1,0
4,5	17,63288913	0,83326191	0,99999998	1,0	1,0
4,7	24,97625842	0,71766322	0,99999678	1,0	1,0
4,9	35,37783740	0,59050415	0,99986741	1,0	1,0
5,1	50,11124397	0,46758096	0,99816964	1,0	1,0
5,3	70,98050522	0,35917587	0,98832146	1,0	1,0
5,5	100,54095094	0,26960072	0,95678810	0,99999985	1,0
5,7	142,41210012	0,19892071	0,89116839	0,99998473	1,0
5,9	201,72085176	0,14494066	0,79108841	0,99960206	0,99999984
6,1	285,72924632	0,10465522	0,66894279	0,99602337	0,99998419
6,3	404,72366387	0,07507647	0,54179664	0,97980279	0,99959207
6,5	573,27433648	0,05360772	0,42361605	0,93638502	0,99595313
6,7	812,01939548	0,03815167	0,32225561	0,85700210	0,97955160
6,9	1150,19190057	0,02708815	0,24013767	0,74667704	0,93582748
7,1	1629,19927221	0,01920092	0,17624035	0,62068276	0,85611843

Table E6. Return periods (in years) and probability of occurrence of an event with local magnitude Ml for time horizons of 1, 10, 50, and 100 years, considering only cortical events (≤60 km) from the Campo Colorado (CC) subcatalog. Note: Probabilities are expressed as values between 0 and 1.

Magnitude	Return period CC crustal	1-year probability	10-year probability	50-year probability	100-year probability
0,1	0,00141572	1,0	1,0	1,0	1,0
0,3	0,00211391	1,0	1,0	1,0	1,0
0,5	0,00315641	1,0	1,0	1,0	1,0
0,7	0,00471304	1,0	1,0	1,0	1,0
0,9	0,00703735	1,0	1,0	1,0	1,0
1,1	0,01050792	1,0	1,0	1,0	1,0
1,3	0,01569005	1,0	1,0	1,0	1,0
1,5	0,02342782	1,0	1,0	1,0	1,0
1,7	0,03498159	1,0	1,0	1,0	1,0
1,9	0,05223327	1,0	1,0	1,0	1,0
2,1	0,07799286	1,0	1,0	1,0	1,0
2,3	0,11645617	1,0	1,0	1,0	1,0
2,5	0,17388821	1,0	1,0	1,0	1,0
2,7	0,25964370	1,0	1,0	1,0	1,0
2,9	0,38769074	1,0	1,0	1,0	1,0
3,1	0,57888604	1,0	1,0	1,0	1,0
3,3	0,86437207	1,0	1,0	1,0	1,0
3,5	1,29064966	1,0	1,0	1,0	1,0
3,7	1,92715221	0,99999992	1,0	1,0	1,0
3,9	2,87755520	0,99998279	1,0	1,0	1,0
4,1	4,29666319	0,99935545	1,0	1,0	1,0
4,3	6,41562481	0,99270378	1,0	1,0	1,0
4,5	9,57958301	0,96294244	1,0	1,0	1,0
4,7	14,30389298	0,88996010	1,0	1,0	1,0
4,9	21,35806476	0,77190890	0,99999962	1,0	1,0
5,1	31,89110342	0,62836789	0,99994975	1,0	1,0
5,3	47,61866251	0,48465646	0,99867880	1,0	1,0
5,5	71,10249491	0,35851589	0,98820062	1,0	1,0
5,7	106,16771905	0,25720527	0,94886855	0,99999965	1,0
5,9	158,52586584	0,18055758	0,86348372	0,99995258	1,0
6,1	236,70519027	0,12485162	0,73647796	0,99872918	0,99999839
6,3	353,43977972	0,08544246	0,59063534	0,98850387	0,99986784
6,5	527,74372098	0,05806202	0,45017677	0,94975239	0,99747518
6,7	788,00817287	0,03926800	0,33008057	0,86506865	0,98179353
6,9	1176,62580494	0,02647209	0,23531234	0,73853087	0,93163390
7,1	1756,89584514	0,01780728	0,16446023	0,59277388	0,83416689

Table E7. Return periods (in years) and probability of occurrence of an event with local magnitude Ml for time horizons of 1, 10, 50, and 100 years, considering only deep events (>60 km) from the Full Catalog (FC) subcatalog. Note: Probabilities are expressed as values between 0 and 1.

Magnitude	Return period FC deep	1-year probability	10-year probability	50-year probability	100-year probability
0,1	0,00000402	1,0	1,0	1,0	1,0
0,3	0,00000635	1,0	1,0	1,0	1,0
0,5	0,00001005	1,0	1,0	1,0	1,0
0,7	0,00001590	1,0	1,0	1,0	1,0
0,9	0,00002514	1,0	1,0	1,0	1,0
1,1	0,00003977	1,0	1,0	1,0	1,0
1,3	0,00006290	1,0	1,0	1,0	1,0
1,5	0,00009948	1,0	1,0	1,0	1,0
1,7	0,00015733	1,0	1,0	1,0	1,0
1,9	0,00024884	1,0	1,0	1,0	1,0
2,1	0,00039357	1,0	1,0	1,0	1,0
2,3	0,00062248	1,0	1,0	1,0	1,0
2,5	0,00098452	1,0	1,0	1,0	1,0
2,7	0,00155713	1,0	1,0	1,0	1,0
2,9	0,00246279	1,0	1,0	1,0	1,0
3,1	0,00389519	1,0	1,0	1,0	1,0
3,3	0,00616069	1,0	1,0	1,0	1,0
3,5	0,00974385	1,0	1,0	1,0	1,0
3,7	0,01541104	1,0	1,0	1,0	1,0
3,9	0,02437436	1,0	1,0	1,0	1,0
4,1	0,03855090	1,0	1,0	1,0	1,0
4,3	0,06097275	1,0	1,0	1,0	1,0
4,5	0,09643552	1,0	1,0	1,0	1,0
4,7	0,15252404	1,0	1,0	1,0	1,0
4,9	0,24123457	1,0	1,0	1,0	1,0
5,1	0,38154063	1,0	1,0	1,0	1,0
5,3	0,60345104	1,0	1,0	1,0	1,0
5,5	0,95442827	1,0	1,0	1,0	1,0
5,7	1,50953971	1,0	1,0	1,0	1,0
5,9	2,38751326	0,99999820	1,0	1,0	1,0
6,1	3,77613090	0,99976706	1,0	1,0	1,0
6,3	5,97239180	0,99495183	1,0	1,0	1,0
6,5	9,44603477	0,96470013	1,0	1,0	1,0
6,7	14,94000660	0,87927184	1,0	1,0	1,0
6,9	23,62936434	0,73729991	0,99999843	1,0	1,0
7,1	37,37259790	0,57051763	0,99978647	1,0	1,0

Table E8. Return periods (in years) and probability of occurrence of an event with local magnitude Ml for time horizons of 1, 10, 50, and 100 years, considering only deep events (>60 km) from the Bucaramanga Seismic Nest (BSN) subcatalog. Note: Probabilities are expressed as values between 0 and 1.

Magnitude	Return period BSN deep	1-year probability	10-year probability	50-year probability	100-year probability
0,1	0,00000491	1,0	1,0	1,0	1,0
0,3	0,00000774	1,0	1,0	1,0	1,0
0,5	0,00001221	1,0	1,0	1,0	1,0
0,7	0,00001926	1,0	1,0	1,0	1,0
0,9	0,00003037	1,0	1,0	1,0	1,0
1,1	0,00004791	1,0	1,0	1,0	1,0
1,3	0,00007558	1,0	1,0	1,0	1,0
1,5	0,00011922	1,0	1,0	1,0	1,0
1,7	0,00018805	1,0	1,0	1,0	1,0
1,9	0,00029664	1,0	1,0	1,0	1,0
2,1	0,00046792	1,0	1,0	1,0	1,0
2,3	0,00073811	1,0	1,0	1,0	1,0
2,5	0,00116430	1,0	1,0	1,0	1,0
2,7	0,00183658	1,0	1,0	1,0	1,0
2,9	0,00289704	1,0	1,0	1,0	1,0
3,1	0,00456982	1,0	1,0	1,0	1,0
3,3	0,00720849	1,0	1,0	1,0	1,0
3,5	0,01137076	1,0	1,0	1,0	1,0
3,7	0,01793636	1,0	1,0	1,0	1,0
3,9	0,02829301	1,0	1,0	1,0	1,0
4,1	0,04462972	1,0	1,0	1,0	1,0
4,3	0,07039943	1,0	1,0	1,0	1,0
4,5	0,11104885	1,0	1,0	1,0	1,0
4,7	0,17516972	1,0	1,0	1,0	1,0
4,9	0,27631469	1,0	1,0	1,0	1,0
5,1	0,43586193	1,0	1,0	1,0	1,0
5,3	0,68753353	1,0	1,0	1,0	1,0
5,5	1,08452317	1,0	1,0	1,0	1,0
5,7	1,71073911	0,99999999	1,0	1,0	1,0
5,9	2,69853923	0,99999175	1,0	1,0	1,0
6,1	4,25670630	0,99940107	1,0	1,0	1,0
6,3	6,71457667	0,99094234	1,0	1,0	1,0
6,5	10,59164919	0,94931843	1,0	1,0	1,0
6,7	16,70738724	0,84901298	0,99999999	1,0	1,0
6,9	26,35442162	0,69836015	0,99999376	1,0	1,0
7,1	41,57176276	0,53224134	0,99949856	1,0	1,0

Table E9. Return periods (in years) and probability of occurrence of an event with local magnitude Ml for time horizons of 1, 10, 50, and 100 years, considering only deep events (>60 km) from the Campo Colorado (CC) subcatalog. Note: Probabilities are expressed as values between 0 and 1.

Magnitude	Return period CC deep	1-year probability	10-year probability	50-year probability	100-year probability
0,1	0,00013260	1,0	1,0	1,0	1,0
0,3	0,00020670	1,0	1,0	1,0	1,0
0,5	0,00032221	1,0	1,0	1,0	1,0
0,7	0,00050228	1,0	1,0	1,0	1,0
0,9	0,00078297	1,0	1,0	1,0	1,0
1,1	0,00122054	1,0	1,0	1,0	1,0
1,3	0,00190264	1,0	1,0	1,0	1,0
1,5	0,00296594	1,0	1,0	1,0	1,0
1,7	0,00462346	1,0	1,0	1,0	1,0
1,9	0,00720728	1,0	1,0	1,0	1,0
2,1	0,01123508	1,0	1,0	1,0	1,0
2,3	0,01751382	1,0	1,0	1,0	1,0
2,5	0,02730145	1,0	1,0	1,0	1,0
2,7	0,04255891	1,0	1,0	1,0	1,0
2,9	0,06634301	1,0	1,0	1,0	1,0
3,1	0,10341891	1,0	1,0	1,0	1,0
3,3	0,16121471	1,0	1,0	1,0	1,0
3,5	0,25130979	1,0	1,0	1,0	1,0
3,7	0,39175463	1,0	1,0	1,0	1,0
3,9	0,61068728	1,0	1,0	1,0	1,0
4,1	0,95197076	1,0	1,0	1,0	1,0
4,3	1,48398101	1,0	1,0	1,0	1,0
4,5	2,31330597	0,99999882	1,0	1,0	1,0
4,7	3,60610039	0,99984216	1,0	1,0	1,0
4,9	5,62137486	0,99635940	1,0	1,0	1,0
5,1	8,76288842	0,97274180	1,0	1,0	1,0
5,3	13,66004143	0,90083129	1,0	1,0	1,0
5,5	21,29397555	0,77292129	0,99999964	1,0	1,0
5,7	33,19414493	0,61364325	0,99992589	1,0	1,0
5,9	51,74474135	0,45668215	0,99775849	1,0	1,0
6,1	80,66236571	0,32385838	0,98003006	1,0	1,0
6,3	125,74064672	0,22201806	0,91877398	0,99999646	1,0
6,5	196,01099097	0,14874991	0,80021094	0,99968168	0,99999990
6,7	305,55201986	0,09815517	0,64410803	0,99429059	0,99996740
6,9	476,31021289	0,06412649	0,48456781	0,96362042	0,99867653
7,1	742,49687175	0,04162415	0,34632987	0,88065804	0,98575750

Appendix F.

This appendix presents the results of the fractal dimension (Dc) estimation for the three subcatalogs analyzed in this study. All results can be reproduced using the Notebooks available in the public repository referenced in the Data Availability section.

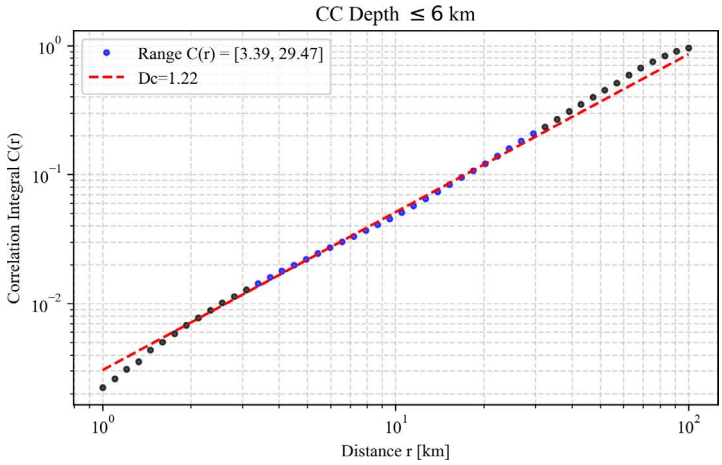


Figure F1. Fractal dimension (Dc) estimation for seismic events shallower than 6 km in the Campo Colorado.

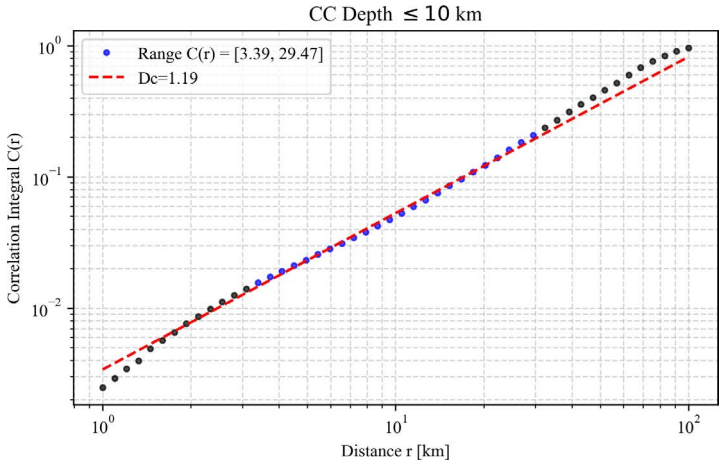


Figure F2. Fractal dimension (Dc) estimation for seismic events shallower than 10 km in the Campo Colorado.

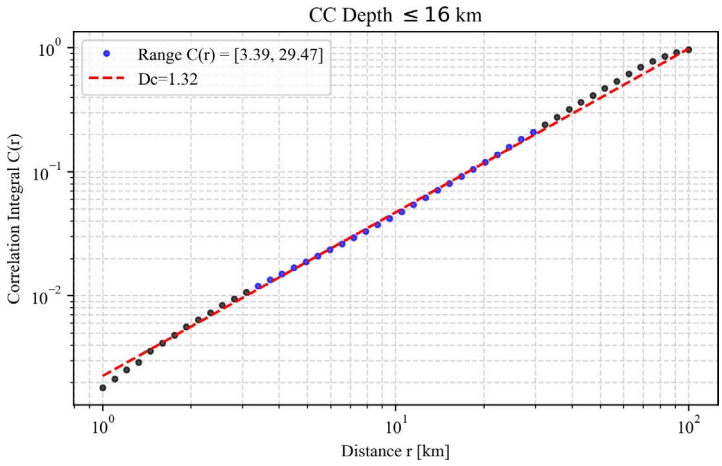


Figure F3. Fractal dimension (Dc) estimation for seismic events shallower than 16 km in the Campo Colorado.

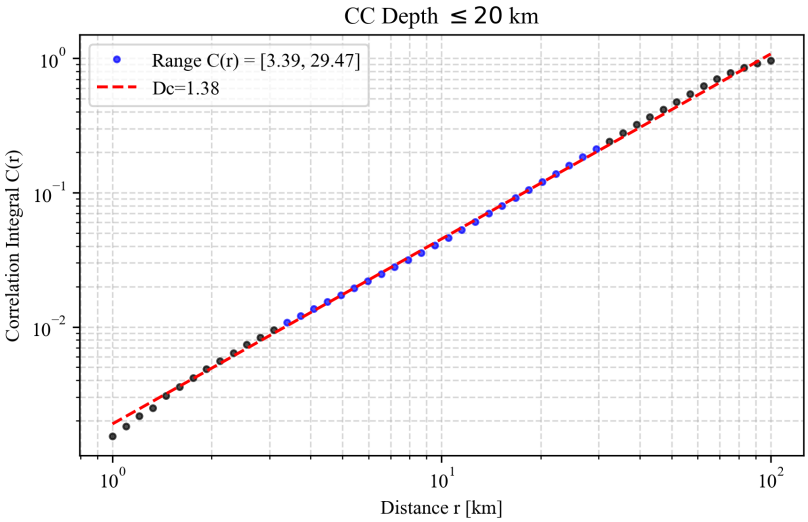


Figure F4. Fractal dimension (Dc) estimation for seismic events shallower than 20 km in the Campo Colorado.

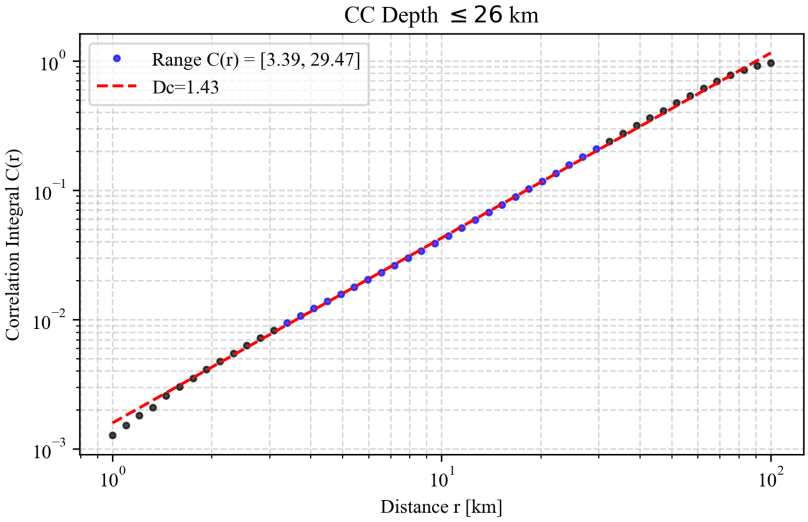


Figure F5. Fractal dimension (Dc) estimation for seismic events shallower than 26 km in the Campo Colorado.

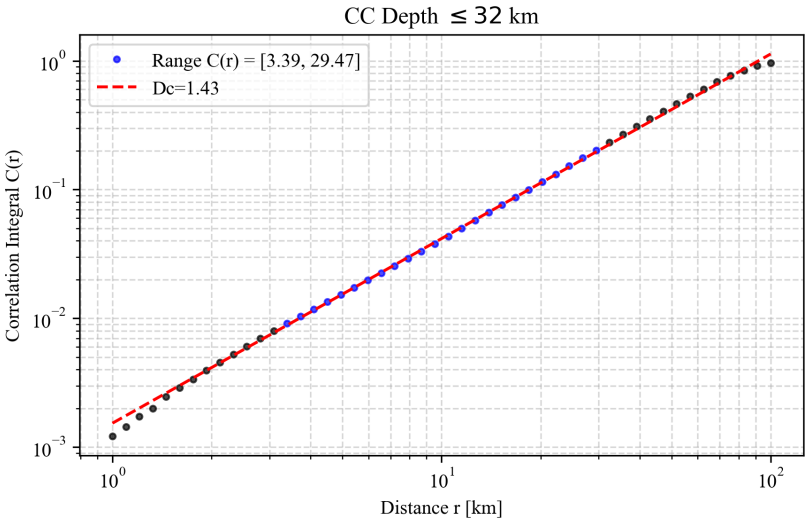


Figure F6. Fractal dimension (Dc) estimation for seismic events shallower than 32 km in the Campo Colorado.

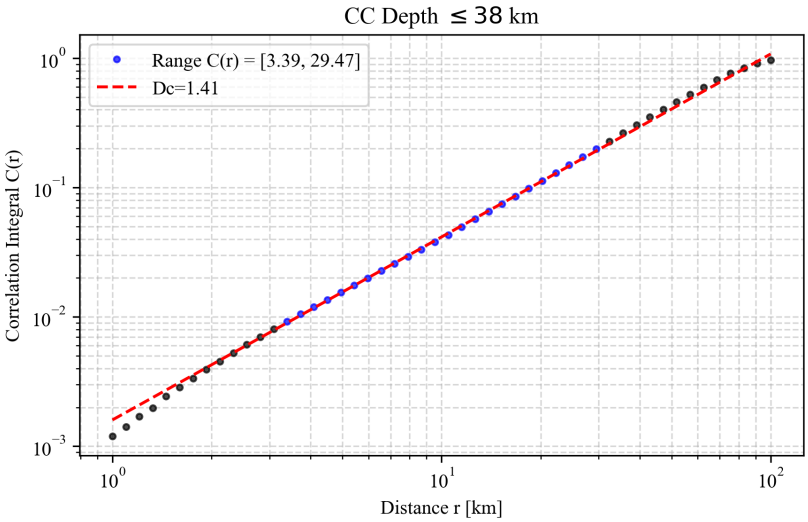


Figure F7. Fractal dimension (Dc) estimation for seismic events shallower than 38 km in the Campo Colorado.

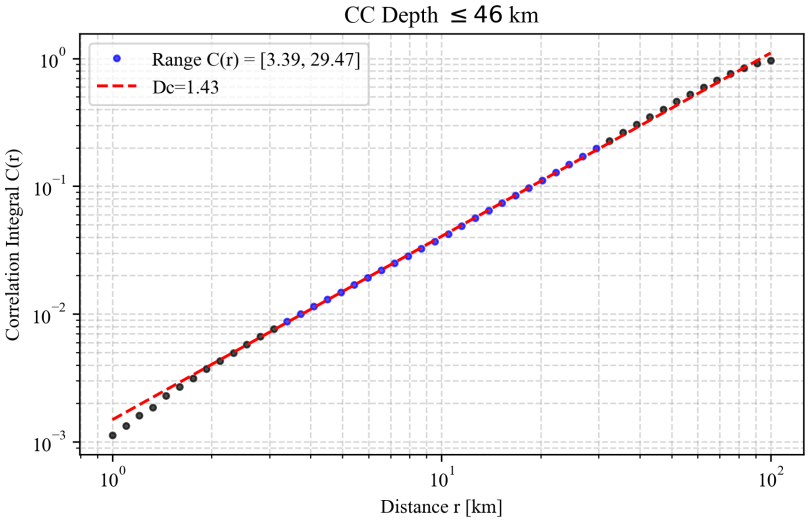


Figure F8. Fractal dimension (Dc) estimation for seismic events shallower than 46 km in the Campo Colorado.

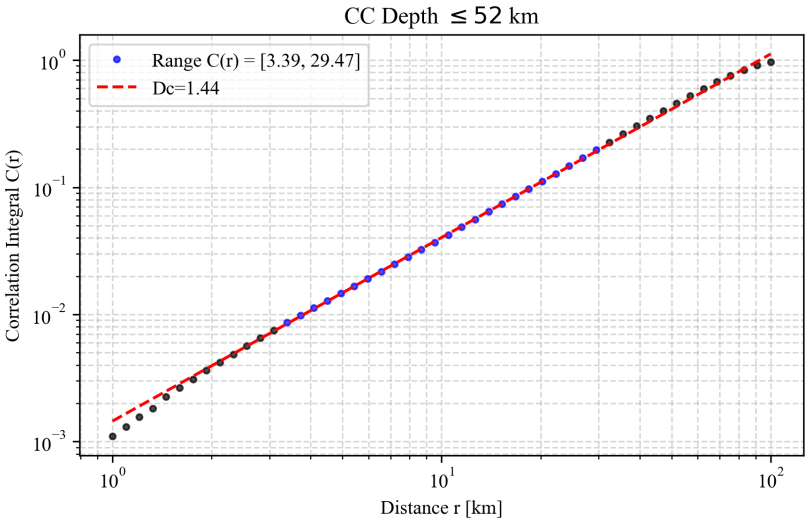


Figure F9. Fractal dimension (Dc) estimation for seismic events shallower than 52 km in the Campo Colorado.

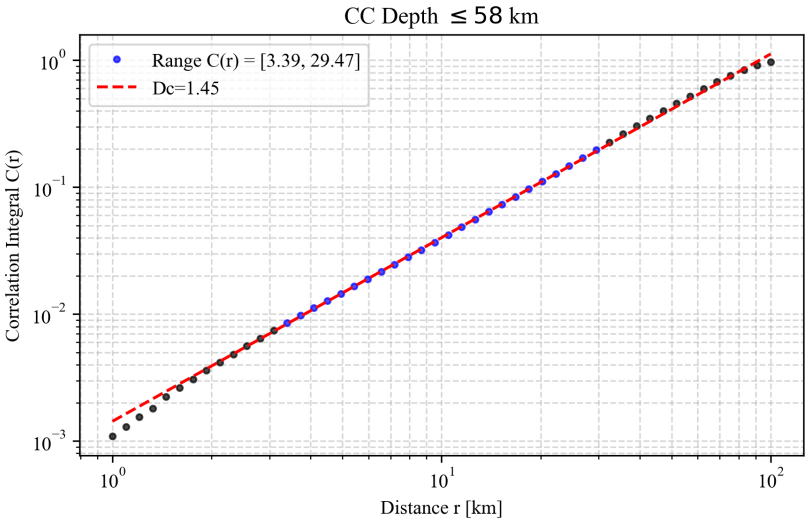


Figure F10. Fractal dimension (Dc) estimation for seismic events shallower than 58 km in the Campo Colorado.

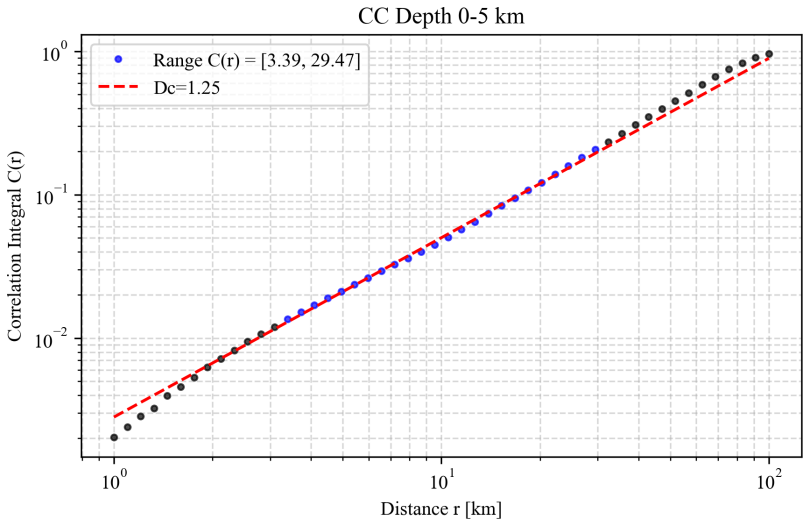


Figure F11. Estimated fractal dimension (Dc) for seismic events within the 0-5 km depth interval in the Campo Colorado.

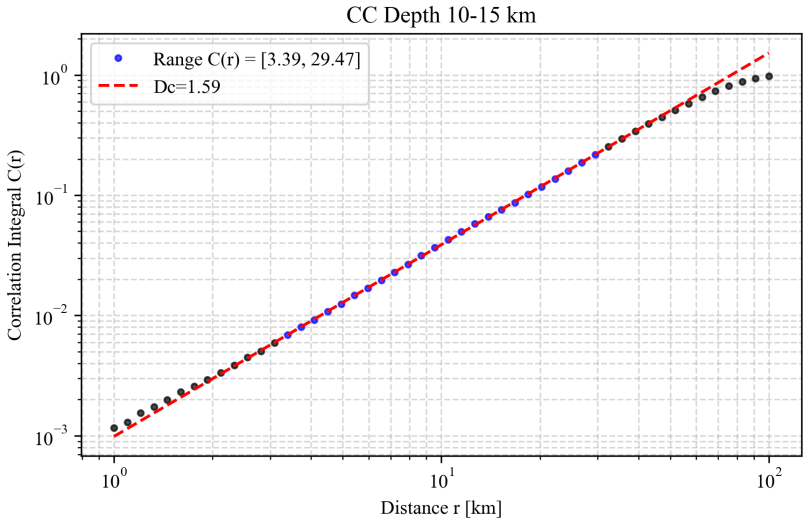


Figure F12. Estimated fractal dimension (Dc) for seismic events within the 10-15 km depth interval in the Campo Colorado.

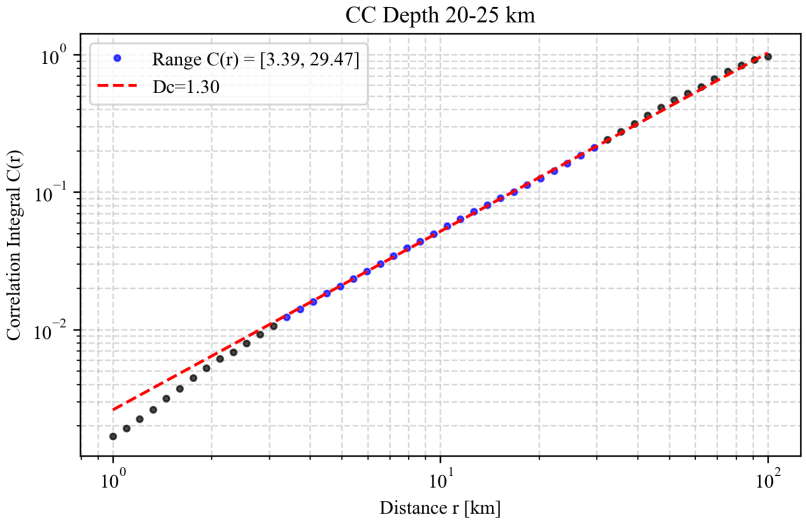


Figure F13. Estimated fractal dimension (Dc) for seismic events within the 20-25 km depth interval in the Campo Colorado.

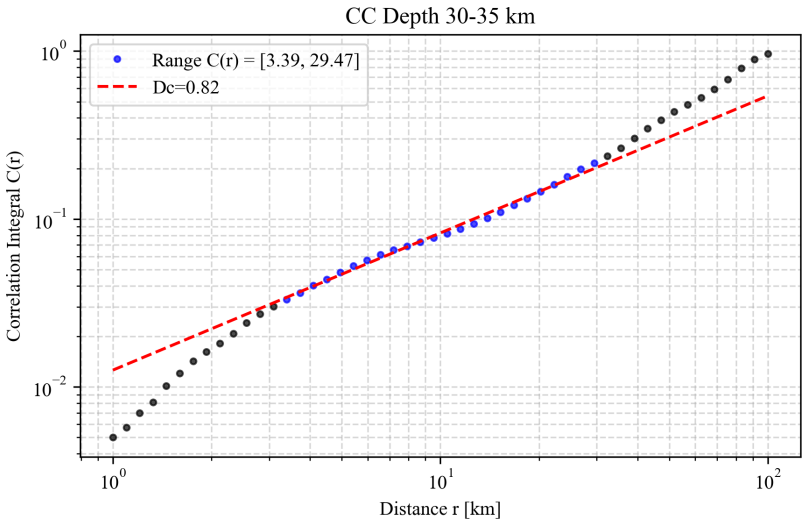


Figure F14. Estimated fractal dimension (Dc) for seismic events within the 30-35 km depth interval in the Campo Colorado.

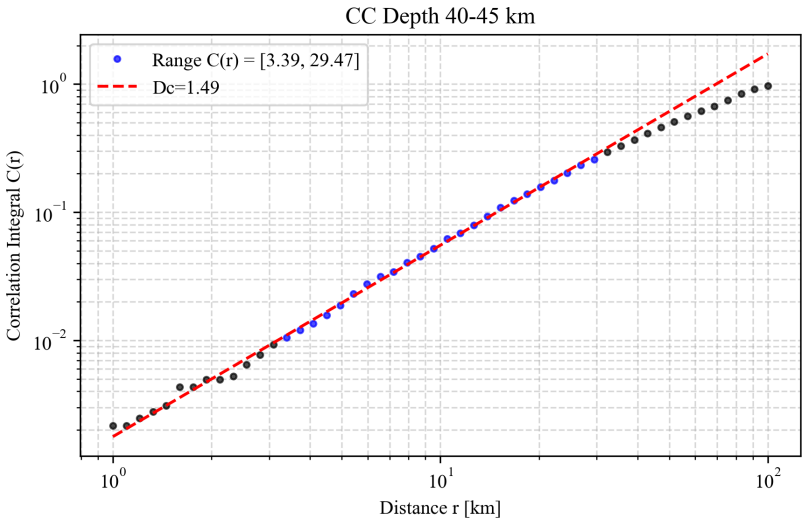


Figure F15. Estimated fractal dimension (Dc) for seismic events within the 40-45 km depth interval in the Campo Colorado.

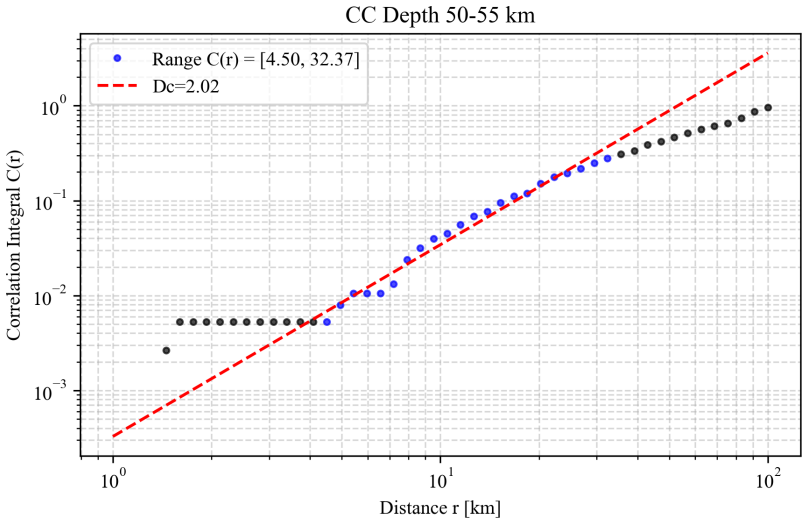


Figure F16. Estimated fractal dimension (Dc) for seismic events within the 50-55 km depth interval in the Campo Colorado.

References

Acevedo Acosta, V. (2023). Influencia de la inyección de CO_2 sobre la recuperación de metano en yacimientos de roca generadora mediante el estudio del fenómeno de adsorción, M.Sc. thesis, Universidad Industrial de Santander, Bucaramanga, Colombia, https://noesis.uis.edu.co/handle/20.500.14071/15457.

Acosta, J. (2002). Estructura tectónica y modelos en 3D del Piedemonte Occidental de la Cordillera Oriental y del Valle Medio del Magdalena, Colombia, Publicaciones Especiales de INGEOMINAS, Bogotá, Colombia.

Ali, S. M., K. Abdelrahman and N. Al-Otaibi (2021). Tectonic stress regime and stress patterns from the inversion of earthquake focal mechanisms in NW Himalaya and surrounding regions, J. King Saud Univ. Sci., 33, 2, 101351, doi:10.1016/j.jksus.2021.101351.

Aminu, M. D., S. A. Nabavi, C. A. Rochelle and V. Manovic (2017). A review of developments in carbon dioxide storage, Appl. Energy, 208, 1389-1419, doi:10.1016/j.apenergy.2017.09.015.

Anaya, C., G. Jiménez and D. A. Martínez-Sánchez (2018). Modelo estructural del Campo Escuela Colorado a partir de modelos análogos, Rev. Acad. Colomb. Cienc. Exactas Fís. Nat., 42, 165, 402, doi:10.18257/raccefyn.673.

Angelier, J. and P. Mechler (1977). Sur une methode graphique de recherche des contraintes principales egalement utilisables en tectonique et en seismologie: la methode des diedres droits, Bull. Soc. Géol. Fr., S7-XIX, 6, 1309-1318, doi:10.2113/gssgfbull.S7-XIX.6.1309.

Bachmann, C. E., S. Wiemer, B. P. Goertz-Allmann and J. Woessner (2012). Influence of pore-pressure on the event-size distribution of induced earthquakes, Geophys. Res. Lett., 39, 9, doi:10.1029/2012GL051480.

Barrero, D., A. Pardo, C. A. Vargas and J. F. Martínez (2007). Colombian Sedimentary Basins: Nomenclature, Boundaries and Petroleum Geology, a New Proposal, Agencia Nacional de Hidrocarburos (ANH), Bogotá, Colombia, ISBN: 9789589823705, https://www.anh.gov.co/documents/12/colombian_sedimentary_basins.pdf.

Barton, C. A., M. D. Zoback and D. Moos (1995). Fluid flow along potentially active faults in crystalline rock, Geology, 23, 8, 683-686, doi:10.1130/0091-7613(1995)023<0683:FFAPAF>2.3.CO;2.

Caballero, V., M. Parra and A. R. Mora (2010). Levantamiento de la Cordillera Oriental de Colombia durante el Eoceno tardío-Oligoceno temprano: proveniencia sedimentaria en el sinclinal de Nuevo Mundo, cuenca Valle Medio del Magdalena, Bol. Geol., 32, 1, 45-77, https://revistas.uis.edu.co/index.php/revistaboletindegeologia/article/view/1008.

Cabañas, L. and B. Benito (1999). Caracterización del movimiento del suelo en ingeniería sísmica, Fís. Tierra, 11, 49-79.

Cappa, F. and J. Rutqvist (2011a). Impact of CO_2 geological sequestration on the nucleation of earthquakes, Geophys. Res. Lett., 38, 17, doi:10.1029/2011GL048487.

Cappa, F. and J. Rutqvist (2011b). Modeling of coupled deformation and permeability evolution during fault reactivation induced by deep underground injection of CO_2, Int. J. Greenh. Gas Control, 5, 2, 336-346, doi:10.1016/j.ijggc.2010.08.005.

Castillo, E., D. Siervo and G. A. Prieto (2024). Colombian seismic monitoring using advanced machine-learning algorithms, Seismol. Res. Lett., 95, 5, 2971-2985, doi:10.1785/0220240036.

Chajín, P., J. Luna Osorio, L. Delgado Blanco, T. Palmera et al. (2013). Reinterpretación del modelo estructural del Campo Escuela Colorado, VMM, Colombia, In XV Congreso Colombiano del Petróleo y Gas, ACIPET, Bogotá, Colombia, 20-22 November 2013.

Cheng, Y., W. Liu, T. Xu, Y. Zhang et al. (2023). Seismicity induced by geological CO_2 storage: A review, Earth-Sci. Rev., 239, 104369, doi:10.1016/j.earscirev.2023.104369.

Chiarabba, C., P. De Gori, C. Faccenna, F. Speranza et al. (2016). Subduction system and flat slab beneath the Eastern Cordillera of Colombia, Geochem. Geophys. Geosyst., 17, 1, 16-27, doi:10.1002/2015GC006048.

Cook, P. J. and S. M. Benson (2005). Overview and current issues in geological storage of carbon dioxide. In: Proceedings of the 7th International Conference on Greenhouse Gas Control, Elsevier, 15-20, doi:10.1016/B978-008044704-9/50003-3.

Cortés, M. and J. Angelier (2005). Current states of stress in the northern Andes as indicated by focal mechanisms of earthquakes, Tectonophysics, 403, 1-4, 29-58, doi:10.1016/j.tecto.2005.03.020.

Delvaux, D. (2001). Win-Tensor (version 5.9.0), software, http://damiendelvaux.be/Tensor/WinTensor/win-tensor.html.

Delvaux, D., R. Moeys, G. Stapel, A. Melnikov et al. (1995). Palaeostress reconstructions and geodynamics of the Baikal region, Central Asia, Part I. Palaeozoic and Mesozoic pre-rift evolution, Tectonophysics, 252, 1-4, 61-101, doi:10.1016/0040-1951(95)00090-9.

Delvaux, D., R. Moeys, G. Stapel, C. Petit et al. (1997). Paleostress reconstructions and geodynamics of the Baikal region, Central Asia, Part 2. Cenozoic rifting, Tectonophysics, 282, 1-4, 1-38, doi:10.1016/S0040-1951(97)00210-2.

Díaz, A., C. A. Tavera, C. Sánchez Ruiz, C. Perea et al. (2024). Atlas de almacenamiento de CO_2 en Colombia, Agencia Nacional de Hidrocarburos (ANH), Bogotá, Colombia, https://www.anh.gov.co/documents/29509/Atlas_CO2_Espanol_Interactivo.pdf.

Evans, K. F., A. Zappone, T. Kraft, N. Deichmann et al. (2012). A survey of the induced seismic responses to fluid injection in geothermal and CO_2 reservoirs in Europe, Geothermics, 41, 30-54, doi:10.1016/j.geothermics.2011.08.002.

Ferrill, D. A., J. Winterle, G. Wittmeyer, D. Sims et al. (1999). Stressed rock strains groundwater at Yucca Mountain, Nevada, GSA Today, 9, 1-8.

Foulger, G. R., M. P. Wilson, J. G. Gluyas, B. R. Julian et al. (2018). Global review of human-induced earthquakes, Earth-Sci. Rev., 178, 438-514, doi:10.1016/j.earscirev.2017.07.008.

Frohlich, C. and S. D. Davis (1993). Teleseismic b values; Or, much ado about 1.0, J. Geophys. Res. Solid Earth, 98, B1, 631-644, doi:10.1029/92JB01891.

Furre, A. K., O. Eiken, H. Alnes, J. N. Vevatne et al. (2017). 20 years of monitoring CO_2-injection at Sleipner, Energy Procedia, 114, 3916-3926, doi:10.1016/j.egypro.2017.03.1523.

Garcia Ariza, A. L. (2024). Análisis geomecánico de riesgos en el almacenamiento subterráneo de CO_2, caso: pozo Bullerengue Sur 1, Cuenca Sinú-San Jacinto, Colombia, M.Sc. thesis, Universidad Nacional de Colombia, Bogotá, Colombia, https://repositorio.unal.edu.co/handle/unal/86932.

García-Arias, S., F. Velandia, S. Khurama and M. A. Florez (2026). Towards earthquake forecasting in the Bucaramanga nest, a machine learning approach, J. Seismol., 30, 2, 11, doi:10.1007/s10950-026-10364-w.

Goertz-Allmann, B. P., N. Langet, K. Iranpour, D. Kühn et al. (2024). Effective microseismic monitoring of the Quest CCS site, Alberta, Canada, Int. J. Greenh. Gas Control, 133, 104100, doi:10.1016/j.ijggc.2024.104100.

Gutiérrez Barrera, J. C. (2025). Modelado numérico del entrampamiento de CO_2 en un medio poroso durante la inyección alternada de agua y gas (WAG), M.Sc. thesis, Universidad Industrial de Santander, Bucaramanga, Colombia, https://noesis.uis.edu.co/handle/20.500.14071/45375.

Hosseini, S., S. D. Hovorka, A. Savvaidis, F. Kavoura et al. (2022). Current state of knowledge regarding the risk of induced seismicity at CO_2 storage projects, Technical Report 2022-02, IEAGHG, Cheltenham, UK, doi:10.62849/2022-02, https://ieaghg.org/publications/current-state-of-knowledge-regarding-the-risk-of-induced-seismicity-at-co2-storage-projects/.

IEAGHG (2013). Induced seismicity and its implications for CO_2 storage risk, Technical Report 2013-09, IEAGHG, Cheltenham, UK, https://ieaghg.org/publications/induced-seismicity-and-its-implications-for-co2-storage-risk/.

Jaramillo, C. A. and D. L. Dilcher (2001). Middle Paleogene palynology of Central Colombia, South America: a study of pollen and spores from tropical latitudes, Palaeontographica Abt. B, 258, 4-6, 87-259, doi:10.1127/palb/258/2001/87.

Kiyingi, W., R. Xiong, Y. Jin and J. Guo (2025). Geological carbon dioxide storage and subsurface rock mechanics – geomechanical risks, modelling practices, and risk mitigation strategies, Simul. Model. Pract. Theory, 144, 103195, doi:10.1016/j.simpat.2025.103195.

Kohli, A., Y. Li, T. W. Kim and A. R. Kovscek (2023). Induced seismicity hazard assessment for a potential CO_2 storage site in the Southern San Joaquin Basin, CA, GeoHazards, 4, 4, 421-436, doi:10.3390/geohazards4040024.

Londoño, J. M., O. P. Bohórquez and L. F. Ospina (2010). Tomografía sísmica 3D del sector de Cúcuta, Colombia, Bol. Geol., 32, 1, 45-77, https://revistas.uis.edu.co/index.php/revistaboletindegeologia/article/view/1011.

Londoño, J. M., S. Quintero, K. Vallejo, F. Muñoz et al. (2019). Seismicity of Valle Medio del Magdalena Basin, Colombia, J. S. Am. Earth Sci., 92, 565-585, doi:10.1016/j.jsames.2019.04.003.

Londoño, J. M. and J. A. Romero (2017). Local magnitude scale for Valle Medio del Magdalena region, Colombia, J. S. Am. Earth Sci., 80, 237-243, doi:10.1016/j.jsames.2017.09.033.

Londoño, J. M., K. Vallejo and S. Quintero (2020). Detailed seismic velocity structure of the Caribbean and Nazca plates beneath Valle Medio del Magdalena region of NE Colombia, J. S. Am. Earth Sci., 103, 102762, doi:10.1016/j.jsames.2020.102762.

Londoño, J. M., L. V. Velásquez and J. C. Bermúdez (2022). Seismic wave attenuation at Valle Medio del Magdalena, Colombia, J. S. Am. Earth Sci., 119, 103987, doi:10.1016/j.jsames.2022.103987.

Maxwell, S. C., M. Jones, R. Parker, S. Miong et al. (2009). Fault activation during hydraulic fracturing, In: SEG Technical Program Expanded Abstracts 2009, Society of Exploration Geophysicists, Tulsa, OK, USA, 1552-1556, doi:10.1190/1.3255145.

Metz, B., O. Davidson, H. C. de Coninck, M. Loos et al. (2005). IPCC Special Report on Carbon Dioxide Capture and Storage, Cambridge University Press, Cambridge, UK, 442, ISBN: 978-0-521-86643-9.

Mier, R., P. Chajín, L. Delgado, J. Luna et al. (2013). Modelo geológico de Campo Escuela Colorado, Technical Report, Universidad Industrial de Santander, Bucaramanga, Colombia, 143.

Ministerio de Ambiente y Desarrollo Sostenible (2020). Actualización de la Contribución Determinada a Nivel Nacional de Colombia (NDC), Ministerio de Ambiente y Desarrollo Sostenible, Bogotá, Colombia, https://unfccc.int/sites/default/files/NDC/2022-06/NDC%20actualizada%20de%20Colombia.pdf.

Mitchell, J. K. and R. A. Green (2017). Some induced seismicity considerations in geo-energy resource development, Geomech. Energy Environ., 10, 3-11, doi:10.1016/j.gete.2017.01.001.

Mojica, J. and R. Franco (1990). Estructura y evolución tectónica del Valle Medio y Superior del Magdalena, Colombia, Geol. Colomb., 17, 17, 41-64.

Morales, L. G. (1958). General geology and oil occurrences of Middle Magdalena Valley, Colombia. In: L. G. Weeks (ed.), Habitat of Oil, American Association of Petroleum Geologists, Special Publication 18, Tulsa, OK, USA, 641-695, doi:10.1306/SV18350C25.

Mortimer, L., A. Aydin, C. T. Simmons, G. Heinson et al. (2011). The role of in situ stress in determining hydraulic connectivity in a fractured rock aquifer (Australia), Hydrogeol. J., 19, 7, 1293-1312, doi:10.1007/s10040-011-0760-z.

Ochoa Suarez, H. (2010). Análisis estructural del Campo Colorado en la cuenca del Valle del Magdalena Medio, Colombia, B.Sc. thesis, Universidad Industrial de Santander, Bucaramanga, Colombia, https://noesis.uis.edu.co/handle/20.500.14071/24572.

Pérez, J. L., J. S. Vargas Montealegre, M. C. Rodríguez Lasso and E. de J. Salcedo Hurtado (2026). Stress regime and plastic deformation at depth in the Bucaramanga Seismic Nest: analysis based on focal mechanisms, Geociências, 45, 1, 87-96, doi:10.5016/geociencias.v45i1.19602.

Prada Velásquez, S. J. (2024). Estructura de la corteza por debajo del Valle Medio del Magdalena (VMM) a partir de funciones receptoras y curvas de dispersión, B.Sc. thesis, Universidad de los Andes, Bogotá, Colombia, https://hdl.handle.net/1992/74454.

Prieto, G. A., G. C. Beroza, S. A. Barrett and G. A. López et al. (2012). Earthquake nests as natural laboratories for the study of intermediate-depth earthquake mechanics, Tectonophysics, 570-571, 42-56, doi:10.1016/j.tecto.2012.07.019.

Rivas, C. R. (2007). Almacenamiento geológico de CO_2: criterios de selección de emplazamientos, In Actas del Congreso Nacional del Medio Ambiente (CONAMA 9), Madrid, España

Rojas Orduz, K. J. and J. F. Pabón Uribe (2024). Evaluación experimental del potencial daño de formación en reservorios calcáreos como efecto del almacenamiento geológico de CO_2, B.Sc. thesis, Universidad Industrial de Santander, Bucaramanga, Colombia, https://noesis.uis.edu.co/handle/20.500.14071/44495.

Roncancio, J. and M. Martínez (2011). Upper Magdalena Basin. In: Petroleum Geology of Colombia, Vol. 14: Upper Magdalena Basin, Agencia Nacional de Hidrocarburos (ANH) and Fondo Editorial Universidad EAFIT, Medellín, Colombia, 183, https://www.anh.gov.co/es/hidrocarburos/información-geológica-y-geofísica/estudios-integrados-y-modelamientos/petroleum-geology-of-colombia/.

Royero, J. and J. Clavijo (2001). Mapa geológico generalizado del departamento de Santander, Instituto Colombiano de Geología y Minería (INGEOMINAS), Bogotá, Colombia.

Rutqvist, J. (2011). Status of the TOUGH-FLAC simulator and recent applications related to coupled fluid flow and crustal deformations, Comput. Geosci., 37, 6, 739-750, doi:10.1016/j.cageo.2010.08.006.

Rutqvist, J. (2012). The geomechanics of CO_2 storage in deep sedimentary formations, Geotech. Geol. Eng., 30, 3, 525-551, doi:10.1007/s10706-011-9491-0.

Rutqvist, J., A. P. Rinaldi, F. Cappa, P. Jeanne et al. (2016). Fault activation and induced seismicity in geological carbon storage: lessons learned from recent modeling studies, J. Rock Mech. Geotech. Eng., 8, 6, 789-804, doi:10.1016/j.jrmge.2016.09.001.

Sarmiento, G., J. Puentes and C. Sierra (2015). Evolución geológica y estratigrafía del sector norte del Valle Medio del Magdalena, Geol. Norandina, 12, 1, 51-82.

Sarmiento Isaza, R. C. (2021). Distribución de acuíferos de agua dulce y salada en las formaciones Esmeraldas, Mugrosa y Colorado en el Campo Colorado, Valle Medio del Magdalena, Colombia, B.Sc. thesis, Universidad Industrial de Santander, Bucaramanga, Colombia, https://noesis.uis.edu.co/handle/20.500.14071/41141.

Shapiro, S. A. and C. Dinske (2009). Scaling of seismicity induced by nonlinear fluid-rock interaction, J. Geophys. Res. Solid Earth, 114, B9, doi:10.1029/2008JB006145.

Sierra Reyes, C. A. (2025). Análisis del efecto de la inyección de CO_2 sobre la interacción química y características morfológicas de una roca almacén representativa del Valle Medio del Magdalena, B.Sc. thesis, Universidad Industrial de Santander, Bucaramanga, Colombia, https://noesis.uis.edu.co/handle/20.500.14071/45405.

Sminchak, J., N. Gupta, C. Byrer and P. Bergman (2001). Issues related to seismic activity induced by the injection of CO_2 in deep saline aquifers. In: Proceedings of the First National Conference on Carbon Sequestration, Washington, DC, USA, May 14-17, 2001, https://www.osti.gov/biblio/1200684.

Streit, J. E., A. F. Siggins and B. J. Evans (2005). Predicting and monitoring geomechanical effects of CO_2 injection. In: Carbon Dioxide Capture for Storage in Deep Geologic Formations, Elsevier, 751-766, doi:10.1016/B978-008044570-0/50132-X.

Taboada, A., L. A. Rivera, A. Fuenzalida, A. Cisternas et al. (2000). Geodynamics of the northern Andes: subductions and intracontinental deformation (Colombia), Tectonics, 19, 5, 787-813, doi:10.1029/2000TC900004.

van Eck, N. J. and L. Waltman (2010). Software survey: VOSviewer, a computer program for bibliometric mapping, Scientometrics, 84, 2, 523-538, doi:10.1007/s11192-009-0146-3.

Vergara Espinosa, C. A. (2024). Sismicidad e implicaciones sismotectónicas de una zona del centro-oriente de la cuenca del Valle Medio del Magdalena (VMM) y Nido Sísmico de Bucaramanga, M.Sc. thesis, Universidad Industrial de Santander, Bucaramanga, Colombia, https://noesis.uis.edu.co/handle/20.500.14071/44389.

Vesga Esparza, F. A. and P. A. Mendoza Vecino (2020). Factibilidad técnica del almacenamiento del dióxido de carbono (CO_2) en la Formación La Luna de la cuenca del VMM, B.Sc. thesis, Universidad Industrial de Santander, Bucaramanga, Colombia, https://noesis.uis.edu.co/handle/20.500.14071/40059.

Vilarrasa, V., J. Carrera, S. Olivella, J. Rutqvist et al. (2019). Induced seismicity in geologic carbon storage, Solid Earth, 10, 3, 871-892, doi:10.5194/se-10-871-2019.

Villalobos-Escobar, G. P., R. R. Castro and T. A. Peña-Alonso (2024). Empirical ground-motion relations of peak ground acceleration in the region of the Gulf of California, Nat. Hazards, 120, 3, 2599-2615, doi:10.1007/s11069-023-06295-1.

Wo, S., J. T. Liang and L. R. Myer (2005). CO_2 storage in Coalbeds. In: Carbon Dioxide Capture for Storage in Deep Geologic Formations, 2, Elsevier, 1263-1291, doi:10.1016/B978-008044570-0/50161-6.

Zafra, E. (2013). Cartografía geológica del Campo Colorado a escala 1:25,000, B.Sc. thesis, Universidad Industrial de Santander, Bucaramanga, Colombia, https://noesis.uis.edu.co/handle/20.500.14071/28100.

Zarifi, Z., J. Havskov and A. Hanyga (2007). An insight into the Bucaramanga nest, Tectonophysics, 443, 1-2, 93-105, doi:10.1016/j.tecto.2007.06.004.

***CORRESPONDING AUTHOR: Sergio GARCIA-ARIAS**,
Universidad Industrial de Santander, Escuela de Geología, Bucaramanga, Colombia
e-maill: sergio.garcia.910815@gmail.com

© 2026 the Author(s).
Open Access. This article is licensed under a Creative Commons Attribution 4.0 International License